

University of Windsor

Scholarship at UWindor

Electronic Theses and Dissertations

Theses, Dissertations, and Major Papers

2015

Vibration Damping Via Acoustic Treatment Attached To Vehicle Body Panels

Carlo Gambino
University of Windsor

Follow this and additional works at: <https://scholar.uwindsor.ca/etd>

Recommended Citation

Gambino, Carlo, "Vibration Damping Via Acoustic Treatment Attached To Vehicle Body Panels" (2015). *Electronic Theses and Dissertations*. 5268.
<https://scholar.uwindsor.ca/etd/5268>

This online database contains the full-text of PhD dissertations and Masters' theses of University of Windsor students from 1954 forward. These documents are made available for personal study and research purposes only, in accordance with the Canadian Copyright Act and the Creative Commons license—CC BY-NC-ND (Attribution, Non-Commercial, No Derivative Works). Under this license, works must always be attributed to the copyright holder (original author), cannot be used for any commercial purposes, and may not be altered. Any other use would require the permission of the copyright holder. Students may inquire about withdrawing their dissertation and/or thesis from this database. For additional inquiries, please contact the repository administrator via email (scholarship@uwindsor.ca) or by telephone at 519-253-3000ext. 3208.

Vibration Damping Via Acoustic Treatment Attached To Vehicle Body Panels

By

Carlo Gambino

A Thesis
Submitted to the Faculty of Graduate Studies
Through Mechanical, Automotive & Materials Engineering
in Partial Fulfillment of the Requirements for
the Degree of Master of Applied Science
at the University of Windsor

Windsor, Ontario, Canada

2015

© 2015 Carlo Gambino

Vibration Damping Via Acoustic Treatment Attached To Vehicle Body Panels

by

Carlo Gambino

APPROVED BY:

Dr. N. Kar
Department of Electrical & Computing Engineering

Dr. R. Gaspar
Department of Mechanical, Automotive & Materials Engineering

Dr. C. Novak, Advisor
Department of Mechanical, Automotive & Materials Engineering

January 20th, 2015

DECLARATION OF ORIGINALITY

I hereby certify that I am the sole author of this thesis and that no part of this thesis has been published or submitted for publication.

I certify that, to the best of my knowledge, my thesis does not infringe upon anyone's copyright nor violate any proprietary rights and that any ideas, techniques, quotations, or any other material from the work of other people included in my thesis, published or otherwise, are fully acknowledged in accordance with the standard referencing practices. Furthermore, to the extent that I have included copyrighted material that surpasses the bounds of fair dealing within the meaning of the Canada Copyright Act, I certify that I have obtained written permission from the copyright owner(s) to include such material(s) in my thesis and have included copies of such copyright clearances to my appendix.

I declare that this is a true copy of my thesis, including any final revisions, as approved by my thesis committee and the Graduate Studies office, and that this thesis has not been submitted for a higher degree to any other University or Institution.

ABSTRACT

Currently, in the automotive industry, the control of noise and vibration is the subject of much research, oriented towards the creation of innovative solutions to improve the comfort of the vehicle and to reduce its cost and weight. This thesis fits into this particular framework, as it aims to investigate the possibility of integrating the functions of sound absorption\insulation and vibration damping in a unique component.

At present the bituminous viscoelastic treatments, which are bonded to the car body panels, take charge of the vibration damping, while the sound absorption and insulation is obtained by means of the poroacoustic treatments. The solution proposed here consists of employing porous materials to perform both these functions, thus allowing the partial or complete removal of the viscoelastic damping treatments from the car body. This should decrease the weight of the vehicle, reducing fuel consumption and emissions, and it might also benefit production costs.

ACKNOWLEDGEMENTS

I would like to express the deepest appreciation to FIAT, Chrysler, Politecnico di Torino, and University of Windsor, for giving me the opportunity to take part to the Joint Master Degree program and to work on this thesis.

My gratitude goes to all the people who have collaborated on this project, in particular, Marco Danti and Daniele Stanga, for their constant support, Dilal Rhazi, for his valuable suggestions, and to my academic tutors Colin Novak and Marco Carlo Masoero for their wise advice.

TABLE OF CONTENTS

DECLARATION OF ORIGINALITY	iii
ABSTRACT	iv
ACKNOWLEDGEMENTS	v
LIST OF TABLES	ix
LIST OF FIGURES	x
LIST OF ABBREVIATIONS.....	xv
NOMENCLATURE	xvi
CHAPTER 1 INTRODUCTION	1
1.1 Introduction	1
1.2 Motivations	2
1.3 Objectives	3
1.4 Methodologies	4
1.5 Thesis Organization	5
CHAPTER 2 REVIEW OF LITERATURE	6
2.1 Noise and vibration in vehicles	6
2.2 Vibration damping treatments	11
2.3 Poroacoustic treatments	12
<i>2.3.1 Different categories of poroacoustic treatments and their properties</i>	14
<i>2.3.2 Vibroacoustic behaviour of porous materials</i>	21
2.4 Finite element vibroacoustic analysis of panels treated with poroacoustic materials	27
<i>2.4.1 Modal analysis</i>	28
<i>2.4.2 Finite element vibroacoustic analysis of systems composed by structural components and poroacoustic materials</i>	33
2.5 Summary and final remarks on the review of literature	43
CHAPTER 3 METHODOLOGIES AND RESULTS	45
3.1 Experimental tests	45

3.1.1	<i>Experimental setup</i>	45
3.1.2	<i>Tests carried out on the steel plate</i>	47
3.1.3	<i>Experimental results</i>	49
3.2	<i>Introduction to the FEA software</i>	52
3.2.1	<i>Modal frequency response step 1: Normal modes extraction</i>	54
3.2.2	<i>Modal frequency response step 2: Reduced impedance matrixes of the porous trim</i>	55
3.2.3	<i>Modal frequency response step 3: Structure-acoustic cavity coupling</i>	57
3.2.4	<i>Modal frequency response step 4: Projection of the reduced impedance matrix</i>	59
3.2.5	<i>Modal frequency response step 5: Modal frequency response solver</i>	59
3.3	<i>Numerical modeling</i>	60
3.3.1	<i>Mesh of the elastic component</i>	60
3.3.2	<i>Mesh of the porous trim</i>	61
3.3.3	<i>Presence of an acoustic cavity</i>	63
3.3.4	<i>Sampling frequencies for the calculation of the reduced impedance matrices</i>	64
3.4	<i>Validation of the numerical model</i>	67
3.4.1	<i>Frequency response of the bare plate</i>	67
3.4.2	<i>Effect of the porous treatments on the frequency response of the plate</i>	70
3.5	<i>Sensitivity analysis on porous material properties</i>	75
3.5.1	<i>Methodology</i>	75
3.5.2	<i>Relationship between the porous material properties and the response of the system</i>	77
3.5.3	<i>Negligible parameters</i>	83
3.6	<i>Vibration damping performances of poroacoustic treatments</i>	83
3.6.1	<i>Performance index</i>	83
3.6.2	<i>Comparison between different materials</i>	84
3.7	<i>Use of the poroacoustic treatments on a vehicle for damping the vibration of the floor</i>	87
3.7.1	<i>Comparison among different layouts of the treatments</i>	88
CHAPTER 4 CONCLUSIONS AND RECOMMENDATIONS		96
4.1	<i>Introductory comments</i>	96
4.2	<i>Conclusions</i>	97
4.3	<i>Recommendations</i>	99

REFERENCES/BIBLIOGRAPHY.....	102
VITA AUCTORIS	107

LIST OF TABLES

Table 2.1: Average fiber diameter and density of various fibrous acoustic materials [4]	16
Table 2.2: Density of various fibrous materials used for noise control [4].....	18
Table 2.3: Principal properties of the poroelastic materials.....	18
Table 2.4: Nomenclature of the principal FRF used in modal analysis.	32
Table 3.1: Characteristics of the felts employed for the validation of the numerical model, provided by the supplier of the treatments.....	47
Table 3.2: Optimized frequency set for the calculation of the impedance matrices.	67
Table 3.3: Material properties database, with the maximum and minimum values underlined for each variable.	76
Table 3.4: Nominal values and range of variation for the porous material properties.....	77
Table 3.5: Material properties of the optimized treatment.....	85

LIST OF FIGURES

Figure 2.1: Schematic representation of the engine noise transmission paths.	7
Figure 2.2: General layout of the NVH treatments within a passenger vehicle [4].	10
Figure 2.3: Free layer and constrained layer damping treatments layouts [5].	12
Figure 2.4: Interaction between a sound pressure wave and an obstacle placed on the airborne transmission path.	13
Figure 2.5: Champoux porosimeter [8].	14
Figure 2.6: Examples of microstructures for cellular and fibrous poroacoustic materials [4].	15
Figure 2.7: Experimental setup for the measurement of the air flow resistivity [8].	17
Figure 2.8: Setup used for the electrolytic measurement of tortuosity [8].	19
Figure 2.9: Setup used for the ultrasound measurement of tortuosity [8].	19
Figure 2.10: Graphical representation of the thermal and viscous characteristic lengths	20
Figure 2.11: Schematic representation of the Biot’s theory of poroelasticity [17].	25
Figure 2.12: Representation of a system composed by elastic, acoustic and porous domains [22].	28
Figure 2.13: Schematic representation of the FRF [24].	31
Figure 2.14: Example of a magnitude Bode plot of an FRF, highlighting the contribution of each mode shape to the overall response function [24].	32
Figure 2.15: Experimental setup used for measuring the transmission loss and the frequency response of the roof panel to a mechanical excitation in the Göransson research work [30].	36
Figure 2.16: Different kinds of porous treatments tested in Kobayashi et al. research [17].	37
Figure 2.17: Comparison between the response calculated with the numerical model and the one measured experimentally on the dashboard treated with poroacoustic materials in the research conducted by Duval et al. [32].	39
Figure 2.18: Comparison between the response calculated with the numerical model and the one measured experimentally on the bare dashboard in the research conducted by Duval et al. [32]. ...	39

Figure 2.19: RMS mobility of the bare and the treated plate, evaluated by means of numerical simulations and experimental tests the research conducted by Rieter Automotive [22].....	40
Figure 2.20: Envelope of mobility calculated for four different layouts of the treatments and for various load cases, with zoom below 100 Hz. (Rieter Automotive [22]).	42
Figure 2.21: Measured (red) and simulated (blue) accelerance FRF of a plate treated with a poroacoustic material in the research work conducted by the CRF [33].	43
Figure 3.1: Schematic representation of the experimental setup for the tests conducted on the steel plate.....	46
Figure 3.2: Positioning of the excitation point (E) and the three accelerometers (A1, A2 and A3)	46
Figure 3.3: Different tape layouts for joining the acoustic treatment to the plate: attached in five points (1), on diagonals (2) and on diagonals and sides (3).....	48
Figure 3.4: Experimental setup for the tests conducted on the steel plate.	49
Figure 3.5: Accelerance FRF of the plate treated with the felt "1N" calculated from the accelerometer A3.	50
Figure 3.6: Accelerance FRF of the plate treated with the felt "1S" calculated from the accelerometer A3.	50
Figure 3.7: Comparison between the accelerance FRF curves of the plate treated with the felt "1S" and "1N".	51
Figure 3.9: Deformation patterns of a plate at increasing natural frequencies.	55
Figure 3.11: Comparison between different kinds of mesh elements for the plate.....	60
Figure 3.12: Comparison between different kinds of mesh elements for the plate.....	62
Figure 3.13: Computational time increment for smaller mesh size.	62
Figure 3.14: Mesh of the treated steel plate coupled to the acoustic cavity.....	63
Figure 3.15: Comparison between the response of the system depicted in Figure 3.14 in the two cases when the presence of the acoustic cavity is neglected or taken into account.	64

Figure 3.16: Comparison between the FRF curves obtained using different steps for the sampled frequencies at which the reduced impedance matrices are calculated.	65
Figure 3.17: Computational time increment related to the accuracy of the discretization and comparison with the optimized frequencies set.	66
Figure 3.18: Comparison between the results obtained with the smallest frequency sampling step and with the optimized frequencies set.	66
Figure 3.19: Steel plate and equivalent FE model.	68
Figure 3.20: Comparison between the experimental and the numerical FRF curves, evaluated for the bare plate in correspondence of the accelerometer A1.	69
Figure 3.21: Comparison between the experimental and the numerical FRF curves, evaluated for the bare plate in correspondence of the accelerometer A2.	69
Figure 3.22: Comparison between the experimental and the numerical FRF curves, evaluated for the bare plate in correspondence of the accelerometer A3.	70
Figure 3.23: Exploded view of the finite element model of the treated plate.	70
Figure 3.24: Comparison between experimental and numerical FRF curves, evaluated at accelerometer A3 for the plate treated with the porous 1N joined with the tape layout 1.	71
Figure 3.25: Comparison between experimental and numerical FRF curves, evaluated at accelerometer A3 for the plate treated with the porous 1N joined with the tape layout 2.	72
Figure 3.26: Comparison between experimental and numerical FRF curves, evaluated at accelerometer A3 for the plate treated with the porous 1N joined with the tape layout 3.	72
Figure 3.27: Comparison between experimental and numerical FRF curves, evaluated at accelerometer A3 for the plate treated with the porous 1S joined with the tape layout 1.	73
Figure 3.28: Comparison between experimental and numerical FRF curves, evaluated at accelerometer A3 for the plate treated with the porous 1S joined with the tape layout 2.	73
Figure 3.29: Comparison between experimental and numerical FRF curves, evaluated at accelerometer A3 for the plate treated with the porous 1s joined with the tape layout 3.	74

Figure 3.30: Effect of the input porous skeleton density on the output frequency response.	78
Figure 3.31: Effect of the input porosity on the output frequency response.	78
Figure 3.32: Effect of the input air flow resistivity on the output frequency response.	80
Figure 3.33: Effect of the input air flow resistivity on the output frequency response.	80
Figure 3.34: Effect of the input air flow resistivity on the output frequency response.	81
Figure 3.35: Effect of the input air flow resistivity on the output frequency response.	81
Figure 3.36: Effect of the input Young’s modulus parameter on the output response.	82
Figure 3.37: Average RMS acceleration of the treated plate in 1/3 octave bands between 14.1 and 112 Hz.	84
Figure 3.38: Average RMS acceleration of the treated plate in 1/3 octave bands between 112 and 891 Hz.	85
Figure 3.39: Weighted mean calculated over the 1/3 frequency bands of the average RMS acceleration of the plate treated with different poroacoustic materials.	86
Figure 3.40: Layout of the treatments applied to the floor of a mid-segment vehicle.	87
Figure 3.41: Example of damping treatments layout on a vehicle’s floor.	87
Figure 3.42: Alternative treatments layouts compared.	89
Figure 3.43: Randomly selected response nodes for the evaluation of the average vibration level of the floor.	90
Figure 3.44: Comparison among the normalized average RMS acceleration in 1/3 octave measured on the bare floor and on the floor treated as in layout 1 and layout 2.	91
Figure 3.45: Comparison among the normalized average RMS acceleration in 1/3 octave measured on the bare floor and on the floor treated as in layout 1 and layout 3.	92
Figure 3.46: Comparison among the normalized average RMS acceleration in 1/3 octave measured on the bare floor and on the floor treated as in layout 1 and layout 4.	92
Figure 3.47: Comparison among the normalized average RMS acceleration in 1/3 octave measured on the bare floor and on the floor treated as in layout 1 and layout 5.	93

Figure 3.48: Comparison among the mean value of the normalized average RMS acceleration over the frequency range 0-1000 Hz, calculated for the bare floor and for the floor with the different layouts of the treatments93

Figure 3.49: Comparison among the mass of the treatments in the various layouts and weight saving achievable with the alternative solutions proposed.94

LIST OF ABBREVIATIONS

AFR	Air Flow Resistivity
CLDT	Constrained Layer Damping Treatment
DOF	Degrees Of Freedom
FE	Finite Element
FEA	Finite Element Analysis
FEM	Finite Element Method
FLDT	Free Layer Damping Treatment
FRF	Frequency Response Function
MDOF	Multiple degrees of freedom
NVH	Noise Vibration and Harshness
OFAT	One Factor At Time
RMS	Root Mean Square
SDOF	Single degree of freedom
SEA	Statistical Energy Analysis
SIMO	Single-Input Multiple-Output
SoS	Speed of Sound
SPL	Sound Pressure Level
SRI	Sound Reduction Index
STL	Sound Transmission Loss
VDPI	Vibration Damping Performance Index

NOMENCLATURE

A	Amplitude of the response acceleration
A_p	Amplitude of the pressure wave
B	Damping coefficient in the Atalla's formulation
c_b	Speed of the flexural wave within a plate
c_p	Fluid specific heat at constant pressure
c_v	Fluid specific heat at constant volume
D	Bending stiffness
E	Young's modulus
E_a	Absorbed energy of an incident sound wave
E_i	Energy of an incident sound wave
E_r	Reflected energy of an incident sound wave
E_s	Young's modulus of the porous skeleton
E_t	Transmitted energy of an incident sound wave
F	Force
$\{F_F\}$	Excitation vector on the fluid
f_{h_b}	Upper limit of the 1/3 octave band

f_{lb}	Lower limit of the 1/3 octave band
f_n	Natural frequency
f_s	Sampling step of the frequencies for the \overline{RMS}_{A_b}
$\{F_S\}$	Excitation vector on the structure
F_R	Viscous force
H	Thickness of the sample for AFR measurement
H	Generic frequency response function
H_A	Accelerance FRF
K	Wave number
$[K]$	Stiffness matrix of a generic multiple DOF system
$[k]$	Stiffness diagonal matrix
$[K_s]$	Stiffness matrix of the structure
$[K_f]$	Stiffness matrix of the fluid
$[M]$	Mass matrix of a generic multiple DOF system
$[m]$	Mass diagonal matrix
$[M_s]$	Mass matrix of the structure
$[M_f]$	Mass matrix of the fluid
M_{plate}	Mass of the plate

m_{tot}	Total mass of the system
N	Number of points considered for the \overline{RMS}_{A_b}
P	Pressure
p_0	Reference pressure in the Champoux porosimeter
p_0	Balance pressure
p_i	Amplitude of an incident sound pressure wave
p_r	Amplitude of a reflected sound pressure wave
$P_{T,inner}$	Porous domain inner pressure
P_{T,r_F}	Porous domain pressure at the interface with the cavity
Q	Fluid bulk modulus
$\{q\}$	Displacement vector of a generic multiple DOF system
\tilde{Q}	Johnson-Champoux-Allard equivalent bulk modulus
R	Air flow resistivity
R	Sound reflection coefficient
r_c	Electrical resistivity of a saturated porous sample
r_f	Electrical resistivity of a fluid
\overline{RMS}_{A_b}	Average RMS acceleration in 1/3 octave band
S	Section of the pipe for AFR measurement

T	Thickness of the plate
$[t_{in}]$	Forces modal participation factor
U	Displacement of the fluid phase in porous materials
U	Displacement of the solid phase in porous materials
$U_i(r_i)$	Microscopic displacement of the fluid inside the pore
$U_i(r_w)$	Microscopic displacement of the fluid at the pore surface
$u_{T,inner}$	Porous domain inner displacement
u_{T,Γ_s}	Porous domain displacement with the structure
V	Volume
V_{ext}	Unfilled volume in Champoux porosimeter
V_f	Volume of fluid phase of porous material
V_s	Volume of solid phase of porous material
V_t	Total volume of porous material
$V_{treatment}$	Volume of the porous treatment
X	Spatial coordinate of a linear sound wave
X	Amplitude of the response displacement
Y	Amplitude of the response velocity
Z_c	Acoustic impedance

$[Z'_{red}]$	Reduced impedance matrix projected into modal space
A	Receptance FRF
α_{∞}	Tortuosity
α_A	Sound absorption coefficient
α_F	Acoustic cavity modal factor
α_S	Elastic component modal factor
$[\zeta]$	Modal damping
A	Fluid thermal conductivity
λ_B	Bending wavelength
λ_i	Eigenvalues
A_t	Thermal Length
A_v	Viscous length
M	Fluid dynamic viscosity
N	Poisson ratio
ξ_i	Modal participation factors
$\tilde{\rho}$	Johnson-Champoux-Allard equivalent fluid density
$\tilde{\rho}_{ii}$	Atalla's formulation equivalent densities
ρ_f	Solid phase density

ρ_{ii}	Biot theory equivalent densities
ρ_s	Solid phase density
$\rho_{treatment}$	Density of the porous treatment
σ^F	Stress tensor for fluid phase in a porous material
σ^S	Stress tensor for solid phase in a porous material
T	Sound transmission coefficient
$\{\phi_i\}$	Eigenvectors
$[\phi_{\Gamma_F}]$	Acoustic cavity mode shapes
$[\phi_{\Gamma_S}]$	Elastic component mode shapes
Ω	Angular velocity
ω_{oi}	Natural frequencies

CHAPTER 1

INTRODUCTION

1.1 Introduction

When a motor vehicle is operated it is subject to several dynamic excitations generated from its subsystems and from the interaction with the road, which causes it to vibrate. The vibrations of the car body are perceived by passengers in two different ways. On one hand they are perceived as a tactile sensation due to the contact with the vehicle; on the other hand they are perceived as an acoustic sensation caused by the sound pressure waves radiated from the vibrating surfaces. As these acoustic and tactile stimuli have a significant impact on the comfort of the passengers, being able to control noise and vibrations represents a key factor to reach customer satisfaction. The adoption of appropriate countermeasures against the generation and transmission of noise and vibration, usually referred as NVH design, has thus become a standard practice in the product development process. Furthermore, as a result of increasing customer expectations and the evolution of motor vehicles towards lighter construction and higher engine power output, NVH design has become more and more challenging, thus motivating research into new solutions aimed at achieving better noise and vibration levels.

In general, the problem of noise and vibration control can be addressed with two opposite approaches, which consist of modifying the characteristics of the excitation sources and in acting on the propagation of the acoustics and the mechanical waves. Regarding the modification of the excitation source characteristics, it usually needs to be planned in the very first stages of the vehicle design process and is usually limited by a series of functional constraints. On the contrary, the countermeasures adopted to obstruct the propagation of the acoustics and the mechanical waves can be designed in a later stage of the product development, when the characteristics of the excitation source have already been established. This solution usually involves the usage of particular components that can be placed along the transmission paths and within the receiving

environment; such as vibration dampers, noise absorbers, insulators and barriers. The selection of the suitable materials and layouts for these components represents the most significant part of the NVH design work, which aims to achieve the target noise and vibration levels within the vehicle. Furthermore, since these treatments have a significant contribution in terms of cost and weight of the car, their vibroacoustic performance needs to be balanced with the lightness and cost requirements.

During the vehicle development process the control of noise and vibration is usually addressed in an independent way, and therefore, the design of vibration damping and noise absorbing\insulating treatments are typically carried out separately. For this reason, the contribution of the poroacoustic materials in achieving target vibration levels is generally neglected.

This conventional approach to the problem is motivated by the fact that the poroacoustic treatments presently employed have little damping effect on the vibration of the car body panels. However, by modifying the characteristics of the porous materials and the way they are applied to the vehicle, it might be possible to improve this effect significantly, allowing their use as vibration dampers.

1.2 Motivations

As already mentioned, the vibroacoustic comfort of a vehicle is controlled by imposing specific targets to noise and vibration levels, which are achieved by employing different kinds of treatments. More specifically, porous treatments, like foam and felt, are used for sound absorption and insulation, while viscoelastic treatments, like bitumen and thick rubber, are employed as vibration dampers. In a similar way, different kinds of numerical tools are used to analyze the acoustic and vibration performances of the vehicle. In particular, Statistical Energy Analysis (SEA) is commonly employed in the medium and high frequency range to estimate the value of the acoustic performance indicators, such as the Sound Pressure Level. With a range of frequency

range overlap, the Finite Element Analysis (FEA) is normally used in the low and medium frequency range for the analysis of the vibration performance indicators, such as the resonance peaks of the Frequency Response Functions.

The choice of using a specific kind of treatment, respectively, for vibration damping and sound absorption\insulation is because each one possesses specific characteristics to perform its own function but it is not capable to carry out both tasks. Proving that it is possible to use the poroacoustic materials to dampen the vibrations of the car body panels would mean that they could be used to integrate the two functions in a unique component.

This solution could mean that by replacing the viscoelastic treatments with the poroacoustic ones, either partially or completely, there could be potential benefits in terms of weight or cost reduction.

1.3 Objectives

The primary objective of the project was to evaluate the possibility of employing porous acoustic treatments in place of standard FLDT to damp the vibrations of the car body panels. In addition, two secondary objectives have been pursued. The first one was to establish a numerical procedure for evaluating the impact of the acoustic treatments on the car body panels, in terms of vibration damping. This procedure involved the use of a finite element model based on the Biot's theory of poroelasticity, whose results were validated by means of experimental tests. A further objective was to analyze the way material properties affect the vibration damping performance of the treatments. This analysis should provide a criterion for selecting the most suitable materials among the ones already available, based on their characteristics, and to define the ideal specifications for materials to be produced in the future.

1.4 Methodologies

The research work was carried out following the steps listed below:

- **Experimental tests:** An experimental frequency response analysis was conducted on a system composed of a steel plate and a sound absorbing treatment attached to its surface by means of double-sided tape. The response of the system was determined by exciting the panel with an inertial shaker and measuring the acceleration in various points on its surface.
- **Analysis of the features of the model:** A brief study was conducted to determine how the various features of the numerical model affect the output of the simulations. First, the effects of the characteristics of the mesh on the calculated response of the system were investigated. Then two solutions to reduce the computational effort of the simulations were examined: neglecting the presence of the coupled acoustic cavity and selecting only certain sampled frequencies for the calculation of the reduced impedance matrices.
- **Validation of the model:** The experimental results were compared to the outcomes of the corresponding numerical simulations in order to assess the validity of the numerical model for the frequency response analysis of trimmed structural panels.
- **Sensitivity analysis:** A sensitivity analysis was conducted to determine the effects of the properties of porous materials on the frequency response of the panels to which they were applied. For the sensitivity analysis the OFAT methodology of changing one factor at time was employed.
- **Materials comparison:** Various poroacoustic materials, selected among the ones which are made available from the suppliers, were compared with one another in terms of vibration damping characteristics. In this way it was possible to determine which, among them, was the most suitable for replacing the FLDT.
- **Application to the floor of a vehicle:** Various numerical simulations were conducted on the floor of a vehicle to evaluate the possibility of matching the vibration damping

performance of the FLDT by means of poroacoustic materials, thus allowing the removal of the bitumen patches.

1.5 Thesis Organization

The thesis is divided in four chapters, which are organized as follows.

- Chapter 1 introduces the problem addressed and presents the objectives of the thesis and the methodologies used.
- Chapter 2 contains the review of relevant literature and is divided into two parts. The first part explains how noise and vibration are generated and transmitted on a vehicle; it describes how sound absorbing and damping treatments work, and it provides a general presentation of the finite element techniques used to address the vibroacoustic problems involving the presence of poroelastic materials. In the second part, some of the most significant studies which have been conducted in the same field of investigation as this thesis are presented to highlight the common elements they share with this work and to contrast them with the innovative elements that are introduced by this study.
- Chapter 3 covers the modeling, simulation and experimental work. The first part analyzes the main features of the finite element model and it describes the way the numerical results have been validated by means of experimental tests. In the second part the simulations are used to investigate how the characteristics of the poroacoustic treatments affect the dynamic response of the steel panels to which they are attached. Finally, the numerical frequency response analysis is used to evaluate the possibility of replacing the standard FLDT with the poroacoustic treatments in the floor.
- Chapter 4 summarizes the results and draws the conclusions of the research work and it also provides some suggestions and recommendations for its possible future developments.

CHAPTER 2

REVIEW OF LITERATURE

2.1 Noise and vibration in vehicles

In any operating condition the comfort of a vehicle is negatively affected by noise and vibration, which propagate from the various excitation sources to the passenger cabin. The study of the way noise and vibration are generated and transmitted is usually referred as NVH, and its main task is to limit the influence of the vibroacoustic phenomena on passenger well-being. Over the last decade, because of the rising customer expectations in terms of vibroacoustic comfort, the role of NVH has assumed an even higher importance in the design of new vehicles. In order to understand the significance of this field of research for the automotive industry, one must consider that poor vehicle comfort accounts for more than one quarter of the customer dissatisfaction [1]. Another factor that must be taken into account to understand the central role that NVH has assumed in modern automotive design is the evolution of cars towards higher engine performance and lightweight construction. Maintaining an elevated vibroacoustic comfort in spite of the higher power and the thinner body panels indeed constitutes one of the greatest challenges in the design of new vehicles.

Since noise and vibration are closely connected to each other they are usually analyzed in parallel. Their correlation is because noise is generated from the vibration of a body, while at the same time a sound pressure wave interacting with a body makes it resonate. The inputs for these phenomena are come from the dynamic excitations generated from the subsystems of the vehicle and from the external environment. On a passenger car there are various kinds of excitations, distributed within a wide range of frequencies. The manoeuvring loads usually lie below 1Hz, while the acoustic excitations extend up to about 10 KHz. Both the mechanical and the acoustic stimuli can be perceived by the human body in two different ways according to their frequencies. From 25 up to 100 Hz they are mainly perceived as a tactile sensation, while for frequencies

higher than 100 Hz the predominant sensation is auditory. In the range of frequencies around 100 Hz a partial overlap between the two senses is usually experienced. This latter sensation is usually described as boom noise. [2].

In order to have a better understanding of the correlation between noise and vibration it is useful to refer to the noise transmission paths. In general, it is possible to identify two different paths from the source to the receiver:

- **The airborne path, when the transmission occurs through the air.** It can be “direct” when a sound pressure wave from the outside of the vehicle enters the cabin through holes and gaps (e.g. windows, seals etc.) or “indirect” when a sound pressure wave resonates through the car body panels which radiate noise inside an acoustic cavity.
- **The structure-borne path, when the transmission occurs through the solid medium constituted by the car body.** In this kind of transmission the vehicle subsystems mechanically excite the car body panels with dynamic forces causing them to resonate and therefore to radiate noise.

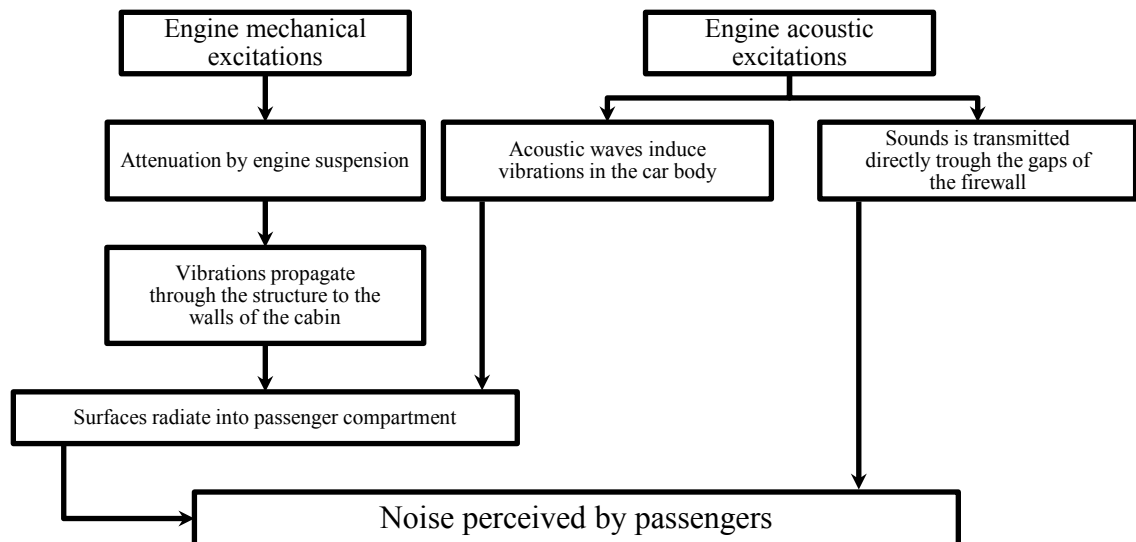


Figure 0.1: Schematic representation of the engine noise transmission paths.

Figure 0.1 shows how the engine noise is transmitted to the passenger cabin and it highlights the role of airborne and structure borne paths in this process. The noise generated by the multiple sources of mechanical and acoustic excitations of the vehicle, like engine, exhaust, fans, etc., usually propagates towards the passenger compartment using both paths. The predominance of one transmission path over the other only depends on the frequency of the signal. For signals below 500 Hz the structure-borne path prevails, while for the ones over 1000 Hz the airborne is the most significant. Knowing the way noise is transmitted in a vehicle is necessary in order to control it; in other words, the identification of the predominant path is essential to adopt the appropriate countermeasures to its propagation.

Over the course of the vehicle development process, the vibroacoustic problem can be addressed in three different ways: at the source, along the propagation path from the source to the receiver, or within the receiving environment. Usually modifying the characteristics of the source represents the most effective solution; however, this requires planning in the very first stages of the development process and can sometimes create conflicts with the other functional requirements. For this reason, the vibroacoustic performance targets can be achieved only by employing additional components along the transmission path or within the receiving environment. The type of these components depends on kind of noise addressed. For the airborne noise, sound insulators and barriers are used to obstruct the transmission from the source to the receiver and sound absorbers are employed directly within the receiving environment, while for the structure-borne noise, the transmission is controlled with vibration dampers and insulators [3]. With noise barriers and insulators, it is possible to minimize the transmission of the acoustic energy by means, respectively, of reflection and dissipation. The materials used for the barriers are generally nonporous and dense, so that they can maximize the reflection of the incoming sound waves. The ideal characteristics of these reflective components include the absence of gaps to avoid sound wave leakages, a high density to reduce vibration, and an optimized stiffness to prevent resonance effects in correspondence of their natural frequencies. The double-walled

firewall, which is placed between the engine and the passenger compartment to prevent powertrain noise from entering the cabin, constitutes a typical example of noise barrier.

In the parts of the vehicle, which require a high STL, barriers are usually combined with insulators. The sound insulators are constructed by foam or felt, which dissipate the energy of the sound waves passing through them. The energy dissipation takes place within the microstructure of the porous material and it is associated to the viscoelastic and viscous losses. The viscoelastic losses are related the deformation of the solid skeleton, while the viscous losses are due to the friction between the skeleton and the fluid flowing inside its channels. Since the energy dissipation is mainly due to the viscous friction and to a smaller extent to the viscoelastic losses, the most important characteristic for the porous material used for sound absorption is the presence of an open cell structure. This means that all the cavities are interconnected through channels that allow the fluid to flow inside them.

The porous materials can also be employed as sound absorber, which means that they can be used to decrease the energy of the reflected sound waves within an acoustic cavity. In this case the dissipation does not occur along the airborne transmission path, as for the noise insulators, but rather within the receiving environment. In most of the practical vehicle applications, however, the function of insulation and absorption is integrated in a unique component, as in the case of door trim.

The principle of dissipating energy to minimize noise transmission is also employed in the case of structure borne noise. The components used for this purpose are referred to as vibration damping treatments and they are bonded to the structure of the vehicle. When the structure vibrates, the damping treatments undergo several deformation cycles characterized by a large hysteresis. The hysteresis is caused by the fact that in every cycle a certain amount of strain energy is converted into heat and then dissipates into the environment. This dissipation allows for a reduction of the amplitude of vibration in the frequency range close to the resonance peaks of the structure, hence limiting the noise radiation.

Another strategy adopted for the control of the structure borne noise uses vibration insulators to separate the car body structure from the excitation sources. The insulators are placed in correspondence of the major sources of vibration, such as the engine and suspensions, and they perform a decoupling function on their excitations.

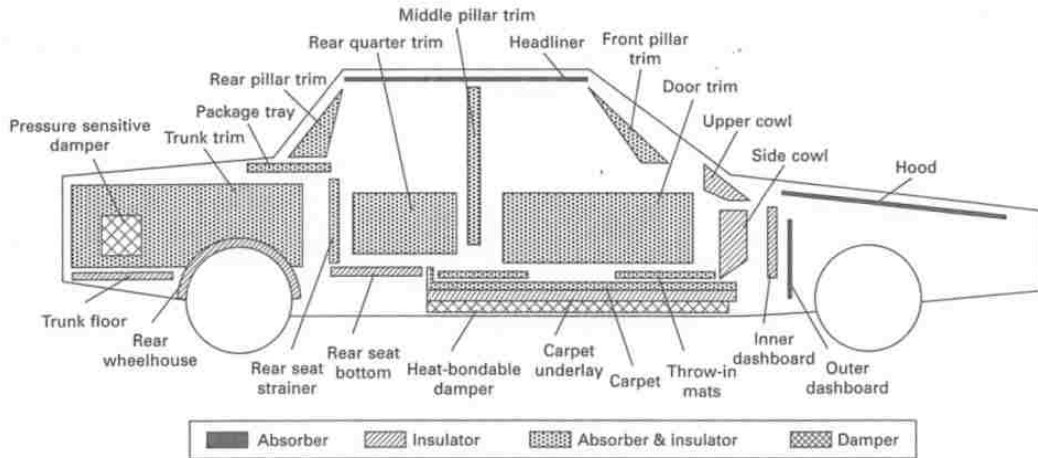


Figure 0.2: General layout of the NVH treatments within a passenger vehicle [4].

Figure 0.2 shows the layout of the principal acoustic treatments used on passenger vehicles, divided by function. The roof panel is the most important sound absorbing treatment of the passenger compartment and it provides about the 25% of the absorption within that cavity; the cumulative contribution of all the other sound absorbing treatments on board is equal to the entire roof, while the remaining 50% is due to the presence of the seats, which are made of open cell foam and fabric [2]. The sound absorbing treatments are also deployed inside the engine compartment to reduce the reverberation of the powertrain noise. The components used for this kind of application are made of fibrous tissue, which are applied to the hood and the outer dashboard. Making reference to Figure 0.2 it can be noted that most part of the thin sound absorbing treatments used inside the passenger compartment are capable of performing insulating functions as well. However, in the areas of the vehicle where noise transmission is most critical, it is necessary to use thicker porous treatments specifically dedicated to the noise insulation. These treatments are usually applied to the firewall to reduce the noise coming from the engine, and to

the floor to insulate the cabin from the noise generated by the contact between the wheels and the road. Finally, as regards the damping treatments, their layout strongly depends on the characteristics of the chassis, because they are placed in correspondence of the areas that are mostly affected by the local modes.

2.2 Vibration damping treatments

Body vibration depends on the excitations themselves and the response. The excitations are generated from the various mechanical subsystems and from interactions with the external environment, while the response is associated with the modes of the chassis. These modes can be classified as global and local, depending on the amount of structure involved in the motion. The global modes, which usually occur below 50 Hz [2], present a deformed shape extending along the entire structure. The elastic strain energy is distributed in a uniform way because of this. In this case, damping vibration is usually very difficult, as it requires the application of elevated loads in correspondence with the points with the highest modal amplitude. On the contrary, local modes are much easier to dampen because their strain energy is localized to smaller areas of the chassis. This means that damping treatments can be positioned on the regions with the highest deformation gradient rather than on the entire car body, thus reducing their impact on the vehicle [1]. In general, the term ‘damping’ refers to the extraction of the mechanical energy from a vibrating system, which is converted into another form of energy (usually heat), then can be dissipated into the environment. Vibration damping is necessary to control the steady state response of the chassis; this prevents the amplitude of the mechanical oscillations from becoming too high in correspondence to resonant frequencies. The characteristics of vibration damping of a chassis can be related to material properties of the panels, more specifically to the loss factor. However, since the metallic materials present a limited degree of hysteresis, this contribution is normally not sufficient. For this reason it is necessary to make use of some kind of viscoelastic treatment such as plastic, rubber, asphalt based materials, etc. [5,6]. These treatments can be

applied to the car body panels in the two different configurations, as illustrated in Figure 0.3. These setups are usually described as Free Layer Damping Treatments (FLDT) and Constrained Layer Damping Treatments (CLDT).

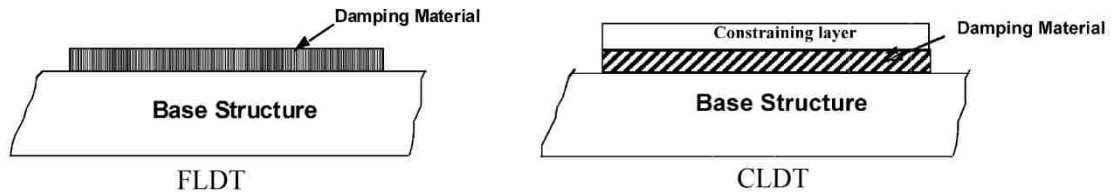


Figure 0.3: Free layer and constrained layer damping treatments layouts [5].

FLDT simply consist in layers of viscoelastic material that can be either sprayed on the chassis or attached to its surface by means of thermal bonding or pressure sensitive adhesives. CLDT has a sandwich structure formed by two outer metal layers (the car body panel and an external sheet metal) and viscoelastic material placed in the middle. The main difference between the two setups is the way they deform. In FLDT, when the car body panels are deflected in bending, the viscoelastic material follows the movements of the structure, deforming primarily in extension and compression within the planes parallel to the metallic substrate. For this reason FLDT are also known as extensional type damping treatments. With CLDT, when the car body panels are deformed in bending, the metallic constrains do not allow the viscoelastic material to deform in extension or compression, but they force it to deform in shear instead. Since shearing deformation leads to an elevated energy dissipation within the viscoelastic layer, CLDT provides a higher level of damping with respect to the FLDT [5], which results in significant weight savings. On the other hand, FLDT is more cost effective. The choice between the two layouts is dependent upon the segment of the vehicle.

2.3 Poroacoustic treatments

The poroacoustic treatments are commonly used in passenger vehicles as they are both used to control noise reverberation within the engine and passenger compartments, and to insulate the

cabin. Poroacoustic material works with noise absorption and energy dissipation that take place when they interact with a sound wave. In order to understand these phenomena it is useful to refer to Figure 0.4, which represents an ideal situation where a sound wave encounters an obstacle placed along the airborne transmission path.

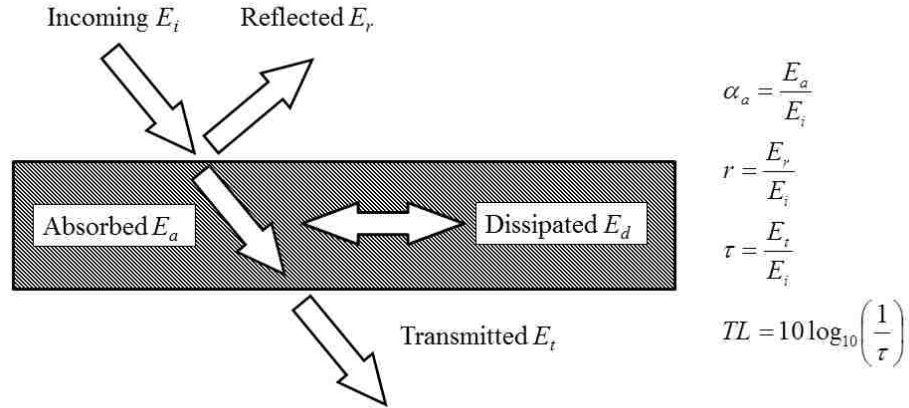


Figure 0.4: Interaction between a sound pressure wave and an obstacle placed on the airborne transmission path.

In this kind of situation the energy of the incident sound wave (E_i) is split in three parts: the reflected energy (E_r), the dissipated energy (E_a) and the transmitted energy (E_t), as indicated in equation (0.1).

$$E_i = E_d + E_r + E_t \quad (0.1)$$

The difference between the energy of the incident and the reflected sound pressure waves represents the amount of energy that is absorbed by the body. Part of this acoustic energy is transmitted through the obstacle and part is transformed into heat, which is then dissipated into the environment. This implies that increasing the percentage of energy dissipated within by the body it is possible to reduce the transmission and the reflection of the incident, sound pressure waves. Therefore, poroacoustic treatments (such as open cell foams and fibrous materials where the percentage of energy dissipated is significantly elevated) are suitable to be used as sound

absorbers and insulators. For these kinds of treatments, the losses are due mostly the viscous friction, which is related to the speed gradient between the fluid excited by the acoustic field and the skeleton. Dissipation can occur through different mechanisms, according to the frequency of the acoustic signal. High frequency signals cause adiabatic process connotation, while with low frequency signals it can be assimilated to a heat exchange process between the fluid and the solid phase [7].

2.3.1 Different categories of poroacoustic treatments and their properties

Poroacoustic treatment refers to a wide range of different materials, which are characterized by the presence of a solid skeleton filled with a fluid. The ratio between the volume of the fluid phase and the total volume of the material is called porosity, and it is one of the most important properties of these materials. In a sample of porous material, its total volume V_t can be divided between the fluid phase, which is indicated as V_f , and the solid phase, which is indicated as V_s . Porosity can then be defined as indicated in equation (0.2).

$$\Omega = \frac{V_f}{V_t} = 1 - \frac{V_s}{V_t} \quad (0.2)$$

The typical values of porosity for commercial sound absorbing materials are generally between 0.50 and 0.99. The measurement of this quantity requires the use of a Champoux porosimeter (Figure 0.5).

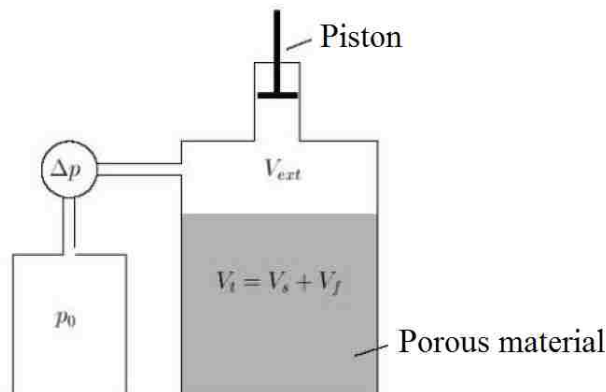


Figure 0.5: Champoux porosimeter [8].

The working principle of this instrument is based on Boyle-Mariotte law for perfect gases (0.3) and it allows measuring the volume of fluid contained inside the pores according to the equation (0.4).

$$(V_f + V_{ext})p_0 = (V_f + V_{ext} + \Delta V)(p_0 + \Delta p) \quad (0.3)$$

$$V_f = -\left(\frac{p_0 + \Delta p}{\Delta p} \Delta V + V_{ext} \right) \quad (0.4)$$

Depending on their morphology, the porous materials can be divided in two different categories: open cell and closed cell. In open cell, the fluid phase contained inside the skeleton of the porous material communicates with the external acoustic field. This allows the sound waves to flow within the porous material, dissipating the acoustic energy by means of viscous friction. In the closed cell, the flow cannot take place due the fact that the fluid phase is enclosed in small blisters inside the skeleton and thus separated from the external acoustic field. Therefore, the open cell materials are usually preferred for acoustic treatments as they provide a higher absorption and insulation as compare to closed cell. When poroacoustic materials are characterized by the presence of both open and closed cells, porosity is usually calculated taking into account only the volume of fluid contained in the open cells. The remaining volume contained in the closed cells is considered to be part of the solid skeleton [7].

Another classification of the poroacoustic materials is usually made according to the kind of microstructure of the skeleton. In particular, it is possible to distinguish between cellular materials (sometimes referred as foams) and fibrous materials, as depicted in Figure 0.6.

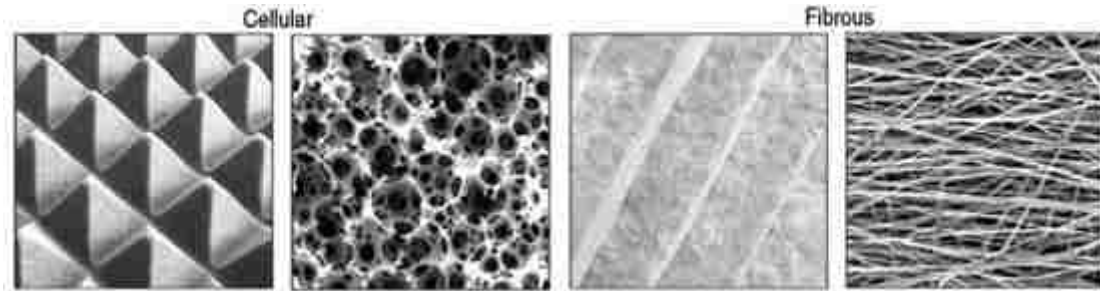


Figure 0.6: Examples of microstructures for cellular and fibrous poroacoustic materials [4].

2.3.1.1 Fibrous materials

Fibrous materials are made by fibers of different nature, which are tied together with chemical agents like resins, or with physical treatments like thermal bonding or pressing. The principal kinds of fibrous materials currently used for noise control are listed in Table 0.1, together with their most important properties.

Material	Average fibers diameter [μm]	Density [kg/m^3]
Mineral wool	4-8	40-100
Fiberglass	1-5	20-40
Polyester fibers	20-40	10-60
Felts	various	20-100
Polylactic acid fiber	20-40	10-60
Vegetal fibers	various	20-80
Animal fibers	various	20-80

Table 0.1: Average fiber diameter and density of various fibrous acoustic materials [4] .

These materials are employed in many industrial areas such as construction, household appliances etc., but only felts and polyester fibers are currently used in the automotive industry. An important parameter that characterizes fibrous materials is the average fibre diameter. This is important because there is a larger amount of surface placed in contact with the fluid when using a smaller fibre. This means that energy dissipation is more elevated in the fibrous materials with a lower average fibre diameter and, therefore, they are more effective in terms of sound absorption and insulation. The average fibre diameter is usually related to a more general parameter called airflow resistivity (AFR), which is used to quantify the viscous friction within the material. The relationship between airflow resistivity and the friction force, which opposes the flow of the fluid through the porous material, is expressed by (0.5).

$$F_R = R(\dot{u} - \dot{U}) \quad (0.5)$$

In equation (0.5) the airflow resistivity represents the coefficient of proportionality between the viscous force and the speed gradient, i.e. the difference between the velocity of the solid frame (\dot{u}) and the velocity of the fluid within the pores (\dot{U}).

The value of the air flow resistivity can be determined by placing a sample of porous material with a thickness h in a pipe with a section S and measuring the steady air flow \dot{V} generated by a pressure differential Δp as indicated in equation (0.6).

$$R = \frac{S\Delta p}{h\dot{V}} = \frac{\Delta p}{h\dot{U}} \quad (0.6)$$

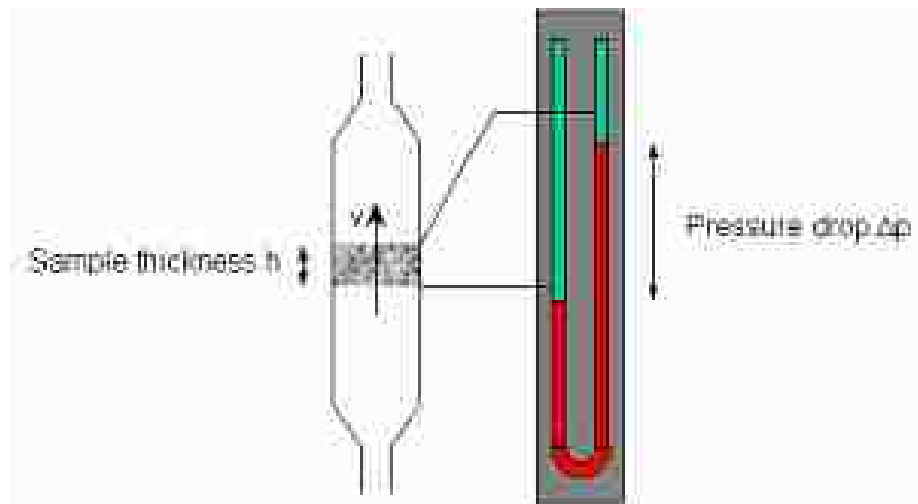


Figure 0.7: Experimental setup for the measurement of the air flow resistivity [8].

2.3.1.2 Foams

The cellular porous materials, which can be produced through a process of foaming, blow moulding, or recycled materials aggregation, are constituted by a skeleton that contains a multitude of interconnected chambers. Table 0.2 reports the principal kinds of cellular materials used for the sound absorbing treatments. Among those listed only the open cell polyurethane foam, the aggregates of expanded elastomers, and the melamine resin foam are currently employed in the automotive industry.

Material	Density [kg/m³]
Polyurethane foam	20-50
Melamine resin foam	10
Polyethylene foam	10-20
Aluminum foam	10-100
Aggregates of expanded elastomers	120-240
Other kinds of aggregates (rubber, plastic, etc.)	40-1500

Table 0.2: Density of various fibrous materials used for noise control [4]

In general, all the porous materials, either cellular or fibrous, are characterized by a series of parameters respectively related to the elastic properties of the skeleton, to the thermo-fluid dynamic properties of the fluid inside the pores, and to the interactions between structure and fluid [7]. These properties, classified as elastic, acoustic and poromechanical, are reported in Table 0.3.

Elastic	Acoustic	Poromechanical
Young's modulus E	Fluid density ρ_f	Porosity Ω
Poisson ratio ν	Fluid specific heat at constant pressure c_p	Flow resistivity R
Solid density ρ_s	Fluid specific heat at constant volume c_v	Tortuosity α_∞
	Fluid dynamic viscosity η	Viscous length A_v
	Fluid thermal conductivity λ	Thermal Length A_t
	Fluid bulk modulus Q	

Table 0.3: Principal properties of the poroelastic materials.

Among the ones listed there are three parameters that are only related to the geometry of the skeleton, they are tortuosity, characteristic viscous length, and characteristic thermal length.

The first geometrical parameter: tortuosity (or sometimes structure shape factor), is used to indicate the degree of complexity of the porous cells interconnections. Since the various communication channels among the pores define the path followed by the fluid flowing inside the

material, tortuosity gives a measure of how the trajectory of the fluid particles is deflected by the presence of a solid phase. Two alternative methodologies can be used for the measurement of this property, depending on the electrical conductivity of the frame of the porous material. When the frame does not conduct electricity the methodology used measures the electrical resistivity r_c between the two ends of a sample saturated with an electrically conductive fluid, as depicted in Figure 0.8 [7]. Inserting the value of the resistivity measured in this way and the one of the fluid itself in equation (0.7) it is then possible to calculate the tortuosity of the material.

$$\alpha_\infty = \Omega \frac{r_c}{r_f} \quad (0.7)$$

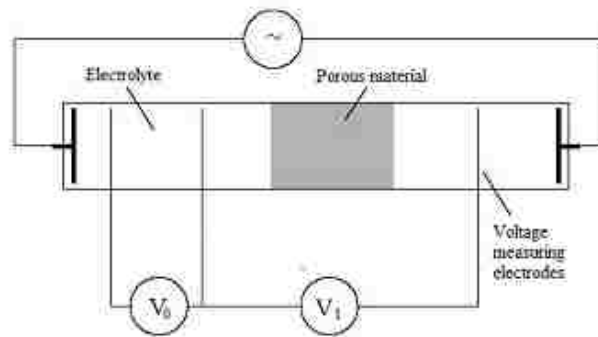


Figure 0.8: Setup used for the electrolytic measurement of tortuosity [8].

Otherwise, if the skeleton of the porous material possesses high electrical conductivity, tortuosity can only be measured with an ultrasound technique. This method is based on the comparison of the travel time of an ultrasound from a source and receiver with and without the interposition of a porous material sample (Figure 0.9).

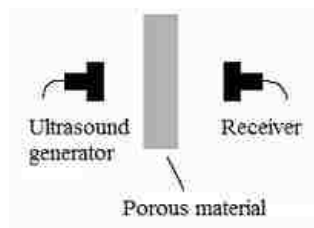


Figure 0.9: Setup used for the ultrasound measurement of tortuosity [8].

The second geometrical parameter is the characteristic viscous length Λ_v , which is usually defined according to the original formulation introduced by Johnson et al. [9] (0.8).

$$\Lambda_v = 2 \frac{\int_V \dot{U}_i^2(r_w) dV}{\int_S \dot{U}_i^2(r_i) dA} \quad (0.8)$$

Making reference to equation (0.8) it can be observed that the viscous characteristic length represents the ratio between the surface of the pore and its volume, weighted by the squared microscopic velocity of the fluid on the surface of the pore and on its inside.

The third geometrical parameter is the characteristic thermal length, which is related to the frequency dependent compressibility of the fluid inside the pores caused by the thermal energy exchange between the fluid and the frame. The characteristic thermal length was introduced for the first time by Champoux-Allard [10], who defined it as indicated in (0.9).

$$\Lambda_t = 2 \frac{\int_V dV}{\int_S dA} \quad (0.9)$$

According to equation (0.9) the characteristic thermal length is proportional to the ratio between the volume of the pore and its surface. Considering the two characteristic lengths in purely geometrical terms it can be stated that the characteristic thermal length provides an estimate of the mean pore size, whereas the characteristic viscous length provides an estimate of the section of the channels among the pores, as depicted in Figure 0.10.

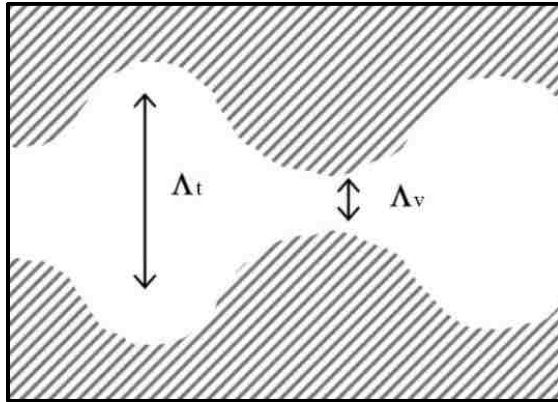


Figure 0.10: Graphical representation of the thermal and viscous characteristic lengths

These porous materials usually have a skeleton with a very complex shape and these two geometrical quantities take on different values depending on the region where they are measured. For this reason, their value is normally defined in terms of statistical average over a certain volume of material.

2.3.2 *Vibroacoustic behaviour of porous materials*

The majority of the vibroacoustic problems of the vehicle concern a vibrating structure attached to an acoustic cavity. In most cases, this scenario can be approached using the standard equations of the theory of elasticity and the laws of acoustics, which describe the propagation of the sound in a homogeneous fluid medium. However, when the problem requires taking into account the presence of a porous material, these formulations are no longer sufficient to find a solution. It is therefore necessary to introduce some additional equations that can represent the vibroacoustic behaviour of the poroacoustic material and the way they interact with the other components. There are many different models to describe how the sound waves interact with porous medium. Before talking about those models it must be introduced the equation which describes the propagation of a linear acoustic wave inside a single-phase medium (0.10).

$$p(x,t) = A_p \exp[j\omega(t - kx)] \quad (0.10)$$

In this equation A_p indicates the amplitude of the pressure wave, k the wave number (which constitutes its spatial frequency), and x the dimensional coordinate [11]. The same equation can be rewritten in terms of particle velocity as indicated in (0.11).

The term Z_c , which appears in equation (0.11), is called acoustic impedance, and it indicates the quantity of sound pressure, which is produced by the vibration of the molecules within the acoustic medium.

$$v(x,t) = \frac{k}{\rho\omega} A_p \exp\left[j\omega\left(t - \frac{x}{c}\right)\right] = \frac{1}{Z_c} p(x,t) \quad (0.11)$$

For a single-phase material, the acoustic impedance is defined as:

$$Z_c(f) = (\rho Q)^{\frac{1}{2}} \quad (0.12)$$

In a similar way the wave number k , which represents the number of radians covered by the sound pressure wave per unit of distance, can be expressed as in equation (0.13).

$$k(f) = \omega \left(\frac{\rho}{Q} \right)^{\frac{1}{2}} \quad (0.13)$$

The acoustic impedance and the wave number completely characterize the way sound propagates within them. For this reason, knowing their value is necessary in order to describe the phenomena related to the sound transmission. For instance, their different impedances can motivate sound reflection at the interface between two materials. In particular, the value of the sound reflection coefficient r , i.e. the ratio between the amplitudes of reflected and incident sound pressure waves (0.14), is related to the impedance of the two different materials at the interface Z_c and Z_c' , as expressed in (0.15) [11].

$$r(f) = \frac{P_r}{P_i} \quad (0.14)$$

$$r(f) = \frac{Z_c - Z_c'}{Z_c + Z_c'} \quad (0.15)$$

Considering that the energy of an incident sound wave is split between the absorbed and the reflected energy, the sound absorption coefficient α_a can be easily derived from r , as indicated in (0.17) [11]. Since both the sound absorption and reflection coefficients are proportional to the value of the impedances, they only depend on the materials at the interface.

All these quantities also depend on the frequency of the sound wave and on the angle formed by the direction of its propagation and the surface of the obstacle. In general, when no further indication is provided, these quantities usually refer to the case when the wave is normal to the surface.

$$\alpha_a(f) = \frac{E_a}{E_i} = 1 - \frac{E_r}{E_i} \quad (0.16)$$

$$\alpha_a(f) = 1 - \sqrt{r^2} \quad (0.17)$$

Since the equations (0.12) and (0.13) only apply to the specific case of a single-phase transmission medium, they cannot be used for the porous materials and it is therefore necessary to refer to some other specific mathematical model.

The first models to describe the propagation of sound within porous media were based on empirical laws, and their application was limited to specific groups of materials. Delaney and Bazley proposed a model in 1970 [12] which has become one of the most significant. This allows calculating the propagation constant and the characteristic impedance of a certain kind of fibrous materials, based on the value of their airflow resistivity. Delaney-Bazley's theory is expressed by equations (0.18) and (0.19) and its validity is restricted into a narrow frequency range and limited by the assumption of perfectly rigid skeleton.

$$Z_c = \rho_0 c \left[1 + 0.0571 \left(\frac{\rho_0 f}{\sigma} \right)^{-0.754} - j 0.087 \left(\frac{\rho_0 f}{\sigma} \right)^{-0.732} \right] \quad (0.18)$$

$$k = \frac{\omega}{c} \left[1 + 0.0978 \left(\frac{\rho_0 f}{\sigma} \right)^{-0.7} - j 0.189 \left(\frac{\rho_0 f}{\sigma} \right)^{-0.595} \right] \quad (0.19)$$

Mechel and Vér then improved upon the original formulation in 1976 [13] and Miki in 1990 [14], introducing specific correction parameters that extend its applicability to a wider range of materials.

More recently, another approach has been adopted to describe the propagation of sound in porous media, which individually analyzes the phenomena of viscous friction, inertia, and heat exchange

occurring within the material. The models developed with this approach are referred as phenomenological. Johnson Champoux and Allard [15] proposed the most significant phenomenological model in 1992. The model is formulated as in equation (0.20) and (0.21), and it has been demonstrated to be more reliable with respect to the empirical models, in particular at the lower frequencies.

$$\tilde{\rho}(\omega) = \rho_0 \left[1 - j \left(\frac{\sigma}{\rho_0 \omega} \right) \sqrt{1 + \frac{j}{2} \left(\frac{\rho_0 \omega}{\sigma} \right) \left(\frac{\rho_0 \omega}{\sigma} \right)} \right] \quad (0.20)$$

$$\tilde{Q}(\omega) = \gamma p_0 \left[\gamma - \frac{\gamma - 1}{1 - \left(\frac{j}{4P_r} \right) \left(\frac{\sigma}{\rho_0 \omega} \right) \sqrt{1 + \frac{j}{2} \left(\frac{\rho_0 \omega}{\sigma} \right) \left(\frac{\rho_0 \omega}{\sigma} \right)^2} (4P_r) \left(\frac{\rho_0 \omega}{\sigma} \right)} \right] \quad (0.21)$$

The validity of the Johnson-Champoux- Allard's equations is limited by the assumption of rigid frame, similar to the theory proposed by Delany-Bazley. Furthermore, it can be observed that four additional parameters need to be provided as input with respect to the empirical models. These parameters are porosity, tortuosity, characteristic viscous length, and characteristic thermal length. The Johnson-Champoux-Allard model is also referred as equivalent-fluid model, because it defines two equivalent values for ρ and Q which allow considering porous material like a single phase medium.

Despite the substantial simplifications involved, the Delany-Bazley and Johnson-Champoux-Allard theories are generally quite reliable for assessing the acoustic performances of the porous treatments. However, when in the vibroacoustic problem, it is necessary to take into account the elastic deformations of the skeleton of the porous material, these two models cannot be employed, as they are based on the assumption of rigid frame.

In this case, it is necessary to refer to the other formulations based on the Biot's theory of poroelasticity. Maurice Anthony Biot proposed this theory in 1941 [16] and it describes the behaviour of the porous materials with an elastic skeleton. In particular, Biot's theory provides

the dynamic equations of the solid and the fluid phase, which also include the coupling terms between the two [4].

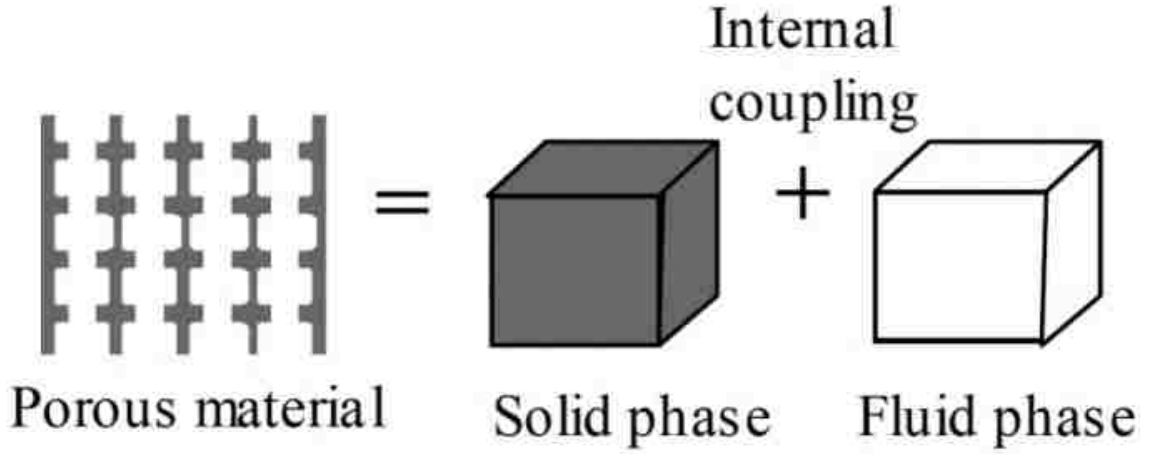


Figure 0.11: Schematic representation of the Biot's theory of poroelasticity [17].

Several variations to the original formulation of the Biot's theory have been proposed over the years by other authors. For instance, the equations reported in (0.22) and (0.23) belong to the $u-U$ formulation, which was described by Jean-Francois Allard [18] in 1993.

$$\nabla \sigma^S = \rho_{11} \ddot{u} + \rho_{12} \ddot{U} + b(\dot{u} - \dot{U}) \quad (0.22)$$

$$\nabla \sigma^F = \rho_{12} \ddot{u} + \rho_{22} \ddot{U} + b(\dot{u} - \dot{U}) \quad (0.23)$$

In equation (0.22) and (0.23) the two variables u and U represent the macroscopic displacement vectors (i.e. the average displacement per unitary cross section) respectively of the solid and the fluid phase while σ^S and σ^F indicate their stress tensors. The equivalent densities ρ_{11} and ρ_{22} are mass coefficients, while ρ_{12} refers to the interactions between the inertia forces of the solid and the fluid phase. In this formulation, the term b is related to the viscous interactions between the fluid and the skeleton. These equations can be employed both in the analysis of vibrating structures and in the study of the propagation of sound within porous media; in particular they can be used for Finite Element Analysis.

The main issue related the use of the Biot's theory in the numerical analysis is the elevated computational power required. The cause of this problem comes about because Biot's equations are characterized by a high number of degrees of freedom, which generate large frequency-dependent matrixes. For this reason, an alternative formulation was proposed by Atalla in 1998 [19,20], which allows the removal of two of the six degrees of freedom. These two degrees of freedom relate to the displacements of the fluid and the solid phase. Atalla's mixed displacement pressure (u - p) formulation the displacement vector U is expressed as a function of the pressure of the fluid contained inside the pores and the displacement of the solid phase, as indicated in equation (0.24).

$$U = \frac{\Omega}{\tilde{\rho}_{22}\omega^2} \nabla p - \frac{\tilde{\rho}_{12}}{\tilde{\rho}_{22}} u \quad (0.24)$$

In (0.24) the effective densities $\tilde{\rho}_{11}$, $\tilde{\rho}_{22}$ and $\tilde{\rho}_{12}$, which values are expressed as in (0.25), are introduced in the equation [4].

$$\tilde{\rho}_{11} = \rho_{11} + \frac{b}{j\omega}, \quad \tilde{\rho}_{22} = \rho_{22} + \frac{b}{j\omega}, \quad \tilde{\rho}_{12} = \rho_{12} + \frac{b}{j\omega} \quad (0.25)$$

Using the pressure of the fluid in place of its macroscopic displacement vector Biot's equations can be rewritten in the mixed displacement-pressure form as follows:

$$\nabla \hat{\sigma}(u) + \omega^2 \tilde{\rho} u + \tilde{\varphi} \nabla p = 0 \quad (0.26)$$

$$\Delta p + \omega^2 \frac{\tilde{\rho}_{22}}{\tilde{R}} p - \omega^2 \frac{\tilde{\rho}_{22}}{\Omega^2} \tilde{\gamma} \nabla u = 0 \quad (0.27)$$

The first two terms of the solid phase in equation (0.26) refers to the dynamic behaviour of the skeleton in vacuum, while the first two terms of the fluid phase in equation (0.27) refers to the dynamic behaviour of the fluid when the structure is considered to be rigid. The last terms of both the equations represent the coupling interactions between the two phases.

In this formulation, the stress tensor is indicated with $\hat{\sigma}$ and, according to the theory of linear elasticity, it is a function of Young's modulus, Poisson ratio and loss factor of the skeleton. The

coefficients $\tilde{\rho}$ and $\tilde{\gamma}$, are related to the values of dynamic density and bulk modulus [17,4], which can be determined using Johnson-Champoux-Allard's theory. This means that Atalla's approach requires all the elastic, fluid and poromechanical properties listed in Table 0.3 to be provided as an input in order to solve the problem.

2.4 Finite element vibroacoustic analysis of panels treated with poroacoustic materials

Finite Element Analysis (FEA) is a widely diffused numerical technique, which can be used to address both static and dynamic boundary problems. In this method a continuous domain is divided into a finite number of elements and certain approximation functions are used to calculate an unknown quantity (e.g. displacement, pressure etc.) through the interpolation of the nodal values. Then, combining the results obtained for each element, it is possible to calculate an approximate value of the unknown quantity over the entire continuous domain. Referring to the vibroacoustic problems described in 2.3.2 it is possible to identify three distinct domains: poroelastic, elastic, and acoustic. Each of these domains is limited by the surfaces that define the coupling conditions between them, as well as the surfaces that determine their boundary conditions [21]. The elastic domain is the one of the structural components (e.g. the car body panels) and is governed by the equations of standard linear elasticity, while the acoustic cavities (e.g. the passenger cabin) belong to the acoustic domain, which is governed by the equations of standard linear acoustics. As for the porous domain, which includes all the sound absorbing and insulating treatments, Biot theory provides a set of partial differential equations and boundary conditions which govern the homogenized porous material [16]. The discretization process of the FEA, however, is not directly conducted using the partial differential equations but rather their integral variational formulation.

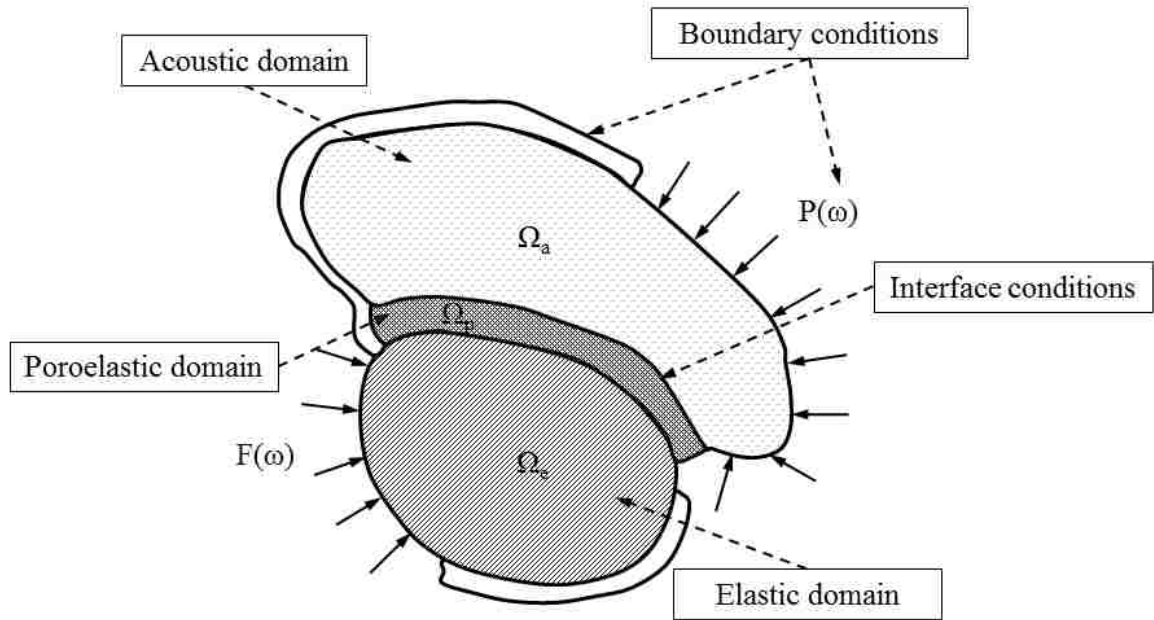


Figure 0.12: Representation of a system composed by elastic, acoustic and porous domains [22].

2.4.1 Modal analysis

As already mentioned in 2.2, the vibroacoustic comfort of a vehicle depends on two factors: the excitations to which the vehicle is subject, and the way it responds to these excitations. The branch of vibroacoustic dealing with the analysis of the response is known as modal analysis. For a generic structure, characterized by multiple DOF, the response can be directly calculated using equation (0.28) [2].

$$[M]\{\ddot{q}\} + [C]\{\dot{q}\} + [K]\{q\} = \{F\} \quad (0.28)$$

The problem can also be addressed in a different way considering the undamped system constituted by (0.29) and the associated homogeneous equation expressed by (0.30).

$$[M]\{\ddot{q}\} + [K]\{q\} = \{F\} \quad (0.29)$$

$$[M]\{\ddot{q}\} + [K]\{q\} = 0 \quad (0.30)$$

Assuming the solution to equation (0.30) to be harmonic and therefore substituting (0.31) in (0.30) the equation of the undamped system can be rewritten as in (0.32).

$$\{q\} = \{\Phi\}e^{st} \quad (0.31)$$

$$\{[M]s^2 + [K]\}\{\Phi\} = 0 \quad (0.32)$$

The form of (0.32) is the one of an eigen equation, which means that it constitutes an eigenvalues/eigenvectors problem, that can be expressed as in (0.33) (0.34) (0.35).

$$\{[M]^{-1}[K] - \lambda[I]\}\{\Phi\} = 0 \quad (0.33)$$

$$\det([M]^{-1}[K] - \lambda[I]) = 0 \quad (0.34)$$

$$s = \pm j\omega = \pm j\sqrt{\lambda} \quad (0.35)$$

Apart from the trivial solution $\{\Phi\} = 0$, which represents the case of a motionless structure and therefore does not provide any useful information from the point of view of the modal analysis, the other solutions to this problem are represented by the n eigenvalues λ_i . Then, inserting the eigenvalues in equation (0.33), it is possible to calculate the eigenvectors Φ_i . From a physical standpoint the eigenvalues and the eigenvectors represent respectively the natural frequencies of the system and the associated mode shapes. An important property of the eigenvectors/mode shapes is their orthogonality, which in the case of symmetric and real mass and stiffness matrices leads to the following relations:

$$\{\Phi\}[M]\{\Phi\}^T = [m] \quad (0.36)$$

$$\{\Phi\}[K]\{\Phi\}^T = [k] \quad (0.37)$$

The fact that $[k]$ and $[m]$ are two diagonal matrices implies that in this form the equations of motion of the undamped system are uncoupled. For this reason, it is possible to represent the displacement vector as a linear combination of mode shapes, as reported in (0.39).

$$\{q\} = \{\Phi_1\}\xi_1 + \{\Phi_2\}\xi_2 + \dots + \{\Phi_n\}\xi_n \quad (0.38)$$

$$\{q\} = [\Phi]\{\xi\}^T \quad (0.39)$$

In equation (0.38) the elements indicated with ξ_i are called modal participation factors and they represent the contribution of each mode shape to the displacement vector.

$$[m]\{\ddot{\xi}\}^T + [K]\{\xi\}^T = [t_{in}]\{F\} \quad (0.40)$$

By inserting (0.39) into (0.30) and multiplying each term by $[\Phi]^T$ it is possible to write the dynamic equation into modal coordinates, as indicated in (0.40). In this equation $[t_{in}]$ is the force modal participation factor and it indicates the extent to which the external forces are able to excite each mode. Furthermore, in the equation of a lightly damped system the viscous effect can be taken into account by means of the diagonal matrix $[\zeta]$. The influence of the elements of this modal damping matrix becomes relevant on the response only in correspondence of the resonance peaks. Finally, taking into account the way the natural frequencies are related to the values of stiffness and mass (0.41) and including the modal damping in (0.40), it is possible to rewrite the dynamic equation of the system as indicated in (0.42).

$$\omega_{0i} = \sqrt{\frac{k_i}{m_i}} \quad (0.41)$$

$$\{\ddot{\xi}\}^T + 2[\zeta][\omega_0]\{\dot{\xi}\}^T + [\omega_0]^2\{\xi\}^T = [t_{in}]\{F\} \quad (0.42)$$

2.4.1.1 Frequency Response Functions (FRF)

In modal analysis, the principal methodology to isolate the inherent dynamic properties of a mechanical structure consists of determining its Frequency Response Functions (FRF). A FRF describes the input-output relationship between two points on a structure as a function of the frequency [23]. Since most of the time both the excitation and the response are defined by means of a vector quantity the FRF need to be referred to a single-input DOF and a single-output DOF (i.e. they must be calculated only in a certain point and in a unique direction). From a mathematical point of view, the FRF consist in frequency dependent quantity defined by ratio $H(\omega)$ between the complex spectrum of the response $X(\omega)$ and the complex spectrum of the excitation $F(\omega)$ [24], as indicated in (0.43) .

$$H(\omega) = \frac{X(\omega)}{F(\omega)} \quad (0.43)$$

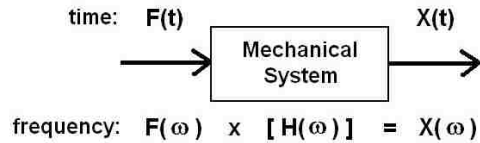


Figure 0.13: Schematic representation of the FRF [24].

In the particular case of a system excited with a sinusoidal signal, the response is always constituted by another sinusoidal signal that has the same frequency as the input and a variable amplitude and phase. In the modal analysis the output signal is constituted by a displacement, velocity or acceleration measured on a particular point of a component and along a certain

direction. Depending on the kind of output, the FRF can be indicated with different names, as reported in Table 0.4.

FRF name	Response	Nomenclature
Receptance	Displacement	$\alpha(\omega) = \frac{X(\omega)}{F(\omega)}$
Mobility	Velocity	$\frac{Y(\omega)}{F(\omega)} = i\omega\alpha(\omega)$
Accelerance	Acceleration	$\frac{A(\omega)}{F(\omega)} = -\omega^2\alpha(\omega)$

Table 0.4: Nomenclature of the principal FRF used in modal analysis.

By plotting the FRF on a Bode or a Nyquist diagram, it is possible to show a graphical representation of the variations of the response over a certain frequency range. The example of magnitude Bode plot in Figure 0.14, for instance, shows how the principal modes of the system can be identified with the peaks of the FRF curves. The overall response is constituted by the sum of the single modes and the contribution of each one characterizes the frequency range around its resonance peak.

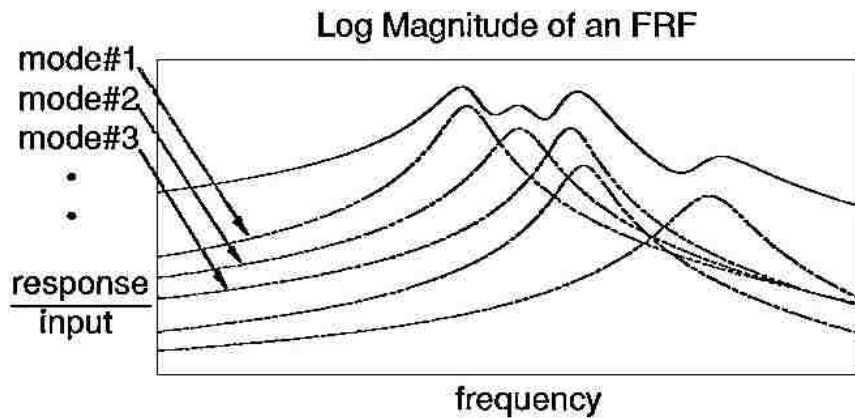


Figure 0.14: Example of a magnitude Bode plot of an FRF, highlighting the contribution of each mode shape to the overall response function [24].

2.4.2 Finite element vibroacoustic analysis of systems composed by structural components and poroacoustic materials

The finite element analysis of structures treated with poroacoustic materials can be used to address a wide range of vibroacoustic problems, such as the evaluation of the STL of a multilayered panel or the frequency response analysis of a soundproofed component. The following sections provide some examples of how it has been used for the study of these kinds of problems.

Kang and Bolton presented one of the first applications of the finite element method for the vibroacoustic analysis of the porous treatments in 1995 [25], consisting in a two-dimensional elastic-absorption model for the isotropic poroelastic materials. In particular, this work focused on the representation of the coupling conditions between the elements of the poroelastic and acoustic domains in the case the interface between them is pervious or sealed by a membrane. The accuracy of the model was verified by comparing its results with the analytical solutions. In the particular case of the propagation of a sound wave in a foam-filled waveguide, the comparison showed a good consistency between the results. The choice of using a bi-dimensional approach allowed reducing the computational effort with respect to a case of 3D porous elements, but it introduced some limitation in the thickness of the analyzed treatments,

A three-dimensional approach was used by Panneton in 1996 [26] to evaluate the sound transmission performance of a multilayered systems composed by a poroelastic material attached to a plate. Specifically, the objective of Panetton's work was to compare two different techniques for calculation of the STL between the sides of such a panel. The comparison was conducted using a Biot based three-dimensional FE model, which took into account the elastic properties of the skeleton of the porous, and an equivalent fluid model, where the solid frame was considered to be rigid. Comparing the numerical results with the ones of the experimental tests, Biot's model has been proven to provide more accurate results especially at low frequency.

Starting from the above-mentioned Panneton approach, in 2003, Duchez [27] studied the dynamic behaviour of a system composed by a porous layer bonded to a plate in the 0-250 Hz frequency range. In this research, numerical analysis was carried out to investigate the relative contribution of the different dissipations, which occur within a porous material. The study was conducted on a double-layered system made with a sound absorbing treatment attached to a mechanically excited plate made of aluminum. For this analysis, under the assumption of heavy structure immersed in a light fluid, the presence of the acoustic cavities was neglected. The simulations were run using poroacoustic treatments made of different materials and having a different thickness. The outcomes of the numerical analysis showed that only the contribution of the structural and viscous dissipations is significant, while the role thermal dissipation mechanism is marginal. The author explained these results with the fact that unlike the acoustic excitations the mechanical ones do not create a straight compression of the fluid inside the pores and to the fact that the free boundary condition of the porous layer does not constrain the fluid within a given volume. Furthermore the effect of the viscoelastic dissipation, related to the skeleton loss factor, was found to be widely dominating for stiff poroelastic materials, while the viscous dissipations, related to the AFR, were demonstrated to be significant only for soft materials and only in for low frequencies. Finally, based on the outcomes of the analysis, Dauchez elaborated on an equivalent plate model, which considers the contribution of the porous layer only in terms of shear stress at the bonding interface and viscoelastic damping losses within the frame. This simplification leads to significant savings in terms of computational costs, but it also limits the applicability of the model to the problems that present a light coupling between the plate and the acoustic domain.

2.4.2.1 Automotive applications

In 2005, DaimlerChrysler-Mitsubishi joint research [28] investigated the potential of using Biot-based finite elements to model carpet-like components. Some experimental tests were conducted using a simplified setup consisting in a two layered mass-spring trim placed on a flat steel plate,

which was clamped in a stiff frame and excited at its base. The vibration of the steel plate and the trim heavy layer surface were measured respectively by means of an accelerometer and a laser-Doppler vibrometer. Furthermore, a microphone placed close to the vibrating system, was used to study the way noise is radiated both in the open field and within closed rectangular cavity. The experimental outcomes were compared to the ones of the numerical simulations showing a good agreement both qualitatively and quantitatively up to 1 kHz. This result demonstrated the reliability of the Biot-based FE model as a tool for studying the vibroacoustic behavior of multilayered system like the car body panels treated with poroacoustic materials.

In 2006, Peter Göransson [29] conducted a purely numerical vibroacoustic analysis on a firewall-like sandwich system composed of polymeric foam enclosed within steel plate and a viscoelastic layer. In this work, the finite element method was used to evaluate the response of the system to an acoustic excitation, measuring the RMS of the displacement for the top viscoelastic surface and the STL between the two sides of the panel. In the simulations, two different configurations of the poroacoustic treatments were investigated. The first one consisted of a single layer of porous material, while the second one consisted of a two layers system formed by different foams bonded together. The results showed that the two layered configuration has better performance in terms of STL as well as a marked decoupling effect between the vibration of the base structure and the viscoelastic layer.

In 2010 Göransson et al. [30] conducted more extensive research that consisted of the measurement of the STL and the modal analysis of a car roof-headliner system, conducted by means of experimental tests and numerical simulations. As for the acoustic analysis, the Sound Reduction Index (SRI) was measured with a full vehicle experimental test and with a component transmission test. In the first test, the vehicle was parked in the middle of an anechoic room and a 100W sound source placed inside the passenger compartment was used to generate a white noise in the frequency range between 250 Hz and 10 kHz. First, the sound pressure within the vehicle was measured using three randomly placed microphones, and then the STL between the two sides

of the roof was evaluated by scanning the outer surface by means of a two-microphone sound intensity probe. For the component test, the excitation and the response side were inverted. The first step of this test consisted of removing the roof from the car, sealing the windows, attaching it to a steel frame and placing it in between a reverberant and an anechoic room. In this set up the outer face of the roof was facing the reverberant room, while the headliner was facing the anechoic room. In the external side, a noise generator was used to produce a white signal in the range of frequencies between 100 Hz and 5 kHz, while in the inner side a set of microphones mounted on a rotating boom were used to measure the average SPL. As for the vibration of the roof, an experimental modal analysis was conducted to evaluate the system response to a dynamic load. The experimental setup employed for the analysis included an inertia shaker attached at the midpoint of the A-Pillar on the driver side, which was used to excite the structure, and a force transducer in the same point, used for measuring the load transmitted by the shaker. A laser vibrometer was employed for the evaluation of the vibration level, which was calculated over the average velocity of 180 points for the outer roof and 21 points for the headliner.

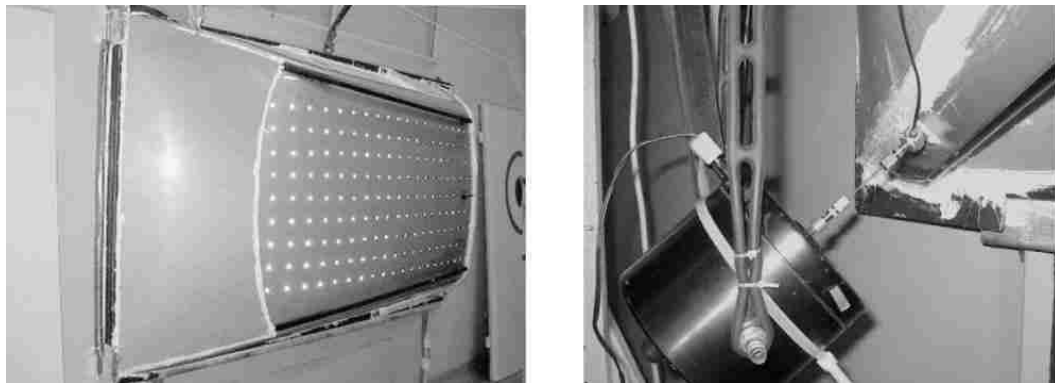


Figure 0.15: Experimental setup used for measuring the transmission loss and the frequency response of the roof panel to a mechanical excitation in the Göransson research work [30].

The numerical analysis was carried out in a similar way as the experimental tests. A series of simulations were conducted to calculate the STL of the roof and the response of the system to the mechanical excitations. Both for the modal analysis and for the computation of the STL the headliner was modeled using three-dimensional Biot elements. For the modal analysis, a full roof

model was employed, while for the STL a simplified representation of the system made with equivalent size rectangular boxes was used. In both cases, the results of the simulations demonstrated a good compliance with the experiments in the entire frequency range.

Kobayashi, Yamakoa et al. did an analogous work in 2008 [31,17], by developing and employing a FE model for the analysis of a multilayered system composed of an aluminum panel, a porous treatment, and top layer with different absorption characteristics (Figure 0.16). The model was validated by comparing the experimental response of the system to a mechanical excitation, evaluated in terms of panel and top layer acceleration, with the results of the numerical simulations conducted with the direct frequency response analysis. This comparison showed a good correlation up to 400 Hz.

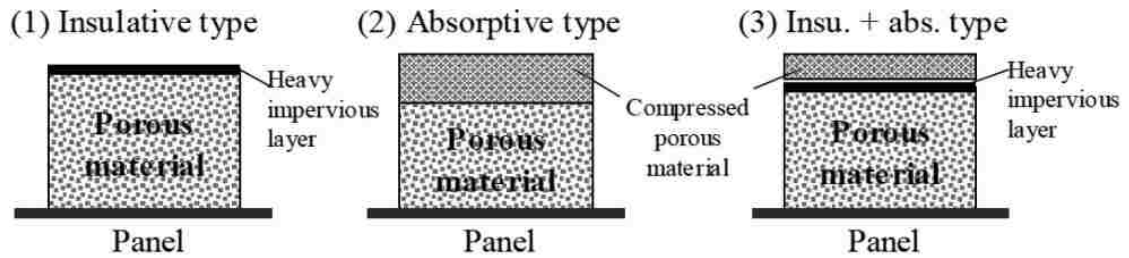


Figure 0.16: Different kinds of porous treatments tested in Kobayashi et al. research [17].

The model was then employed to compare the noise radiated from a panel treated with the three different configurations of poroacoustic materials depicted in Figure 0.16. The comparison was conducted by analyzing the differences among the values of the SPL calculated inside an acoustic cavity coupled with the porous treatment. The outcomes of the analysis showed that the systems with an insulative and hybrid treatment configuration present an additional SPL peak with respect to the base structure, which is due to the mass-spring resonance. Furthermore, in the frequency range above the resonance of the mass-spring system, the noise radiation showed a significant decrease. On the contrary, the purely absorptive treatment did not show the any resonance phenomenon and it presented a higher level of noise radiation.

The numerical procedure developed by Kobayashi, Yamakoa et al. was also used in later research [31,17] for the evaluation of the sound power radiated from the car body panels treated with porous materials. In this case, due to the higher complexity of the problem, the numerical procedure showed an elevated computational cost. For this reason, some simplifications were introduced. The first one was the adoption of the modal approach for the solution of the FE model instead of the original direct approach, and the second one calculated the impedance matrices only for certain sampled frequencies rather than for the entire range. The introduction of these measures allowed a drastic reduction of the computational time, without affecting the reliability of the numerical results, which was confirmed by the experimental validation.

Using the same numerical procedure Duval et al. [32] analyzed the vibroacoustic behaviour of two automotive components: a dashboard and a vehicle floor. The first step of the research analysed the bare dashboard. For this analysis, a shaker was used to excite the structure in a point close to the engine mounts, and the response was measured by means of a laser vibrometer. The results of this test were then used both to determine the modal damping of the dashboard and to assess the validity of the following numerical simulations. The next step of the research analysed the noise radiated from the bare dashboard. For this purpose, an acoustic cavity made with a concrete box was coupled to the component and a microphone was placed inside it to measure the SPL. The same two tests were repeated once again on the dashboard covered with the poroacoustic treatment. Two different kinds of treatments were used for the tests. The first one was of the absorptive type, i.e. formed by a bottom layer made of soft spring felt and a top layer made of compressed felt, while the second one was of the insulative type, with an impervious layer on the top instead of the compressed felt.

The last step of the study conducted by Duval et al. was the comparison of the experimental results with the outcomes of the numerical simulations. Before running the numerical simulations, it was necessary to calculate the material properties of the porous treatments. Since in the thermoformed treatments the Biot parameters presented some significant variations depending on

the thickness, the material properties were measured on over 40 samples, so as to get their value every 5 mm. These quantities were then inserted in the numerical model so that it could be used to calculate the mobility FRF of the dashboard as well as the sound pressure response.

As reported in the comparison between the numerical and the experimental results showed a good correlation up to 600 Hz, both for the velocity of the panel and the pressure in the acoustic cavity. Furthermore the response of the structure treated with the poroacoustic materials (Figure 0.17) presented smoother resonance peaks and a significant reduction of the SPL with respect to the response of the bare structure (Figure 0.18), demonstrating that the presence of the treatments has a significant damping effect on the vibration of the panel, which also reduced the noise radiated.

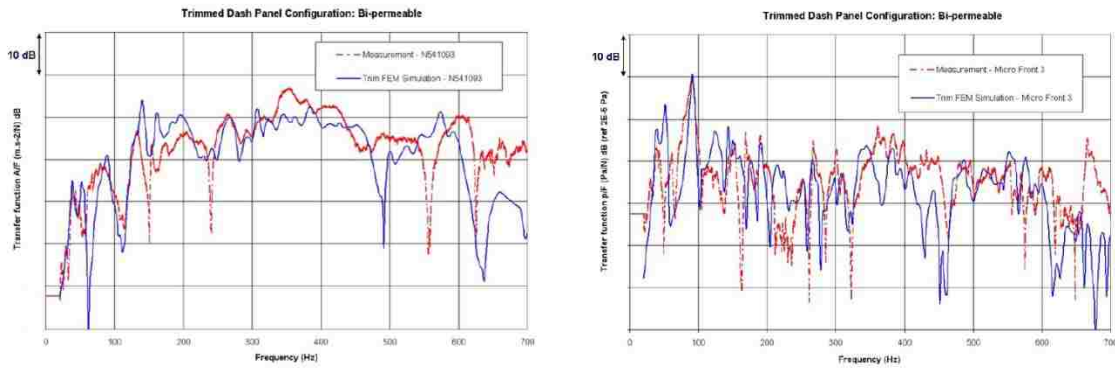


Figure 0.17: Comparison between the response calculated with the numerical model and the one measured experimentally on the dashboard treated with poroacoustic materials in the research conducted by Duval et al. [32].

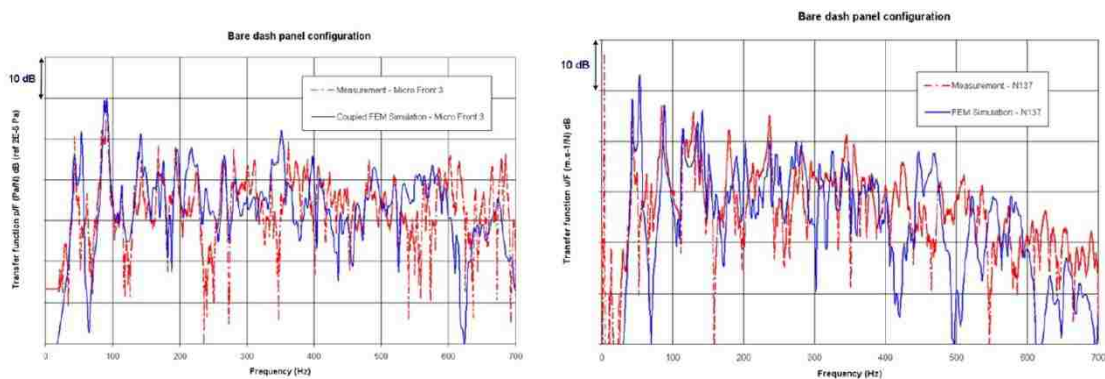


Figure 0.18: Comparison between the response calculated with the numerical model and the one measured experimentally on the bare dashboard in the research conducted by Duval et al. [32].

The same experimental tests and numerical simulations conducted on the dashboard were also repeated on a vehicle floor. In this latter case, the numerical results showed good consistency up to 700 Hz and they highlighted a more pronounced damping effect with respect to the dashboard, because of the more extended contact area between the treatment and the underlying structure.

Rieter Automotive has carried out a deeper analysis of the vibration damping effect of the poroacoustic treatments on the car body panels in 2011 [22]. In this research work, a new FE-based procedure was developed to improve the design of the damping package by taking into account the presence of the poroacoustic treatments. The first part of the study described a procedure to optimize the layout of the damping package applied a layer of viscous material the areas of the panel which showed the highest contribution to its average mobility. In the second step of the research, starting from the Biot's theory, a methodology was introduced for coupling a standard FE model with the boundary representation of the poroacoustic treatments. This model was then validated by means of experimental tests, which were conducted on a flat steel plate excited with an electro-dynamic shaker within the range of frequencies from 0 up to 500 Hz.

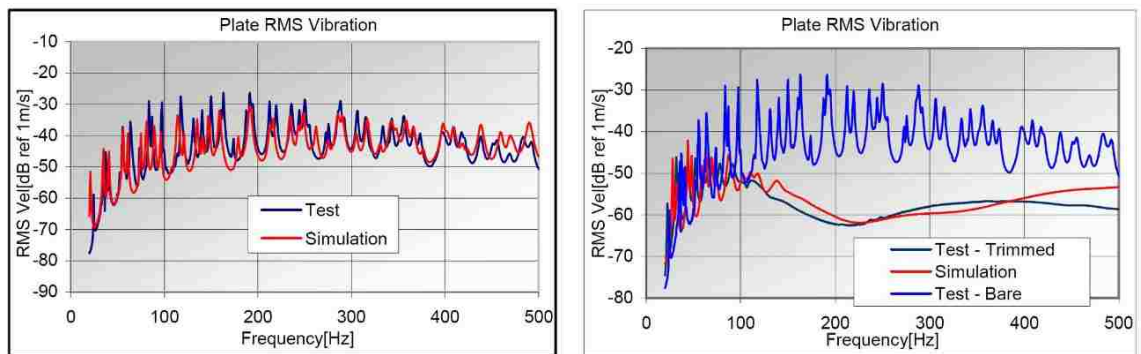


Figure 0.19: RMS mobility of the bare and the treated plate, evaluated by means of numerical simulations and experimental tests the research conducted by Rieter Automotive [22].

The tests were conducted both on the bare panel and on the panel covered with a multilayered treatment composed by a viscous foam material and a surface heavy layer. Using the numerical simulations the average RMS mobility was calculated over the surface of the plate and then

compared to the same quantity measured on the actual component by means of a laser vibrometer (Figure 0.19). The calculation of the RMS was conducted by averaging the mobility measured on 180 points located on the surface of the panel.

In the case of the bare steel plate, the results showed a high consistency between the numerical model and the experimental tests, except at the very low frequencies, where the effect of the frame was suspected to influence the dynamic behaviour of the panel. Some discrepancies were detected for the treated plate, between the numerically evaluated curve and the experimentally measured one, but in general the response was represented quite well both qualitatively and quantitatively. Once the validity of the numerical model was assessed, its use was extended to analysis the vibroacoustic behaviour of a plate covered with both the viscous patches and the spring-mass acoustic treatment. The combined effect of the materials was studied through the comparison of four different configurations:

1. Untreated-bare, with no porous treatment and no damping pad
2. Damped-Untreated”, with the damping pads located on the parts of the plate with highest mobility contribution and without any porous treatment
3. Treated-bare, with the porous treatments covering the whole surface of the plate and without any damping pad
4. Damped- treated, with both the poroacoustic treatments and the damping pads attached to the panel.

In the setup with no sound absorbing treatment the differences between curves of the damped and undamped plate were quite significant: up to 7dB in the frequency range above 200 Hz and around 10 dB at 500Hz. On the contrary, making reference to the results obtained with the porous treatment applied to the plate, the two curves were very close to each other, especially after 100 Hz. In particular, the difference between them at 500 Hz was reduced to 5 dB.

In the last step of the research, the numerical model was employed for the analysis of the acoustic treatments applied to floor. The study consisted of a comparison between the response of the bare

floor and the response of the floor covered with two different multilayered treatments. The first treatment consisted in a layer of foam covered by a heavier material, while the second one consisted in a simple felt constituted the first treatment. Each setup also included 3 Kg of bitumen damping pads applied to the structure in different layouts.

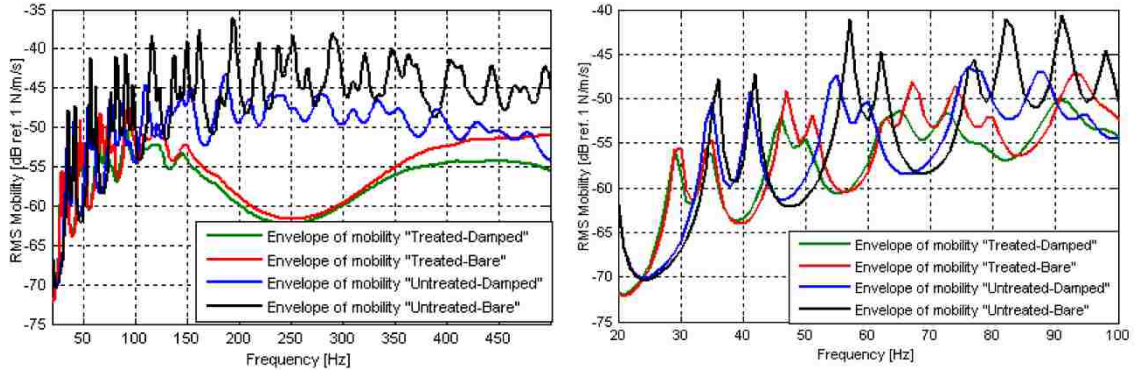


Figure 0.20: Envelope of mobility calculated for four different layouts of the treatments and for various load cases, with zoom below 100 Hz. (Rieter Automotive [22]).

The results of the simulations showed that the presence of the trim reduces the differences in terms of damping effect among different layout of FLDT. This phenomenon is particularly sharp for the treatment array with the foam and the heavy layer. This result demonstrated that the presence of the porous treatments, although influential for the overall vibration level of the floor, have a very small impact on the design of the FLDT layout.

Another research that investigated the possibility to employ the Biot-based finite element method for the frequency response analysis of treated car body panels was carried out at CRF in 2011 [33]. In the first part of this research a series of experimental tests were conducted on a treated steel plate, with the aim to provide a reference set of data for validating the results of the following numerical analysis. The experimental setup consisted in a steel plate excited by a shaker and a series of accelerometers attached on the surface for the measurement of the FRF. The tests were carried out with different configurations of the plate, i.e. untreated and treated with foam or felt, and different joining techniques, i.e. with the treatment completely bonded to the

plate, simply lying on its surface or fastened in different points. For the purpose of validating the numerical model, the experimental outcomes were compared to the ones calculated with a commercial FE solver based on the Biot's theory.

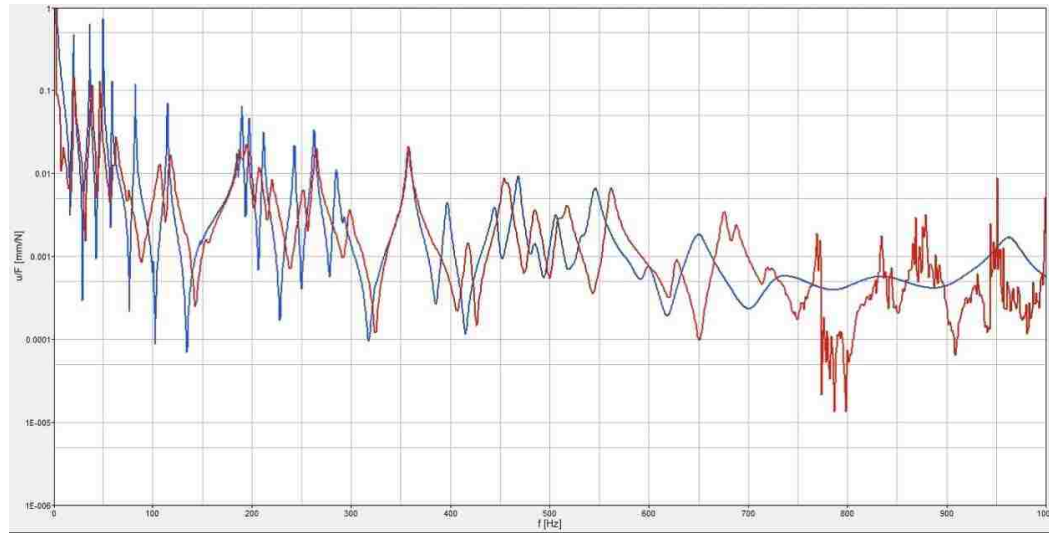


Figure 0.21: Measured (red) and simulated (blue) accelerance FRF of a plate treated with a poroacoustic material in the research work conducted by the CRF [33].

The comparison showed a high consistency between the results in a frequency range from 0 up to 400 Hz, while for higher frequencies significant discrepancies were detected.

2.5 Summary and final remarks on the review of literature

Passenger vehicles are fitted with various different treatments, which are used to control the noise and vibration levels, thus ensuring an adequate riding comfort to the occupants. At the moment, each of these treatments is used with a specific function. In particular, the viscoelastic treatments are used for damping the vibration of the car body panels, while the poroacoustic treatments are used to reduce the reverberation within a certain environment and to isolate it from the external noise.

In the vibroacoustic analysis of the vehicle, which is usually carried out by means of numerical tools, the presence of the NVH treatments must always be taken into account. However if for the

viscoelastic materials it is possible to refer to the classic theory of elasticity, for the poroacoustic materials it is necessary to introduce some other specific mathematical model. The fundamental theory which was proposed for this purpose is the one developed by Maurice Anthony Biot in 1941, which has been presented in several different forms over the years. Among these forms, the mixed displacement-pressure formulation is the most diffused for the finite element applications, as it is the most efficient in terms of computational effort.

The various studies carried out during the last few years have demonstrated that the use of Biot-based finite element analysis for addressing the vibroacoustic problems involving the presence of poroelastic materials can lead to reliable results with a significant saving in terms of cost and time compared to experimental testing. However, in these studies the FEA has never been employed to investigate the possibility of replacing the viscoelastic materials with the poroacoustic ones for damping the vibration of the car body panels. For this reason, this particular problem that has never been taken into consideration will be addressed in this thesis.

CHAPTER 3

METHODOLOGIES AND RESULTS

This chapter describes the methodologies employed within the thesis project, presenting the experimental and numerical tests that have been carried out and the results obtained. The initial part introduces the numerical model used for the analysis. First, in order to prove its validity, some experimental tests are conducted, providing a set of data for the comparison with the numerical results. Afterwards, the procedure employed by the solver for the solution of the problems analyzed within the thesis is explained, and the influence of the FE model parameters on the output results is investigated. A sensitivity analysis is then conducted to determine the effects that the characteristics of the treatment have on the dynamic response of a panel subject to a mechanical excitation. In the same way the performances of different materials are compared. Finally a frequency response analysis is conducted on a vehicle floor, with the aim to evaluate the possibility of replacing the FLDT with the poroacoustic treatments for damping the vibration of the panels.

3.1 Experimental tests

In order to prove the validity of the FE software for the analysis of the frequency response of structures treated with poroacoustic materials, a series of experimental test are conducted on a steel plate, providing an initial set of data for the comparison with the numerical results.

3.1.1 Experimental setup

The experimental tests are carried out on a flat rectangular plate made of AISI 1020 steel, having 552 mm width and 699 mm height, suspended in vertical position by means of elastic hangs to an external rigid frame. An electromagnetic shaker, mounted on a tripod by means of springs, excites the plate by applying a dynamic force perpendicularly to its surface. At the top of the stinger, which transmits a white noise signal from the shaker to the plate, an impedance head measures the force that is transferred to the panel and it sends the measured value to the

multichannel acquisition device. At the same time, the response of the system is evaluated using a SIMO (single-input, multiple-output) approach, by means of three uniaxial accelerometers that are mounted in different positions on the plate and connected to the acquisition frontend.

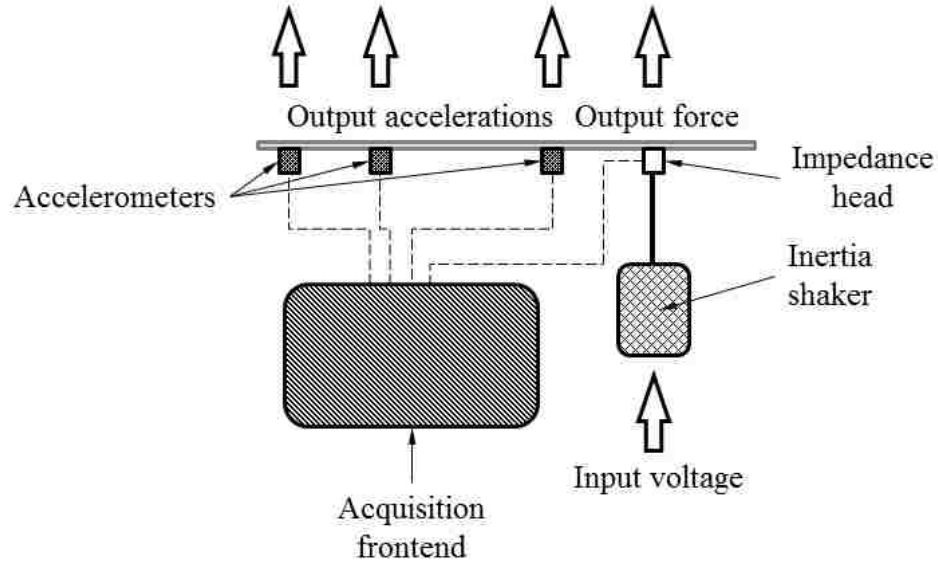


Figure 0.1: Schematic representation of the experimental setup for the tests conducted on the steel plate.

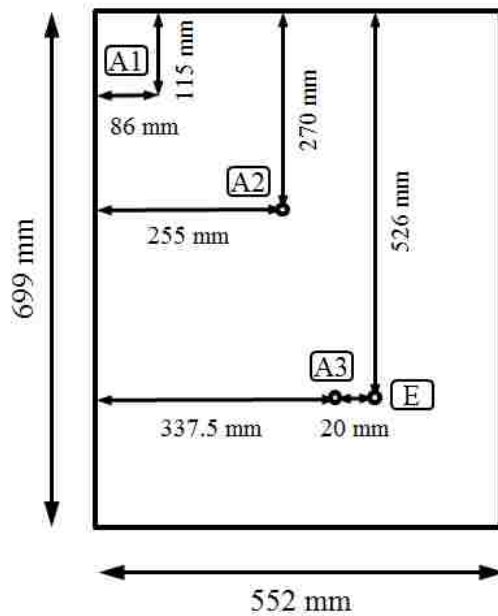


Figure 0.2: Positioning of the excitation point (E) and the three accelerometers (A1, A2 and A3)

Using the amplitude of the accelerations measured with the three accelerometers, and the force acquired from the impedance head, the accelerance FRF (H_{A_i}) is calculated for several sampled frequencies in the range from 0 to 1000 Hz, according to the formulas in (0.1).

$$H_{A_1}(\omega) = \frac{A_1(\omega)}{F(\omega)}; H_{A_2}(\omega) = \frac{A_2(\omega)}{F(\omega)}; H_{A_3}(\omega) = \frac{A_3(\omega)}{F(\omega)} \quad (0.1)$$

3.1.2 Tests carried out on the steel plate

Since the main objective of the thesis is to determine the reduction in terms of vibration level that can be achieved for the car body panels by treating them with poroacoustic materials, the tests are conducted comparing the response of a bare and treated structure to a mechanical excitation.

Initially the bare plate is tested to provide the reference response of the structure, and afterwards the acoustic treatments are attached to its surface by means of a double-sided tape to determine the variation of the response with respect to the untreated panel.

	Treatment "1S"	Treatment "1N"
Skeleton's density[kg/m³]	1793	1810
Skeleton's Young's modulus[Pa]	65085	71468
Skeleton's loss factor	0.1	0.06
Skeleton's Poisson's ratio	0	0
AFR[Ns/m⁴]	104872	21110
Porosity	0.9228	0.9683
Tortuosity	1.1038	1.0751
Viscous length[m]	2.6238E-05	6.9292E-05
Thermal length[m]	7.8715E-05	12.8515E-04
Dimensions [mm]	522x672	517x680
Thickness[mm]	10	17

Table 0.1: Characteristics of the felts employed for the validation of the numerical model, provided by the supplier of the treatments.

In order to investigate the capability of the software to properly represent the effect of the different material properties and interface conditions of the porous trims on the response, two different treatments, which characteristics are indicated in Table 0.1, and three tape layouts, displayed in Figure 0.3, are tested.

In total seven different configurations are examined:

- 1) Bare plate
- 2) Treatment “1N” attached to the plate in five points
- 3) Treatment “1N” attached to the plate on the diagonals
- 4) Treatment “1N” attached to the plate on the diagonals and on the sides
- 5) Treatment “1S” attached to the plate in five points
- 6) Treatment “1S” attached to the plate on the diagonals
- 7) Treatment “1S” attached to the plate on the diagonals and on the sides

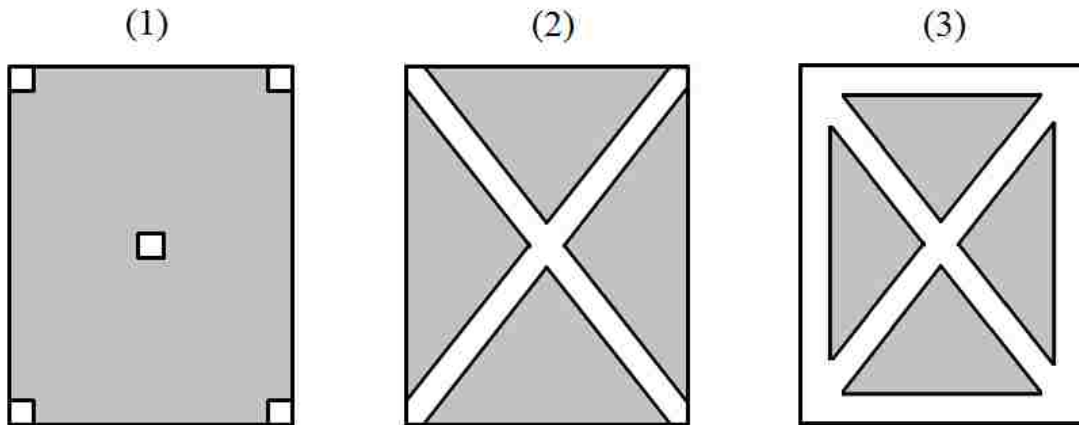


Figure 0.3: Different tape layouts for joining the acoustic treatment to the plate: attached in five points (1), on diagonals (2) and on diagonals and sides (3)

Three runs are performed for each of the seven different tests and the FRF are calculated as the mean value over these three runs. The standard deviation is calculated for each of the 21 runs and

its value never exceeds $2.3 \frac{m}{s^2 N}$, confirming the robustness of the results obtained with this experimental setup.

In order to have a graphical visualization of the response the FRF curves are plotted on a Bode diagram, with the values of the acceleration on the ordinate and the frequency on the abscissa.



Figure 0.4: Experimental setup for the tests conducted on the steel plate.

3.1.3 Experimental results

The two Bode diagrams reported in Figure 0.5 and Figure 0.6 report the FRF calculated from the acceleration of the plate measured in correspondence of the accelerometer A3. The two plots refer to the plate treated respectively with the poroacoustic material samples “1N” and “1S”. In both diagrams, the response of the bare plate is compared to the one of the plate with the acoustic treatment attached by means of the double-sided tape, distributed according to the three different layouts indicated in Figure 0.3.

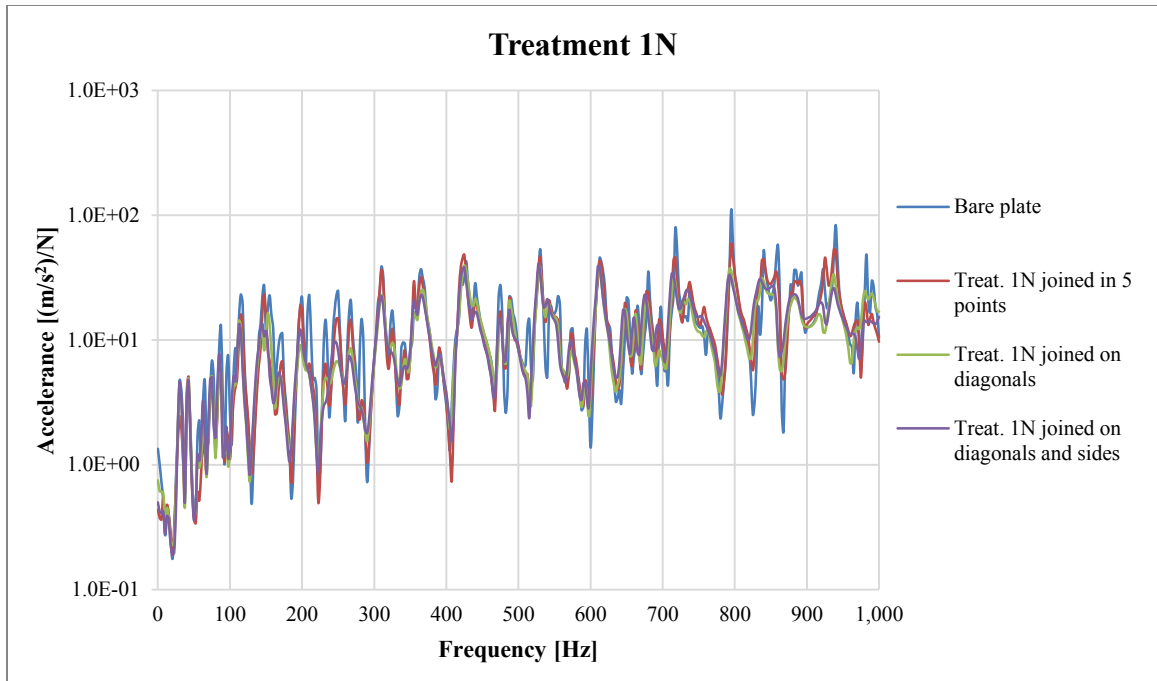


Figure 0.5: Accelerance FRF of the plate treated with the felt "1N" calculated from the accelerometer A3.

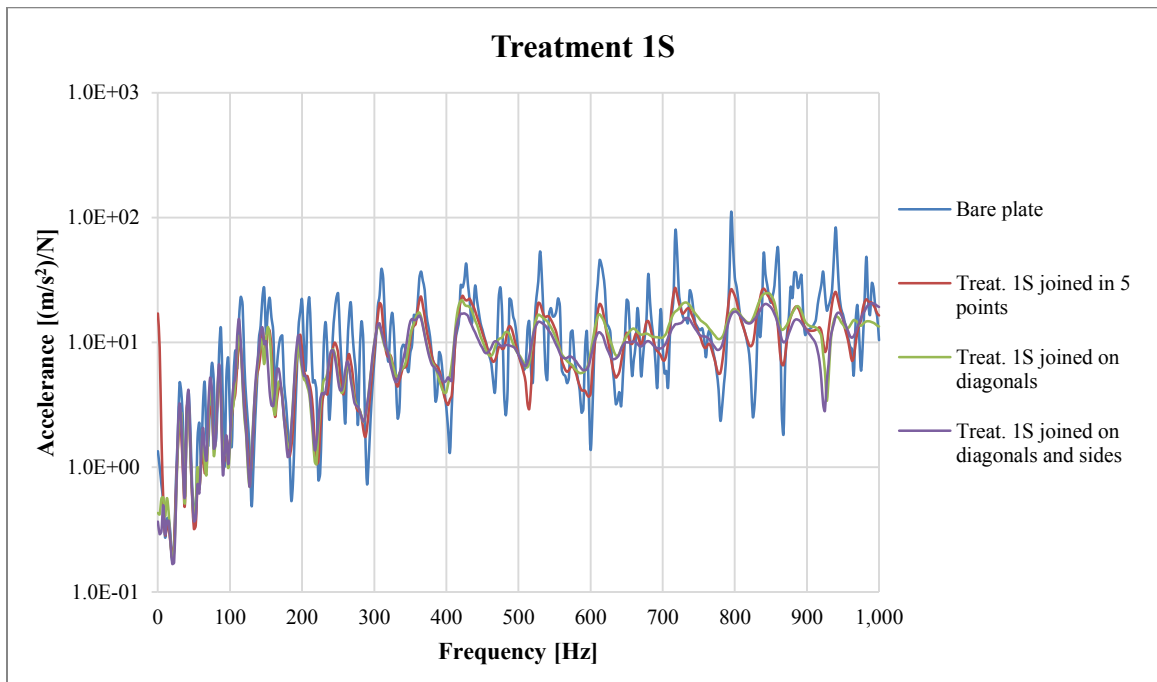


Figure 0.6: Accelerance FRF of the plate treated with the felt "1S" calculated from the accelerometer A3.

For both samples “1N” and “1S” the effect of the treatment on the frequency response of the panel is quite relevant. In both cases the amplitude of the acceleration is significantly decreased with respect to the bare structure, in particular in correspondence of the resonant peaks. As expected, since the energy dissipations that take place within the porous materials are related mainly to the viscous and viscoelastic losses, the damping effect becomes more pronounced at the higher frequencies.

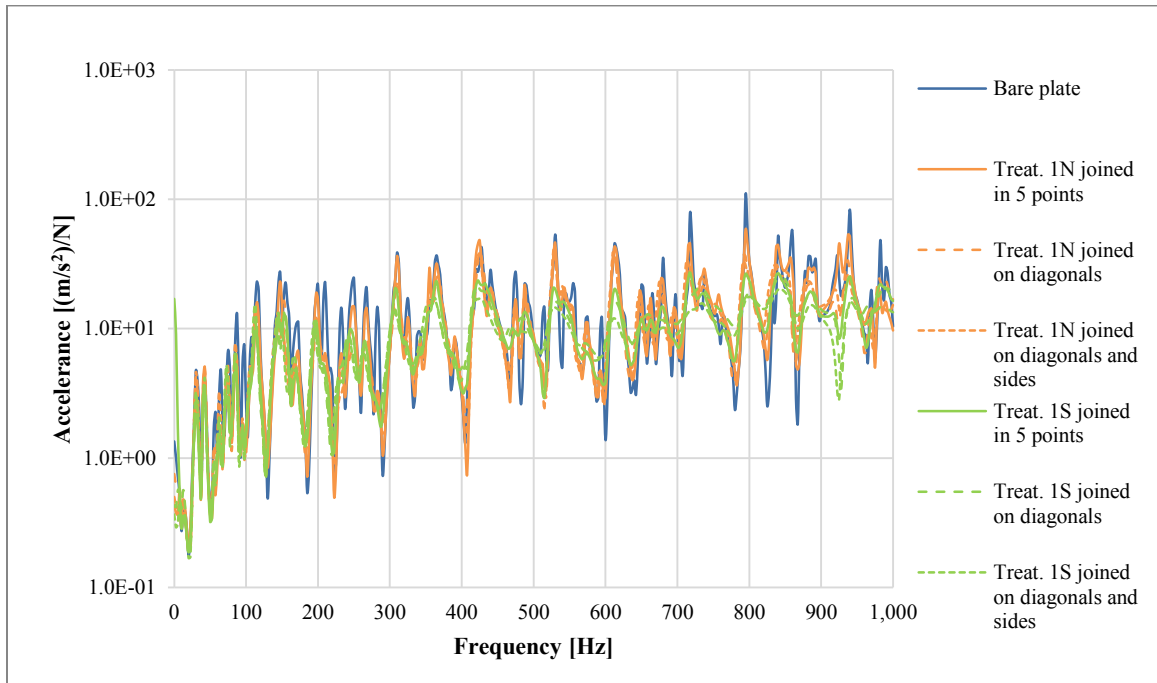


Figure 0.7: Comparison between the accelerance FRF curves of the plate treated with the felt "1S" and "1N".

Comparing the results obtained with the different layouts of the double-sided tape, it can be observed that also the bonding interface between the treatment and the plate has a significant impact on the frequency response of the system. For both treatments, the vibration damping becomes more elevated as the area of the bonded surfaces increases. This behaviour can be explained by taking into consideration the dissipation mechanisms of the porous materials. In particular, since both the viscoelastic losses, which are related to the elastic strain of the solid

phase, and the viscous losses, which are related to the fluid flowing inside the open pores, are caused by the deformation of the porous material, the more the treatment is constrained to the structure, the more it follows its deformations and the more it dissipates energy, damping the vibration. In the Bode plot depicted in **Error! Reference source not found.** the results obtained with the two treatments are compared, highlighting the higher vibration damping level achieved with the treatment “1S” with respect to the “1N”. The different performances of the two samples are related to their material properties and thickness.

3.2 Introduction to the FEA software

In the field of vibroacoustics, the research activities can be divided in numerical simulations and experimental tests. Among the numerical simulation tools the Finite Element Analysis is the most widely diffused for the calculation of the frequency response of car body panels treated with poroacoustic materials. One of the main reasons of its wide application is the consistency between its outcomes and the experimental results, which can be confirmed by the various research works reported in the review of literature. With respect to the experimental tests the numerical simulations are much more flexible and effective in terms of cost and time. The high flexibility makes simulations ideal for certain kinds of applications such as the sensitivity analysis (i.e. the evaluation of the effect that an input parameter has on the output response of a system) or the study of components and materials, which are not yet available for testing. In order to use the Finite Element Analysis for the calculation of the frequency response of car body panels treated with poroacoustic materials it is necessary to employ a solver, which implements the Biot’s theory of poroelasticity. The solver used for the development of this thesis is called Actran and its functioning is briefly described hereafter.

In Actran, two principal approaches are available for the calculation of the frequency response, the direct and the modal approach. The direct approach computes the response of the system in physical coordinates, without first extracting the modes of the various components. On the

contrary, the modal approach computes the response of the system using the modal coordinates, which means that the modal base has to be extracted before running the simulations.

In general, the modal approach is more suitable for larger models because it calculates the solution using a smaller system of uncoupled equations, which allows a higher computational efficiency.

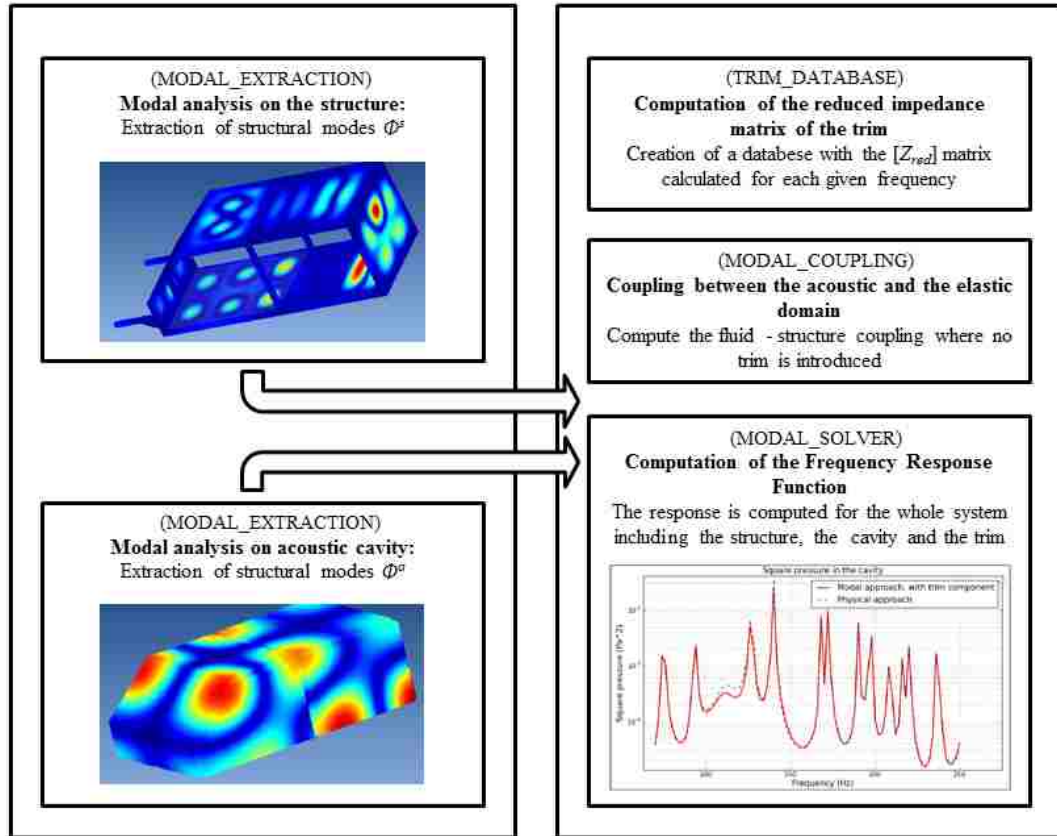


Figure 0.8: Steps of the Actran modal response analysis [8].

The modal approach is also much more flexible, because the natural frequencies and mode shapes of the components can be computed in a preliminary stage of the analysis and then used multiple times to evaluate the response of the system in different configurations (e.g. with other treatments applied) and from different output nodes.

One of the main drawbacks of the modal approach, however, is that the modal base is calculated only within a certain range of frequencies and therefore some of the modes of the systems are

truncated and their contribution to the output response is not considered. On the contrary, the results obtained with the direct approach are not subject to any mode truncation and therefore they are usually more accurate. It is possible, however, to reach an acceptable level of accuracy also with the modal approach, by calculating the modal base within a wider range of frequencies (usually two times the one taken into consideration for the frequency response analysis).

In the course of this thesis project, due to the need of handling complex models (such as the floor of a vehicle) with a very limited computational power, the modal approach has always been preferred to the direct approach for the numerical simulations.

Actran's modal approach for the calculation of the frequency response of a system to a mechanical excitation consists in a sequence of steps (summarized in Figure 0.8), which are described in the following paragraphs.

3.2.1 Modal frequency response step 1: Normal modes extraction

The first step for the calculation of the modal frequency response consists of the extraction of the natural frequencies and mode shapes of the structure and eventually of the acoustic cavity. This step can be performed either within the Actran environment or with another structural\fluid FE solver like Nastran. The meshes of the components of the system must be provided as inputs for the extraction, together with their material properties, i.e. the Young's modulus, Poisson's ratio and solid density for the elastic component and the fluid density and speed of sound for the acoustic component. The output of the modal extraction is an OP2 file where the mode shapes and natural frequencies are stored, which can be used multiple times for different simulations. The information contained in the OP2 file can also be used to graphically represent the mode shapes of the components in the form of deformation patterns, which are projected on the mesh as depicted in Figure 0.9.

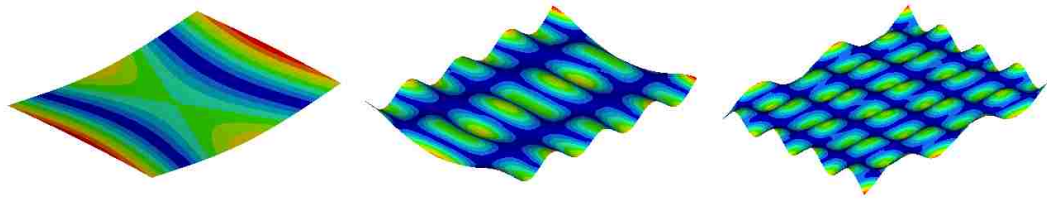


Figure 0.9: Deformation patterns of a plate at increasing natural frequencies.

3.2.2 Modal frequency response step 2: Reduced impedance matrixes of the porous trim

When the modal frequency response analysis is conducted on a system that includes a porous component, the mesh of that component must be included in the FE model of the system and its material properties must be provided to the solver as inputs. Since the behaviour of the porous domain is described with theory of poroelasticity, the material must be characterized by means of a series of quantities called the Biot parameters.

These quantities are:

- Air flow resistivity
- Biot factor (equal to 1 for the majority of the porous materials)
- Viscous characteristic length
- Thermal characteristic length
- Viscosity of the fluid
- Young's modulus of the skeleton (with the imaginary part related to the loss factor)
- Density of the skeleton
- Poisson's ratio
- Specific heat of the fluid for constant volume and for constant pressure
- Tortuosity
- Fluid density
- Thermal conductivity of the fluid
- Fluid bulk modulus
- Porosity

The strategy adopted by Actran to model the interactions between the porous treatments and the structures and cavities to which they are coupled is based on a modal representation of the elastic and acoustic components (the modal bases extracted in the previous step), and a representation of the poroacoustic treatments in physical coordinates. More in details the procedure used for coupling the various components consists in reducing the impedance matrices of the porous treatments by condensing their DOFs at the interface with the structure and the fluid domains, and then projecting them on the global equation of the system composed by the fluid and the structure, which is expressed in modal coordinates.

In order to explain how the reduction of the impedance matrices works it is necessary to make some preliminary consideration on the DOFs of the porous component. With reference to the schematic representation depicted in Figure 0.10 it is possible to define four DOF for the porous trim:

- The inner displacement of the solid phase of the porous $u_{T,inner}$
- The displacement of the solid phase of the porous with the structure u_{T,Γ_S}
- The inner pressure of the fluid phase of the porous $p_{T,inner}$
- The pressure of the fluid phase of the porous at the interface with the cavity p_{T,Γ_F}

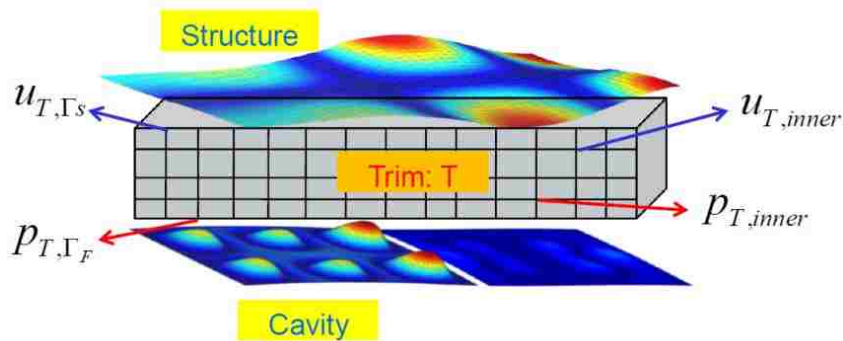


Figure 0.10: Graphical representation of the DOF of the porous trim [8].

The DOF vector is indicated as:

$$[D]^T = (D_{inner}, D_{\Gamma})^T = (u_{inner}, p_{inner}, u_{\Gamma_s}, p_{\Gamma_f})^T \quad (0.2)$$

Given these considerations the impedance matrix $[Z]$ is the one, which correlates the DOF vector $[D]$ to the excitation vector $[h]$, as indicated in equation (0.3).

$$[Z_T(\omega)][D]^T = [h]$$

$$[Z_T(\omega)] = \begin{bmatrix} [Z_{inner}(\omega)] & [Z_{inner,\Gamma}(\omega)] \\ [Z_{\Gamma,inner}(\omega)] & [Z_{\Gamma}(\omega)] \end{bmatrix}, [h] = \begin{bmatrix} [h_{inner}] \\ [h_{\Gamma}] \end{bmatrix} = \begin{bmatrix} [0] \\ [h_{\Gamma}] \end{bmatrix} \quad (0.3)$$

Since the excitation applied to the inner part of the porous treatment is equal to zero it is possible to compute the reduced trim impedance matrix as follows:

$$[Z_{red}(\omega)] = [Z_{\Gamma}(\omega)] - [Z_{\Gamma,inner}(\omega)][Z_{inner}(\omega)]^{-1}[Z_{inner,\Gamma}(\omega)] \quad (0.4)$$

In this way that the excitation acting on the coupling surfaces can be rewritten as:

$$[h_{\Gamma}] = [Z_{red}(\omega)][D_{\Gamma}]^T \quad (0.5)$$

Using the methodology described above, the Actran module “*TRIM DATABASE*” computes the Z_{red} matrices of the trim for each of the requested frequencies and stores them in an OP4 file. Since the calculation of the reduced impedance matrices is the most time consuming operation of the whole simulation process, it is usually performed for a few sampled frequencies rather than for all the frequencies contained in the investigated range and each of the impedance matrices is considered to be piecewise constant over the intervals between two samples.

3.2.3 Modal frequency response step 3: Structure-acoustic cavity coupling

Considering a finite element model constituted by a structure, which interfaces with a cavity, it is possible to write the equations for the elastic and the acoustic domains in a coupled form, which also takes into account the interactions between them, as reported in equation (0.6).

$$\begin{bmatrix} [K_S] - \omega^2 [M_S] & [C_{SF}] \\ [C_{SF}] & \frac{1}{\omega^2} ([K_S] - \omega^2 [M_S]) \end{bmatrix} \begin{bmatrix} \{U(\omega)\} \\ \{P(\omega)\} \end{bmatrix} = \begin{bmatrix} \{F_S(\omega)\} \\ \frac{\{F_F(\omega)\}}{\omega^2} \end{bmatrix} \quad (0.6)$$

In the above equation, it can be noticed that the impedance matrix is not diagonal and therefore the DOFs related to the displacements and the ones related to the pressure are mutually influenced by each other. From a physical point of view, this can be interpreted as the fact that on one hand the presence of the fluid alters the mechanical response of the structure, while on the other hand, the mechanical vibrations of the elastic components are transformed into sound pressure waves radiated inside the acoustic cavity. The coupled equation can be rewritten in modal coordinates as indicated in (0.7) and it is used by the Actran module “*MODAL COUPLING*” to calculate the interactions between the fluid and solid elements which are located at the interfaces between the two domains that are not separated by a porous trim.

$$\begin{bmatrix} [Z_{SS}] & [Z_{SF}] \\ [Z_{SF}^T] & [Z_{FF}] \end{bmatrix} \begin{bmatrix} \alpha_S(\omega) \\ \alpha_F(\omega) \end{bmatrix} = \begin{bmatrix} [\phi_S^T] \{F_S(\omega)\} \\ [\phi_F^T] \left[\frac{F_F(\omega)}{\omega^2} \right] \end{bmatrix} \quad (0.7)$$

Making reference to the coupling between different domains (e.g. between the structure and the porous trim or between the structure and the acoustic cavity), which has been introduced in the computational steps 2 and 3, it must be observed that very often the meshes of the different domains are not coincident. This is because the meshing constraints of the various components are different. On one hand, the density of the structure mesh is guided by the bending wavelength, while on the other hand; the meshes of the cavity and the porous treatment are ruled by the acoustic wavelength. The strategy adopted by Actran to handle those incompatible meshes consists in defining a coupling surface for each of the two domains, creating an interface between them and projecting the nodes of the first coupling surface onto the second one. The projection process consists in finding the face of the second coupling surface, which contains the projection of a particular node of the first surface, and calculating the local coordinates of the projected node

within the considered face. The projection is searched within an extrusion of the first surface along the local normal direction of the second surface. The dimensions of the extrusion are specified by two tolerance input parameter (GAP_TOL and $PLANE_TOL$), which define its depth and width.

3.2.4 Modal frequency response step 4: Projection of the reduced impedance matrix

In order to couple the trim with the acoustic and elastic domain, the impedance matrix is projected into the modal space as follows:

$$[Z'_{red}(\omega)] = \begin{bmatrix} [\phi_{\Gamma_S}^T] & [0] \\ [0] & [\phi_{\Gamma_F}^T] \end{bmatrix} [Z_{red}(\omega)] \begin{bmatrix} [\phi_{\Gamma_S}] & [0] \\ [0] & [\phi_{\Gamma_F}] \end{bmatrix} \quad (0.8)$$

The modal space impedance matrix is then injected into equation (0.7), resulting in a structure-cavity coupled system, which also includes the presence of the trim.

$$\begin{bmatrix} [Z'_{SS}] & [Z'_{SF}] \\ [Z'^T_{SF}] & [Z'_{FF}] \end{bmatrix} \begin{bmatrix} \alpha_S(\omega) \\ \alpha_F(\omega) \end{bmatrix} = \begin{bmatrix} [\phi_S^T] [F_S(\omega)] \\ [\phi_F^T] \left[\frac{F_F(\omega)}{\omega^2} \right] \end{bmatrix} \quad (0.9)$$

3.2.5 Modal frequency response step 5: Modal frequency response solver

Once all the previous steps are completed, it is possible to calculate the response of the elastic and the acoustic components to an external excitation. The excitation is applied to the system as a boundary condition and the output response can be evaluated in any point inside the domains. The output quantity depends only on the component to which the response point is attached; in particular, the response is expressed as a pressure if the point is part of an acoustic component and as a displacement if the node is part of an elastic component. The FRF can then be computed as the ratio between the output response and the force provided as an input, and then reported into a magnitude-frequency plot.

3.3 Numerical modeling

In order to run a modal frequency response analysis, which various steps have been described above, it is necessary to submit to the solver a finite element model, which represents the physical characteristics of the investigated system, and a command file, which defines the various actions that the solver will perform to calculate the response. Since the simulations are only a numerical representation of a physical phenomenon, both the finite element model and the command file are not defined in a unique way, but they can differ in various modeling aspects. The following paragraphs analyze the way these modeling aspects affect the calculated frequency response of a system.

3.3.1 Mesh of the elastic component

The mesh of the panel for the modal frequency response analysis can be created either by means of shell or solid elements.

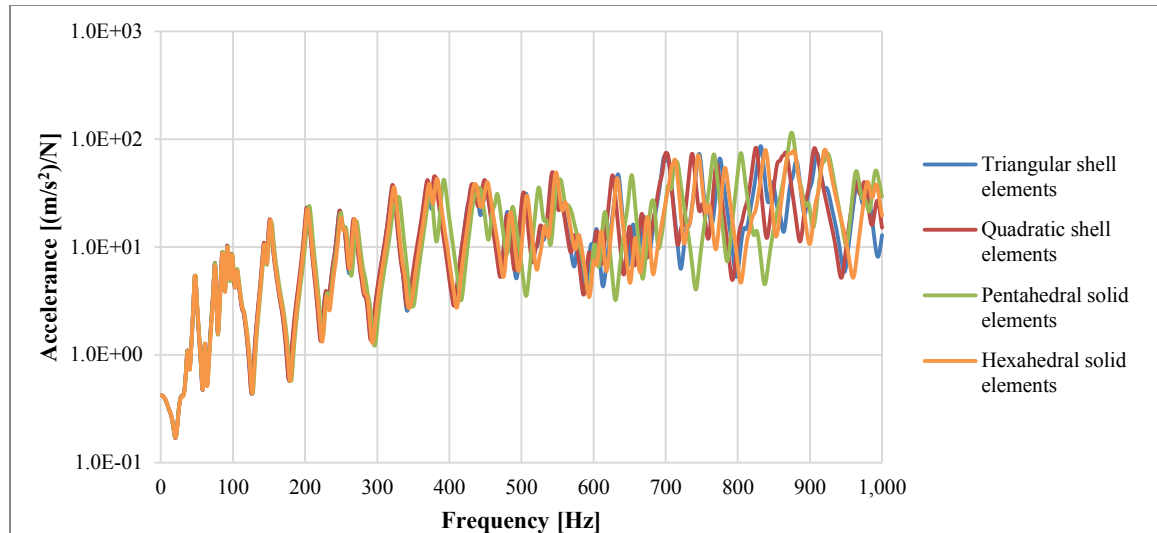


Figure 0.11: Comparison between different kinds of mesh elements for the plate.

Figure 0.11 highlights the differences between the responses calculated using a plate meshed with shell elements (triangular and quadratic) and the one calculated using a plate meshed with solid elements (pentahedral and hexaedral). In Figure 0.11 it can be noticed that the discrepancies

between the responses obtained with the different meshes become more significant at the higher frequencies. The solid elements (especially the pentahedral ones) show a higher stiffness with respect to the shell elements, which causes a frequency shift of the resonance peaks. Usually when two dimensions of a component are much higher than the third one (as in the case of a plate) the shell elements are preferred to the three-dimensional ones, because they are easier to mesh and faster to solve. For what concerns the size of the elements, a common meshing criterion for vibroacoustic problems consists in having more than 6 elements per flexural wavelength (usually 8 or 10), in order to limit the discretization errors that might occur at high frequencies. The smallest wavelength can be evaluated by making reference to the Kirchhoff's theory [34], as indicated in equation (0.8).

$$\lambda_{B_{\min}} = \frac{c_B}{f_{\max}} = \frac{\left(\frac{D}{\rho h}\right)^{\frac{1}{4}}}{2\pi\sqrt{\omega_{\max}}} = \frac{\left(\frac{Et^3}{12(1-\nu^2)\rho h}\right)^{\frac{1}{4}}}{2\pi\sqrt{\omega_{\max}}} \quad (0.10)$$

For instance, inserting the parameters related to the characteristics of the plate (density, Young's modulus, Poisson's ratio and thickness) and the maximum frequency of the experimental tests into equation (0.8) the value of the smallest flexural wavelength corresponds to 121 mm, which means that the size of the elements of the plate should be around 12/15 mm.

3.3.2 Mesh of the porous trim

A porous mesh includes both solid elements, which represent the volume of a treatment, and shell elements with equivalent nodes, which represent its interface with the other components. Since no particular meshing criterion is available for the mesh of the porous trim various configurations are compared, with the aim to evaluate the effect that they have on the calculated frequency response. Considering the results reported in the Bode plot, it could be observed that there is almost no difference between the FRF curves calculated with pentahedral and tetrahedral elements.

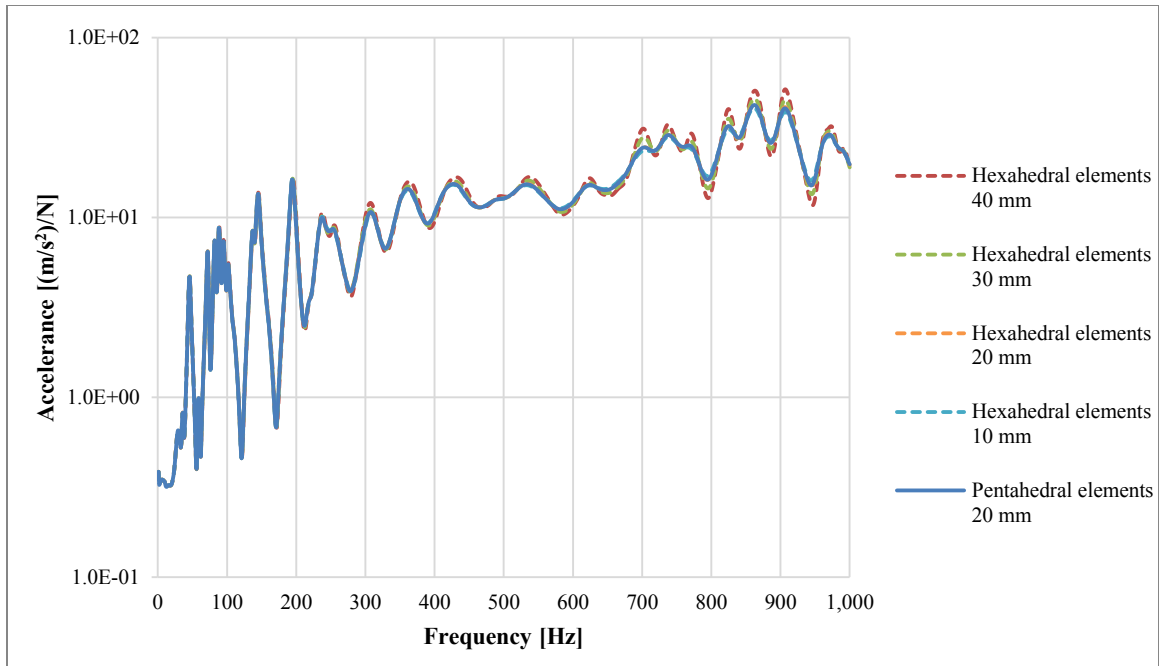


Figure 0.12: Comparison between different kinds of mesh elements for the plate.

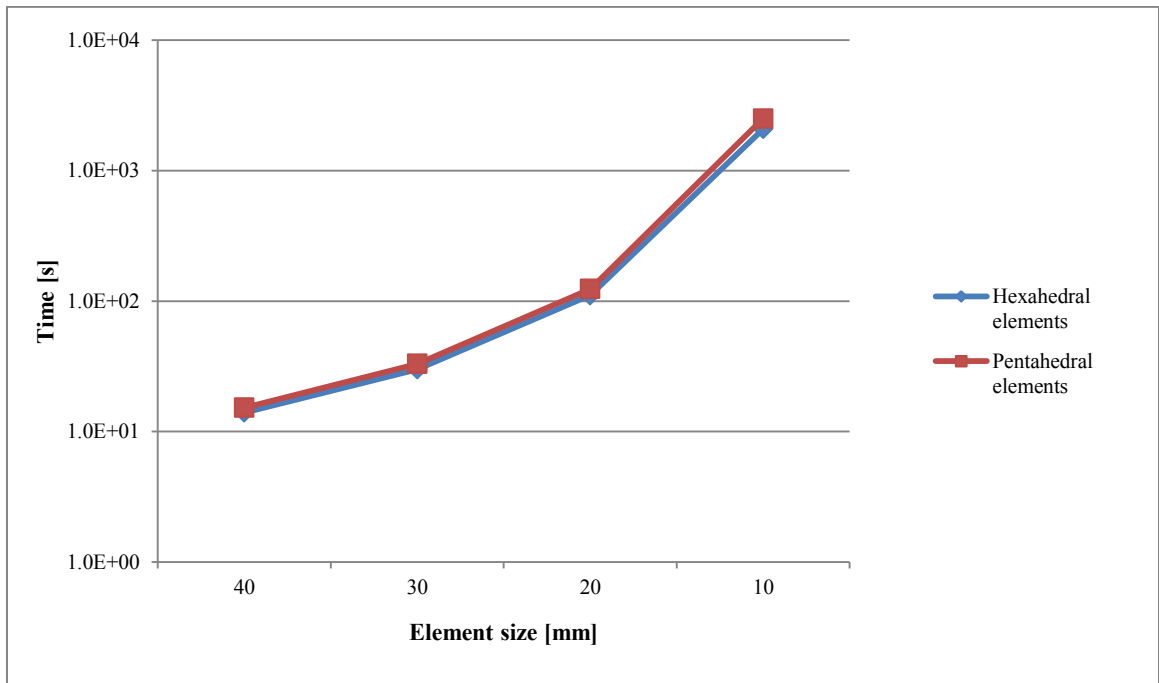


Figure 0.13: Computational time increment for smaller mesh size.

If on one hand a smaller mesh size allows a higher convergence, on the other hand it also introduces a significant increase of the computational time, as showed in Figure 0.13. Based on

this consideration the discretization criterion for the mesh of the porous treatments has to be found in the optimal trade-off between the computational time and the convergence of the results.

3.3.3 Presence of an acoustic cavity

As reported in the review of literature many of the problems studied in the field of vibroacoustics are related to the vibration of a solid structure and to the radiation of noise inside an acoustic cavity. When the numerical analysis requires the calculation of the noise radiated inside the cavity it is obviously necessary to include the acoustic domain in the finite element model, while, on the contrary, for the study of the frequency response of the structure its presence can be neglected. In order to determine the reasonableness of this simplification the frequency response of a treated panel calculated by taking into account its interactions with the acoustic cavity is compared to the response of the same panel calculated without taking into account any interaction.

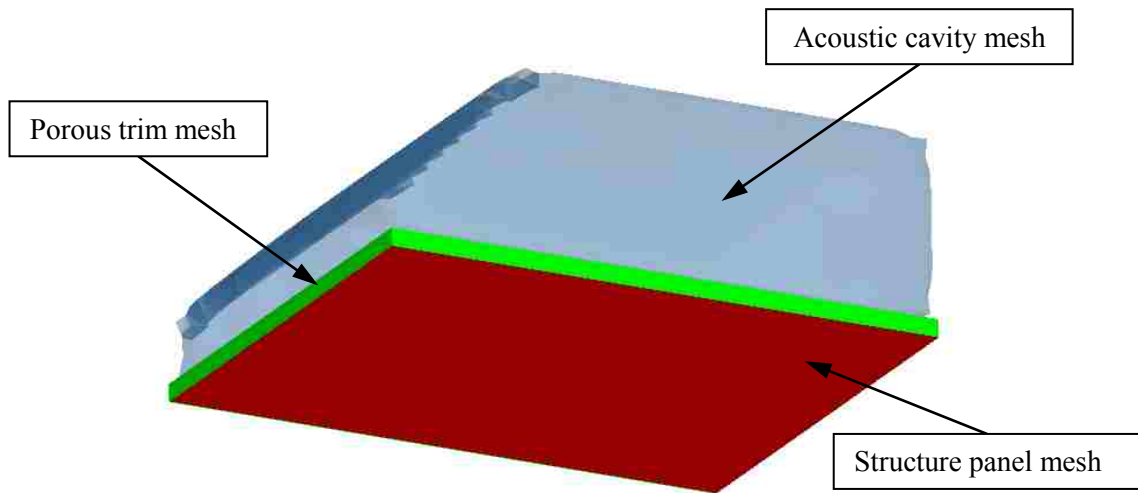


Figure 0.14: Mesh of the treated steel plate coupled to the acoustic cavity.

The acoustic cavity is meshed with tetrahedral and hexahedral elements and then connected to the plate-trim model (Figure 0.14) by means of a coupling surface. For the definition of the fluid characteristics the approximated properties of air at 20° C and 101,325 Pa are employed (1.2 kg/m³ fluid density and 344 m/s speed of sound waves). First, the mode shapes and natural

frequencies of the acoustic cavity are extracted and stored into an OP2 file, and then the acoustic cavity mesh and its modal base are included into the Actran analysis for the calculation of the modal frequency response.

Figure 0.15 compares the two FRF curves calculated for the panel respectively when the effect of the acoustic cavity is omitted and when it is taken into account. In the diagram, it can be observed that the modes of the cavity have a very small influence on the response of the panel below 600 Hz, as most of the natural frequencies of the acoustic component are positioned above that threshold. At the higher frequencies the effects of the interactions between acoustic and structural modes become a little more noticeable, but still negligible for the purpose of the analysis.

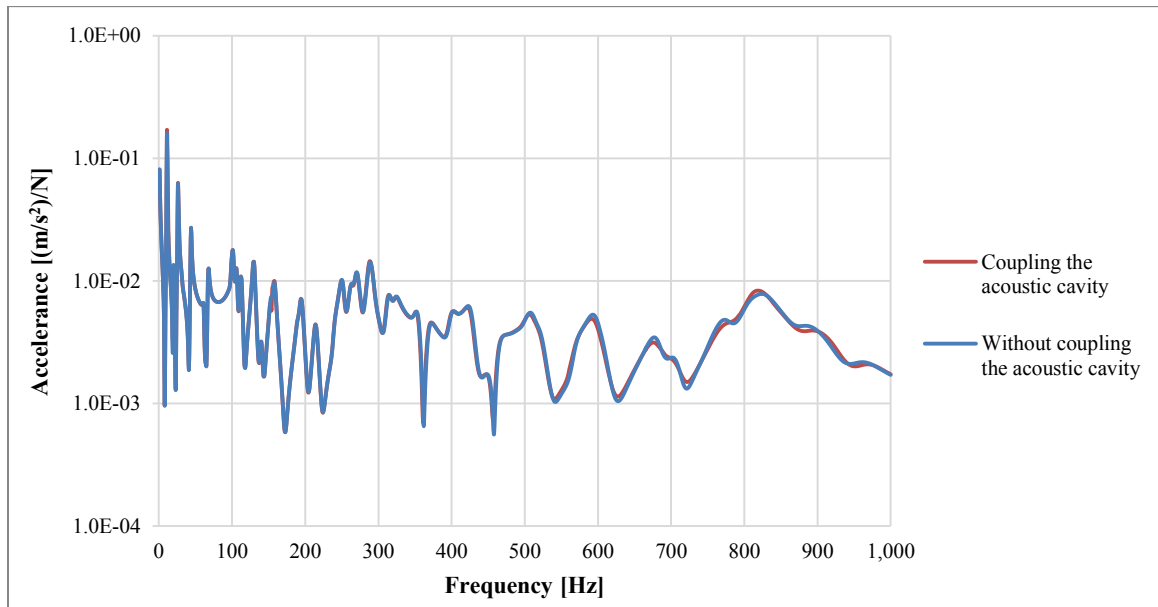


Figure 0.15: Comparison between the response of the system depicted in Figure 0.14 in the two cases when the presence of the acoustic cavity is neglected or taken into account.

3.3.4 Sampling frequencies for the calculation of the reduced impedance matrices

As mentioned in 3.2.2, the numerical approach that Actran uses to account for the effect of the porous treatments in the evaluation of the modal frequency response analysis relies on the calculation of their reduced impedance matrices, which constitutes the most time-consuming step of the simulations. Since the impedance matrices are frequency-dependent, they should be

calculated for each frequency for which the output response is evaluated. However, in order to decrease the computational cost of the analysis, they are usually computed only for a set of sampled frequencies and therefore each matrix is considered to be constant over a certain frequency interval. This approximation clearly introduces an error in the calculated results, which is related to the frequency sampling step and to the rate of change of the impedance matrices.

In Figure 0.16, a comparison among the results obtained using different sampling steps for the calculation of the reduced impedance matrices is presented. From this Bode diagram, it is possible to identify the sampling frequencies which allow reducing the computational cost of the simulations while maintaining a low error level.

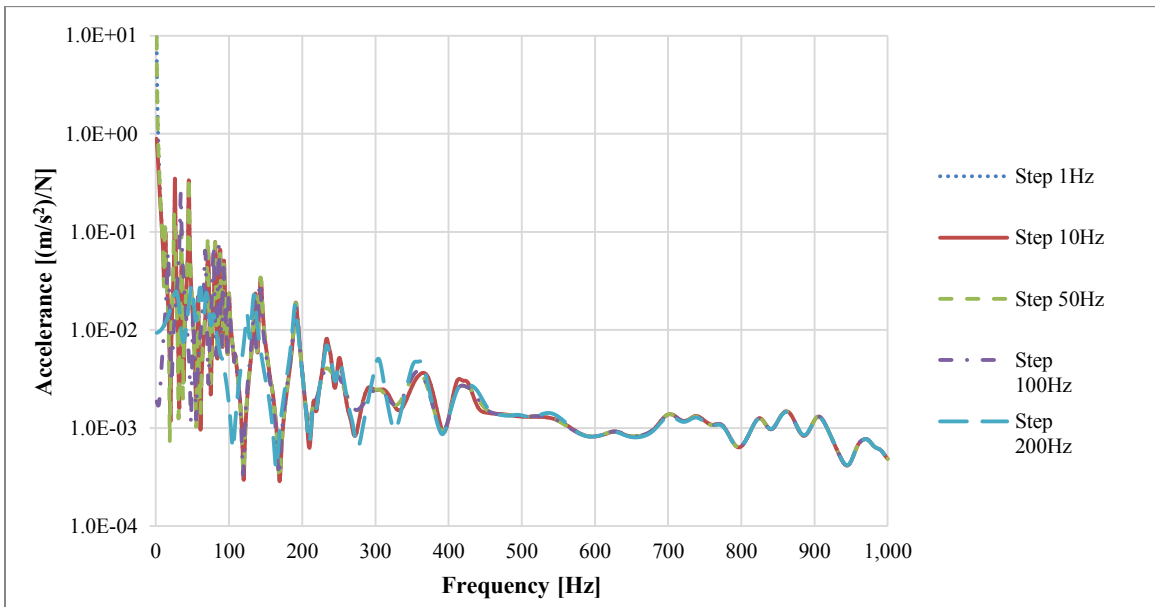


Figure 0.16: Comparison between the FRF curves obtained using different steps for the sampled frequencies at which the reduced impedance matrices are calculated.

As it can be inferred from the FRF curves plotted in Figure 0.16, the error related the discretization becomes significantly smaller at the higher frequencies. The reason for this behaviour is that the variation of the frequency dependent quantities contained in the Biot model is more elevated at low frequencies. Considering that the time required for the simulations is related to the number of calculated matrices (Figure 0.17) it is therefore possible to optimize the

efficiency of the simulations by adopting a sampling step, which becomes wider as the frequency increases.

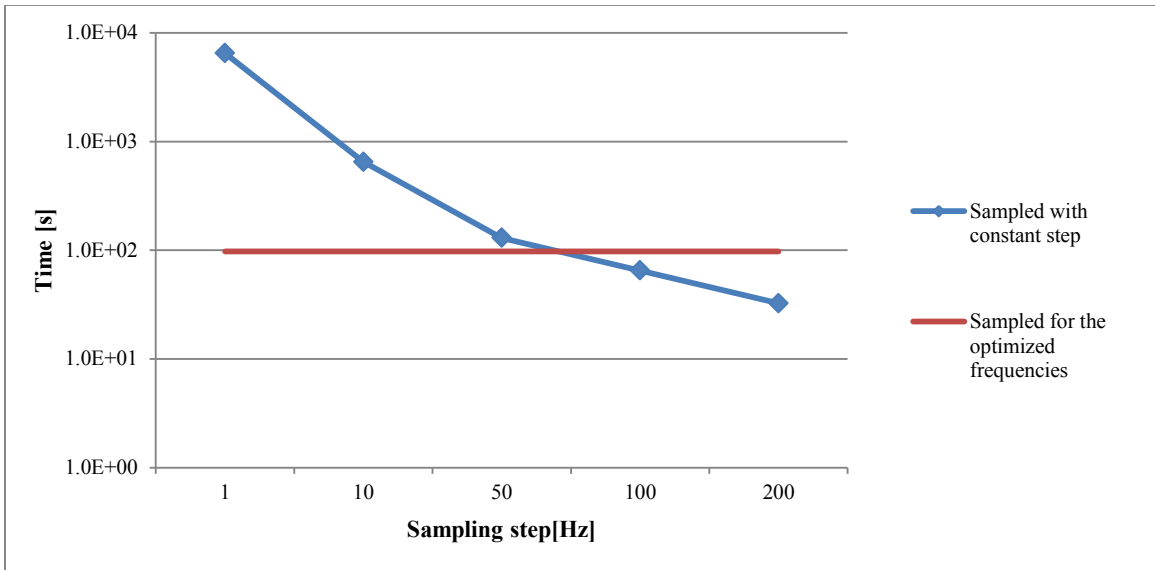


Figure 0.17: Computational time increment related to the accuracy of the discretization and comparison with the optimized frequencies set.

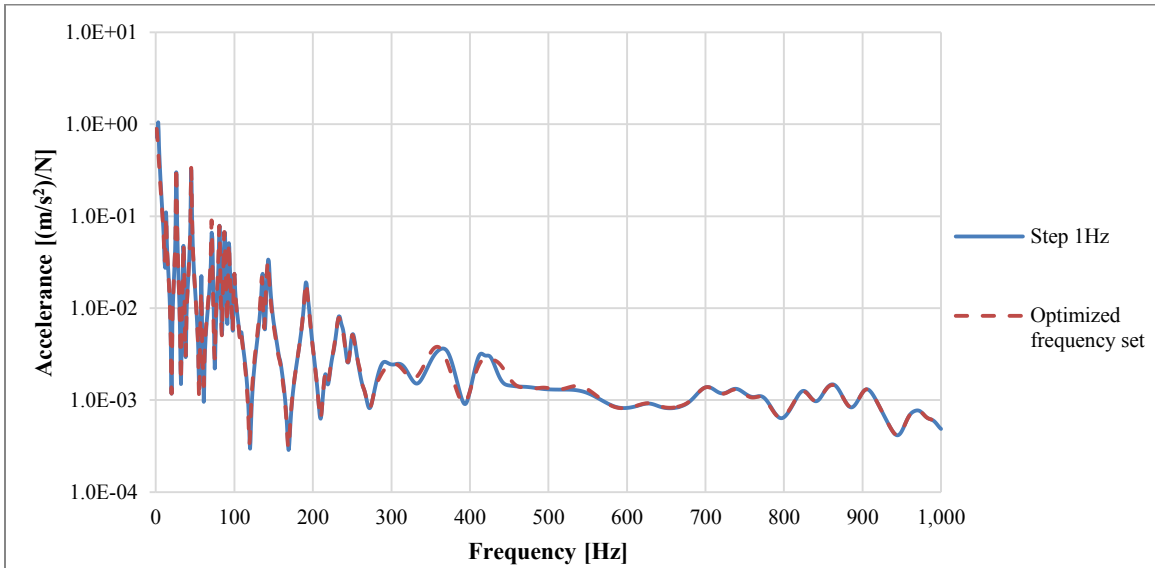


Figure 0.18: Comparison between the results obtained with the smallest frequency sampling step and with the optimized frequencies set.

Making reference to the curves plotted in Figure 0.16 it is possible to observe that the results obtained with the 1Hz and 10Hz steps are equivalent, while the ones calculated with the other steps become fairly coincident after a certain threshold. Hence, using a variable sampling step, it is possible to define an optimized frequency set that offers the best compromise between the computational cost and the sampling error (Table 0.2).

10 Hz	20 Hz	30 Hz	40 Hz	50 Hz	100 Hz	180 Hz	210 Hz
250 Hz	300 Hz	400 Hz	600 Hz	700 Hz	900 Hz	1000 Hz	

Table 0.2: Optimized frequency set for the calculation of the impedance matrices.

The curves depicted in Figure 0.18 show that the results obtained with the optimized frequency set are nearly coincident to the ones computed with the 1Hz step, but with a significant decrease of the computational effort (Figure 0.17).

3.4 Validation of the numerical model

In this section, the results calculated with the Actran's modal frequency response analysis are compared to the ones obtained with the experimental tests to assess their validity.

3.4.1 Frequency response of the bare plate

The first comparison is carried out between the accelerance FRF curves measured with the three accelerometers on the bare plate and the results calculated with the equivalent FE model, built by means of shell elements (Figure 0.19).

Comparing the numerical and the experimental FRF curves evaluated in correspondence of the three points on the surface of the plate, it can be observed that the most significant discrepancies are found for the accelerometers A1 and A2, while the correlation obtained for A3 is quite good up to 700 Hz. A possible explanation for the discrepancies can be found in the position of the two accelerometers. Since A1 and A2 are placed closer to the top with respect to A3, they are more influenced by the interaction between the plate and the hangers, which is not taken into account in

the FE model, where the plate is supposed to be unconstrained. Another factor that might explain the differences between the numerical and the experimental results is the shape of the plate. In the finite element model the plate is supposed to be perfectly flat and with a constant thickness, while the actual component, which is obtained by cold rolling, presents a little curvature and a certain variation of the thickness between the center and the borders. Based on these considerations, a possible improvement in the consistency of the results might be obtained by testing different kinds of hangers, using panels with a more strict flatness tolerance and employing ultrasonic gaging to determine the thickness of the plate in several points on its surface.

Since the results calculated in correspondence of A3 are the most consistent with the experimental measurement, from here on the validation process is conducted by making reference only to that accelerometer, while the other two are not taken into consideration.

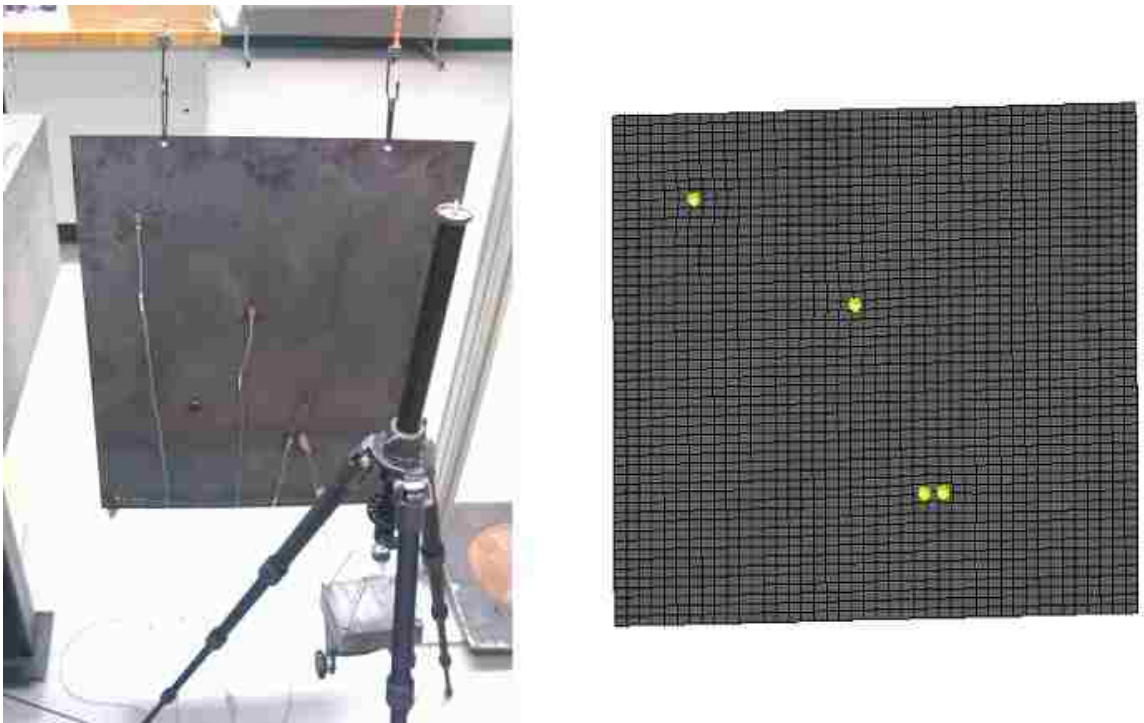


Figure 0.19: Steel plate and equivalent FE model.

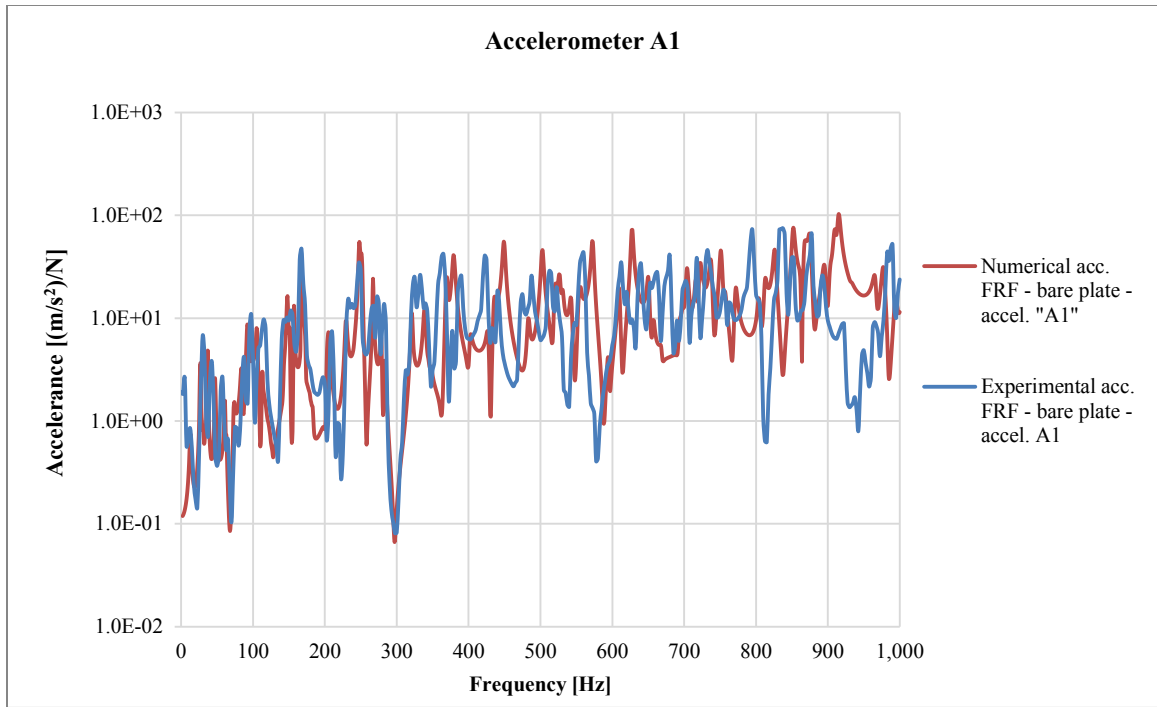


Figure 0.20: Comparison between the experimental and the numerical FRF curves, evaluated for the bare plate in correspondence of the accelerometer A1.

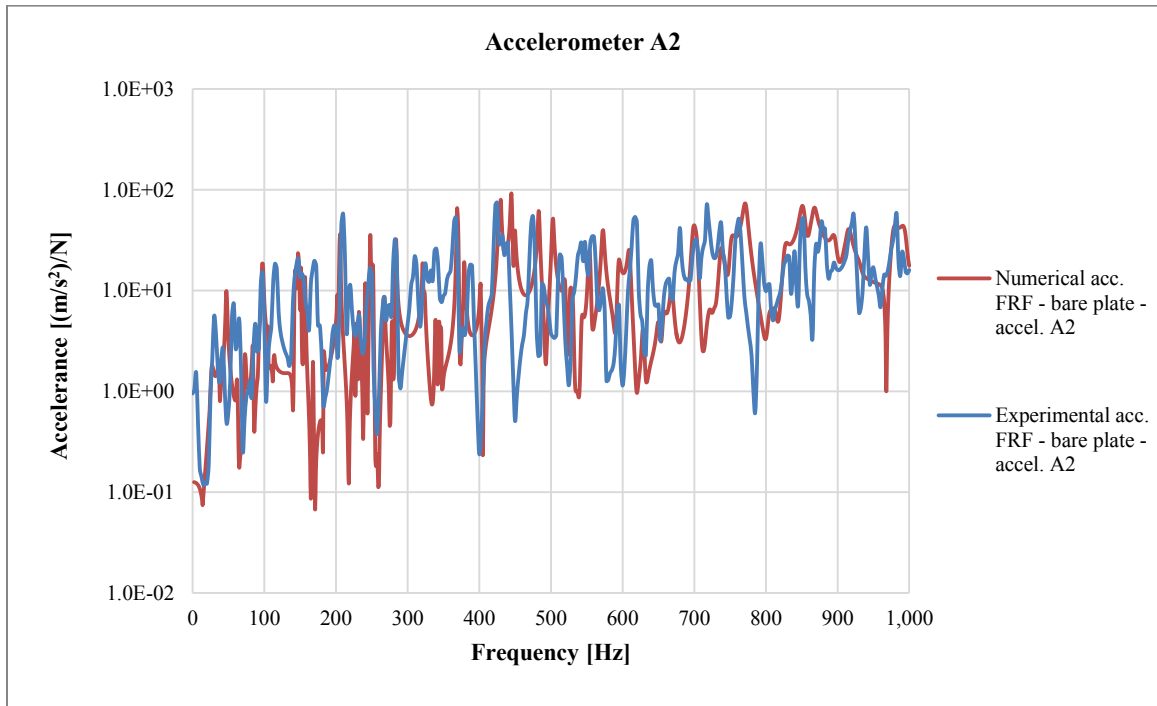


Figure 0.21: Comparison between the experimental and the numerical FRF curves, evaluated for the bare plate in correspondence of the accelerometer A2.

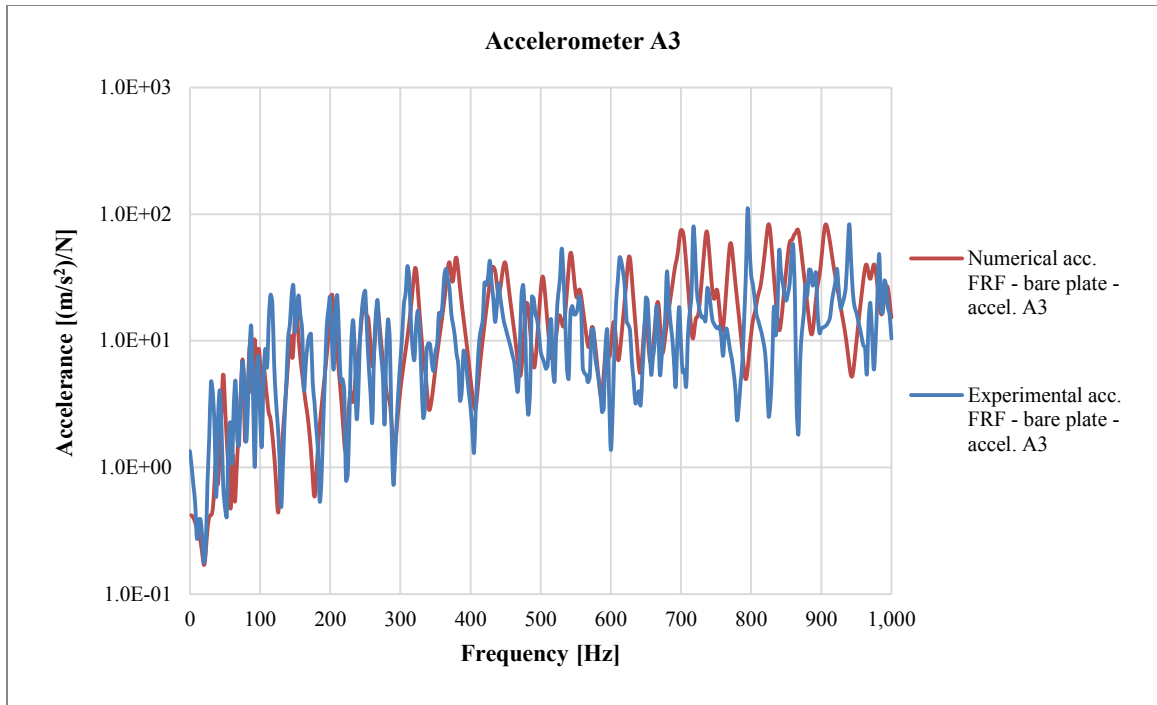


Figure 0.22: Comparison between the experimental and the numerical FRF curves, evaluated for the bare plate in correspondence of the accelerometer A3.

3.4.2 Effect of the porous treatments on the frequency response of the plate

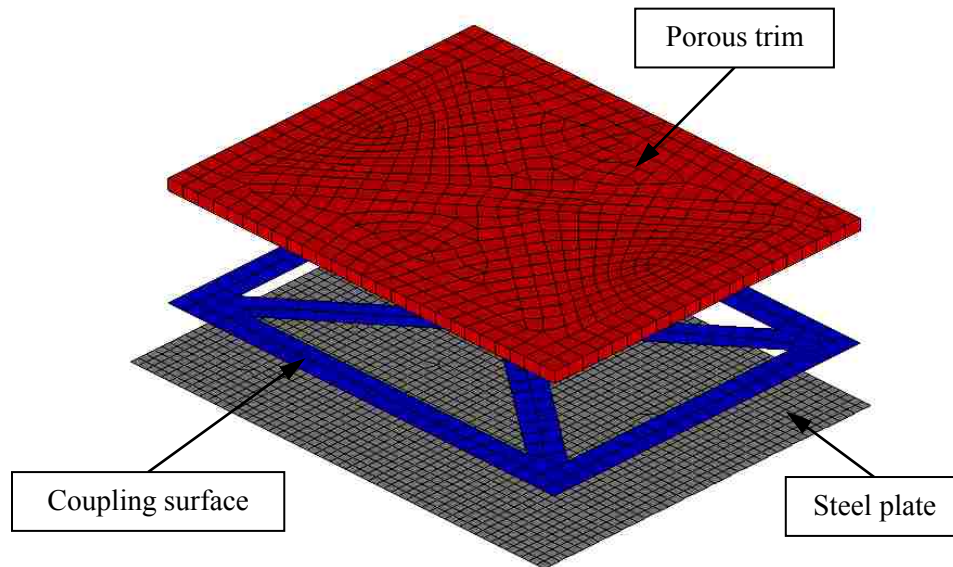


Figure 0.23: Exploded view of the finite element model of the treated plate.

The finite element model used for the calculation of the frequency response of a treated panel is constituted by the meshes of the plate and the porous trim. These meshes are respectively made of shell and solid elements, and by a coupling surface which defines the regions of the treatment where the nodes are projected on the non-coincident mesh of the elastic domain, as depicted in Figure 0.34. In the model used for the validation of the experimental tests, the coupling surface corresponds to the areas where the plate and the treatment are joined by the tape, while in the other regions, where the two component are coupled with a sliding contact, the interaction between the two is not taken into account, as the software cannot model this kind of coupling condition.

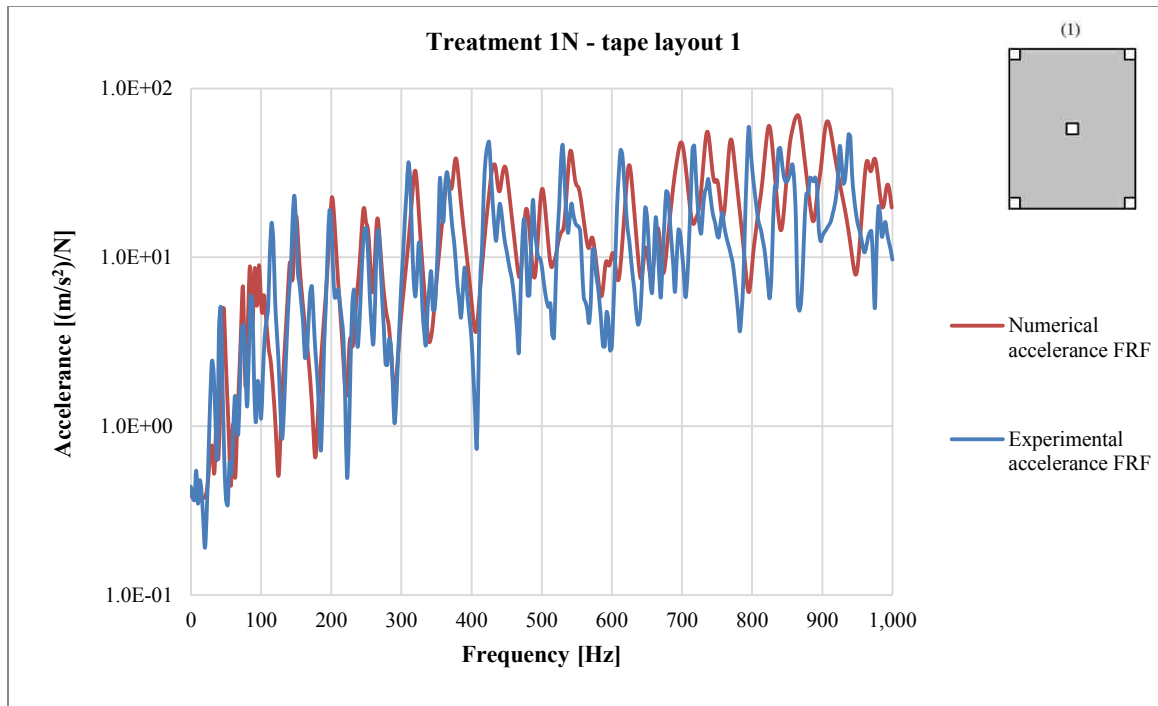


Figure 0.24: Comparison between experimental and numerical FRF curves, evaluated at accelerometer A3 for the plate treated with the porous 1N joined with the tape layout 1.

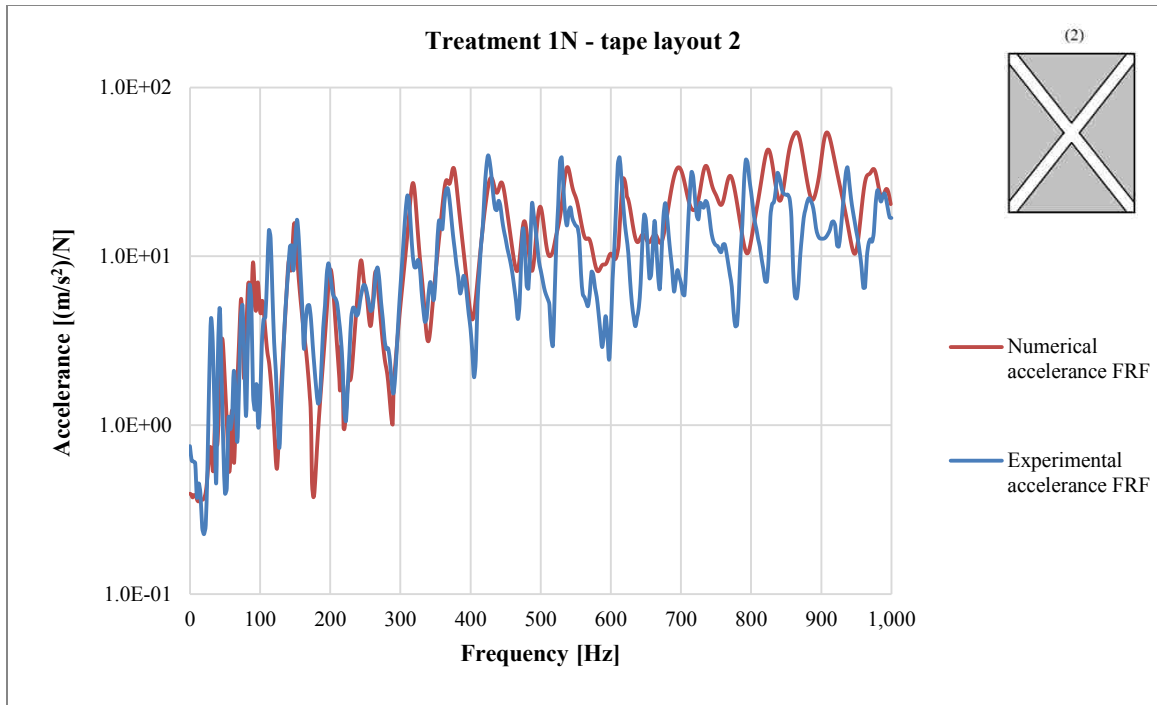


Figure 0.25: Comparison between experimental and numerical FRF curves, evaluated at accelerometer A3 for the plate treated with the porous 1N joined with the tape layout 2.

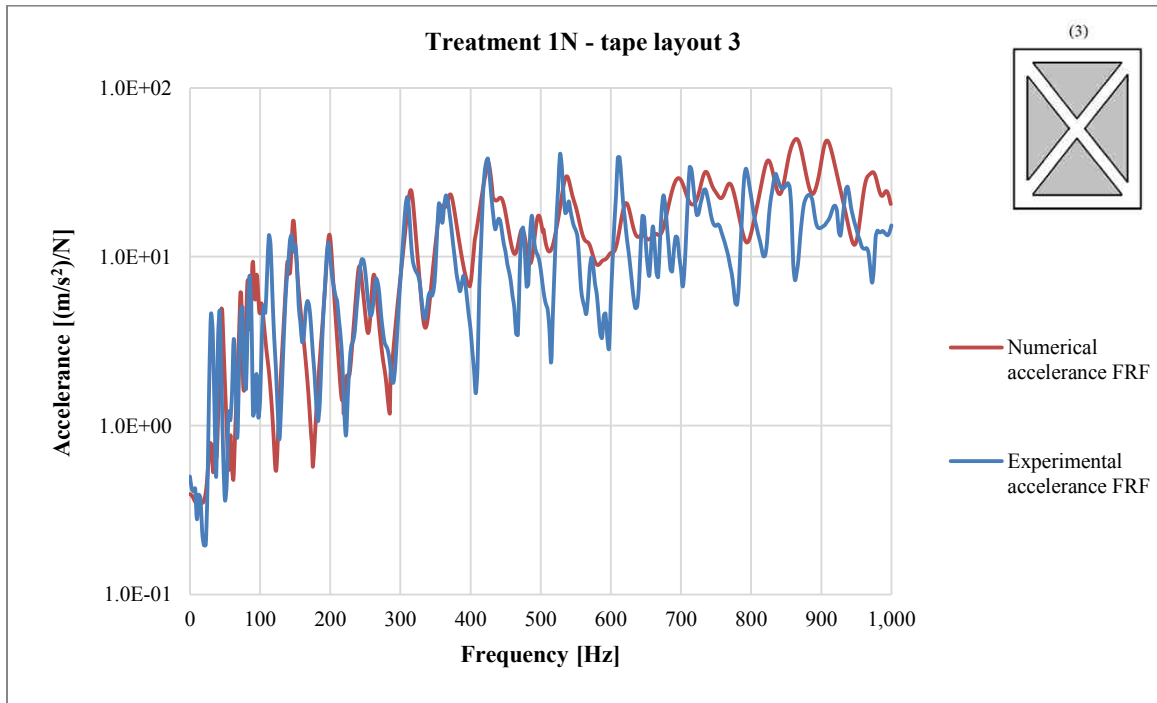


Figure 0.26: Comparison between experimental and numerical FRF curves, evaluated at accelerometer A3 for the plate treated with the porous 1N joined with the tape layout 3.

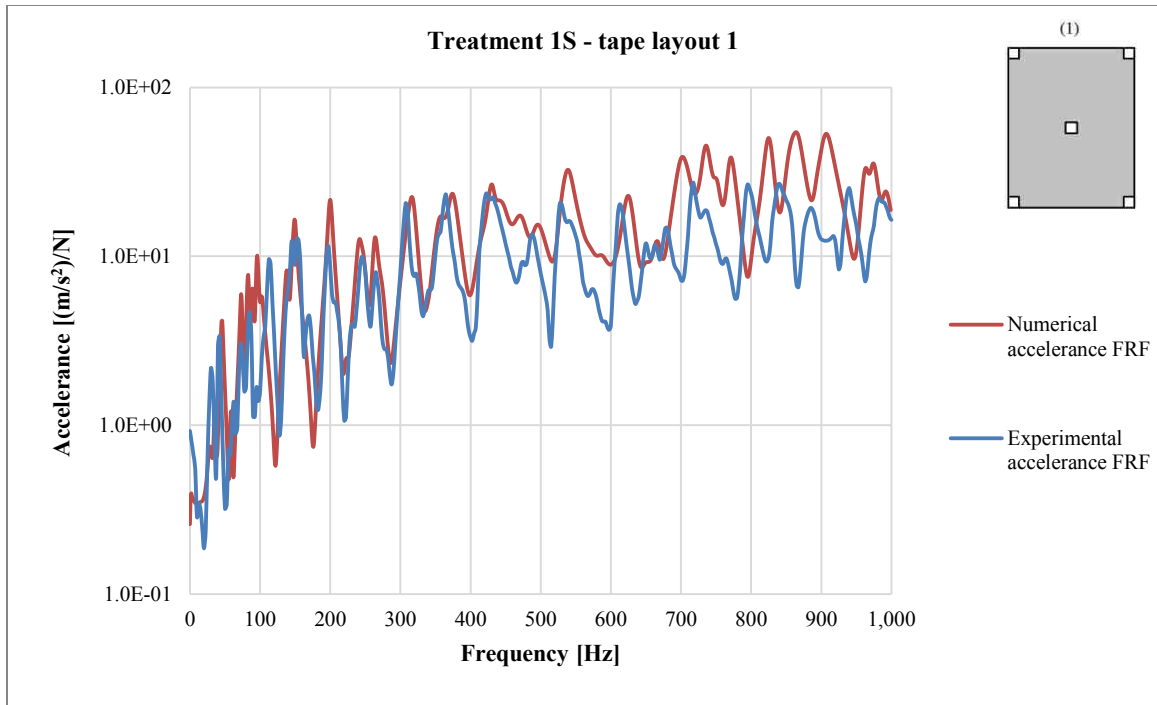


Figure 0.27: Comparison between experimental and numerical FRF curves, evaluated at accelerometer A3 for the plate treated with the porous 1S joined with the tape layout 1.

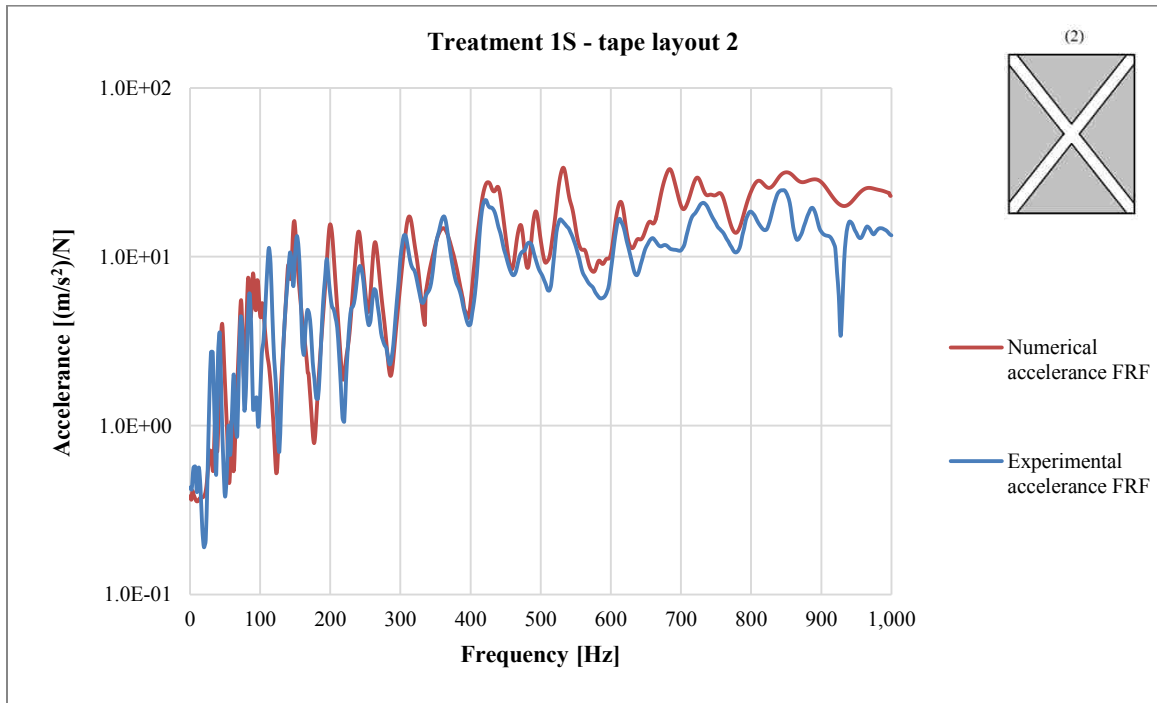


Figure 0.28: Comparison between experimental and numerical FRF curves, evaluated at accelerometer A3 for the plate treated with the porous 1S joined with the tape layout 2.

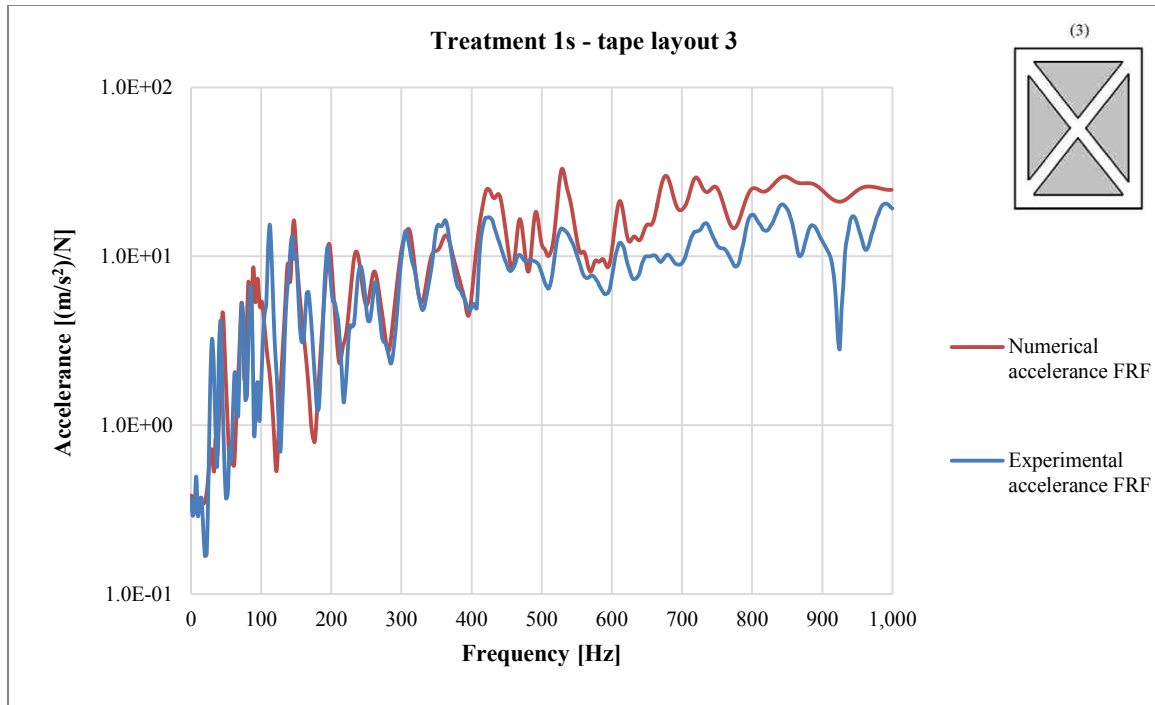


Figure 0.29: Comparison between experimental and numerical FRF curves, evaluated at accelerometer A3 for the plate treated with the porous 1s joined with the tape layout 3.

Comparing the numerical and the experimental FRF curves obtained for the treated plate, it can be observed that the effect of the poroacoustic treatments on the response of the panel is represented more accurately at the lower frequencies, while above 400-500 Hz larger discrepancies arise. In particular, the numerical results tend to overestimate the amplitude of the vibration with respect to the experimental outcomes, yet maintaining the same overall trend of the curve. Despite this amplitude shift, occurring at the higher frequencies, the comparison with the experimental results confirms the validity of the numerical outcomes for the purposes of the current study. In fact, examining the FRF curves obtained with the poroacoustic trims 1S and 1N, it can be stated that the model is capable of interpreting the characteristics of the two different treatments and the impact that they have on the frequency response of the plate.

In addition to that, the comparison also shows that the different joining conditions between the treatment and the plate (which are determined by the layout of the tape), are properly represented with the equivalent coupling surfaces.

3.5 Sensitivity analysis on porous material properties

By comparing the FRF curves obtained for the plate treated with the poroacoustic materials 1N and 1S, it can be observed that the different treatments have a different effect on the response of the system. The differences are not only related to the thickness of the treatment and to the way it is coupled with the plate, but also to the different characteristics of the porous materials.

In order to have a better understanding of how the porous material properties affect the frequency response of the plate-trim system, the numerical model is employed to conduct a sensitivity analysis. Since the final objective of the thesis is to investigate, by means of FE numerical simulations, the possibility of employing the poroacoustic materials for damping the vibration of car body panels, the sensitivity analysis is focused on two principal aspects:

- Evaluation of the relationship between the porous material properties and the response of the plate-trim system, with a focus on the way the vibration damping effect produced by the treatment is influenced by each property.
- Model simplification, obtained by determining if any of the properties of the porous materials have no influence on the response of the plate-trim system, so that number of the input variables necessary for the simulations can be reduced.

3.5.1 Methodology

The study is conducted with the OFAT methodology, which is one of the simplest and most common approaches to the sensitivity analysis. The OFAT methodology allows evaluating the effect that the variation of the input quantity has on the output by changing one input variable at time and keeping the others at their nominal values.

Apart from its simplicity, the OFAT approach has the great advantage of isolating the effects of each variable separately, as any change observed in the output is unambiguously attributed to the change of a single input. On the other hand, since it does not consider the simultaneous variation of the input variables, the interactions between the various parameters cannot be investigated.

With regard to the case considered in this thesis the input variables are constituted by the porous material properties, while the FRF curves represent the output. The analysis is conducted using the same finite element model for every simulation (i.e. the same meshes of the two components and the same coupling surface between them) and measuring the response of the plate each time one of the material properties of the porous treatment is changed. The variation of the input variable occurs about a nominal value and it is defined by a maximum and a minimum. Hence, before proceeding to the analysis, it is necessary to establish the nominal value of each material property as well as its range of variation. Since these quantities must be consistent with the ones of the actual porous treatments, they are derived from a database of physically measured material properties, which is created using the data acquired from the review of literature, the ones contained in the Actran material library and the ones provided from the supplier of the samples used for the experimental tests (Table 0.3).

Material	ρ_s [Kg/m ³]	R [Ns/m ⁴]	Ω	α_∞	Λ_v [m]	Λ_t [m]	E_s [Pa]	η
Polymer foam	-	300000	<u>0.99</u>	2.5	<u>2.00E-04</u>	<u>5.00E-04</u>	<u>800000</u>	0.2
Polymer foam	-	<u>1000</u>	0.94	<u>1</u>	2.00E-05	4.00E-05	50000	0.05
Polymer foam	1420	34614	0.97	1.88	3.10E-05	1.91E-04	75000	0.3
Felt	1460	33400	0.96	1.03	3.20E-05	1.26E-04	<u>12300</u>	0.1
Felt	1460	<u>735007</u>	0.66	<u>3.17</u>	3.20E-05	<u>5.00E-06</u>	207000	0.2
Felt	1810	21110	0.97	1.08	6.93E-05	1.29E-04	71468	0.06
Felt	1793	104872	0.92	1.1	2.62E-05	7.87E-05	65085	0.1
Various (max. val.)	<u>2000</u>	-	0.97	2.33	-	-	-	<u>0.49</u>
Various (min. val.)	1400	-	<u>0.56</u>	1.3	-	-	-	<u>0.016</u>
Polymer foam	<u>827</u>	22000	0.97	1.38	<u>1.70E-05</u>	4.00E-05	192000	0.13

Table 0.3: Material properties database, with the maximum and minimum values underlined for each variable.

	ρ_s [Kg/m ³]	R [Ns/m ⁴]	Ω	α_∞	E_s [Pa]	Λ_v [m]	Λ_t [m]	η
Max	2000	735007	0.99	3.17	800000	2.00E-04	5.00E-04	0.49
Avg	1521	156500	0.89	1.71	184107	5.34E-05	1.39E-04	0.16
Min	827	1000	0.56	1.00	12300	1.70E-05	5.00E-06	0.02

Table 0.4: Nominal values and range of variation for the porous material properties.

3.5.2 Relationship between the porous material properties and the response of the system

The following sections examine the effects of the variation of each porous material property on the response of a treated panel. In particular, the FRF curves calculated using the maximum and the minimum values of each property are compared on the same Bode plot.

3.5.2.1 Solid density and porosity

In Figure 0.30 and Figure 0.31, the FRF curves relative to the maximum and the minimum values of porosity and solid density of the acoustic treatment are presented. Comparing the curves corresponding to the maximum and the minimum values of the material properties in each of the two diagrams, it can be observed that the resonance peaks present a certain frequency shift, which is particularly evident in the range of frequencies between 0 and 250 Hz, where the peaks are closer to each other. In a similar way to a single DOF system (e.g. a mass connected to a spring), for which the natural frequency is equivalent to (0.11), the shift observed in the FRF curves of the treated plate is related to the variation of the mass of treatment.

$$f_n = \frac{1}{2\pi} \sqrt{\frac{k}{m}} \quad (0.11)$$

The relationship between the overall mass of the system and the two material parameters of porosity and skeleton density is expressed in (0.12) .

$$m_{tot} = m_{plate} + V_{treatment} [\Omega \rho_f + (1 - \Omega) \rho_s] \quad (0.12)$$

Apart from the frequency shift, the principal consequence of the increased mass of the treatment is the reduction of the amplitude of the response and the suppression of certain resonance peaks.

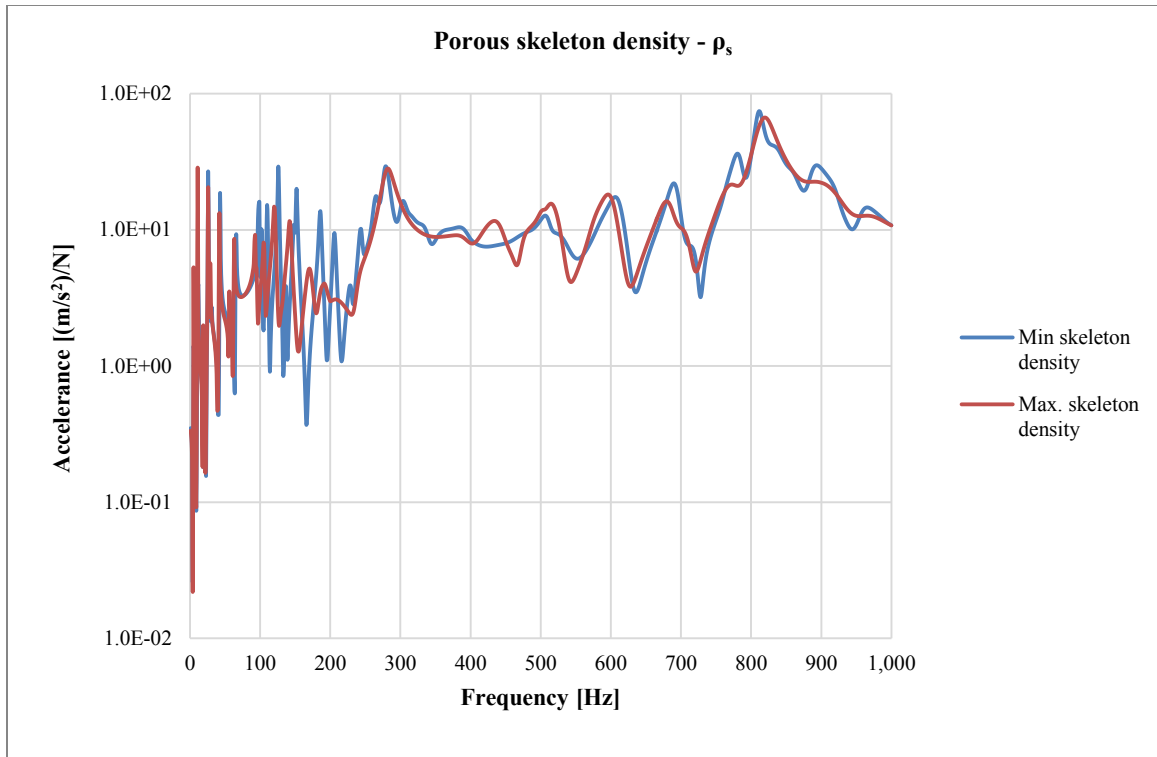


Figure 0.30: Effect of the input porous skeleton density on the output frequency response.

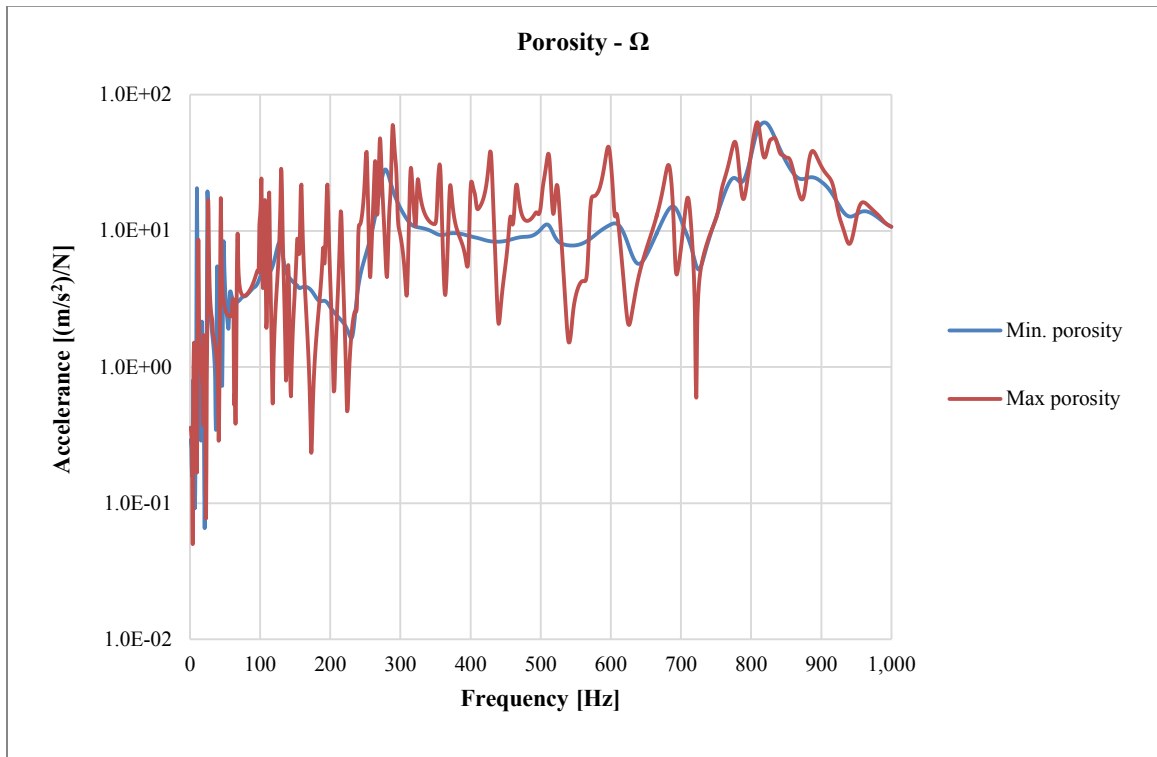


Figure 0.31: Effect of the input porosity on the output frequency response.

This effect is quite limited for the treatment with a high solid density while it is particularly sharp for the one with a low porosity. In the first case, the vibration reduction is related only to the additional mass, while in the second case it is associated also to the elevated amount of material in the solid phase, which allows higher viscous dissipations.

3.5.2.2 Air flow resistivity and skeleton loss factor

As reported in the review of literature, the energy dissipations that occur within the porous treatments are caused mainly by the friction between the surface of the porous skeleton and the fluid flowing inside its channels, which is associated to the value of the airflow resistivity, and by the hysteresis of the elastic skeleton during a deformation cycle, which is associated the loss factor. In this section, the effects of these two dissipation mechanisms on the output response of a treated plate are reviewed.

Figure 0.32 and Figure 0.33 show the different frequency responses related to the maximum and minimum values of airflow resistivity, while Figure 0.34 and Figure 0.35 illustrate the ones related to the loss factor. Due to the fact that, according to a research reported in the review of literature [27], the relative importance of each dissipation mechanisms depends on the stiffness of the porous material, the comparison is carried out taking into consideration both a stiff and a soft material (i.e. with a high and low Young's modulus). In general, it can be observed that increasing the values of airflow resistivity and loss factor the amplitude of the response drops in correspondence of the resonance peaks, indicating that the porous material has a higher vibration damping effect on the panel. Since both the dissipation phenomena are related to the speed of the deformation, this effect becomes more significant at the higher frequencies. The comparison between the FRF curves calculated for the stiff and the soft material indicates that the variation of the air-flow resistivity has a smaller impact on the response of the system when the Young modulus increases, while on the contrary the impact of the loss factor becomes more significant.

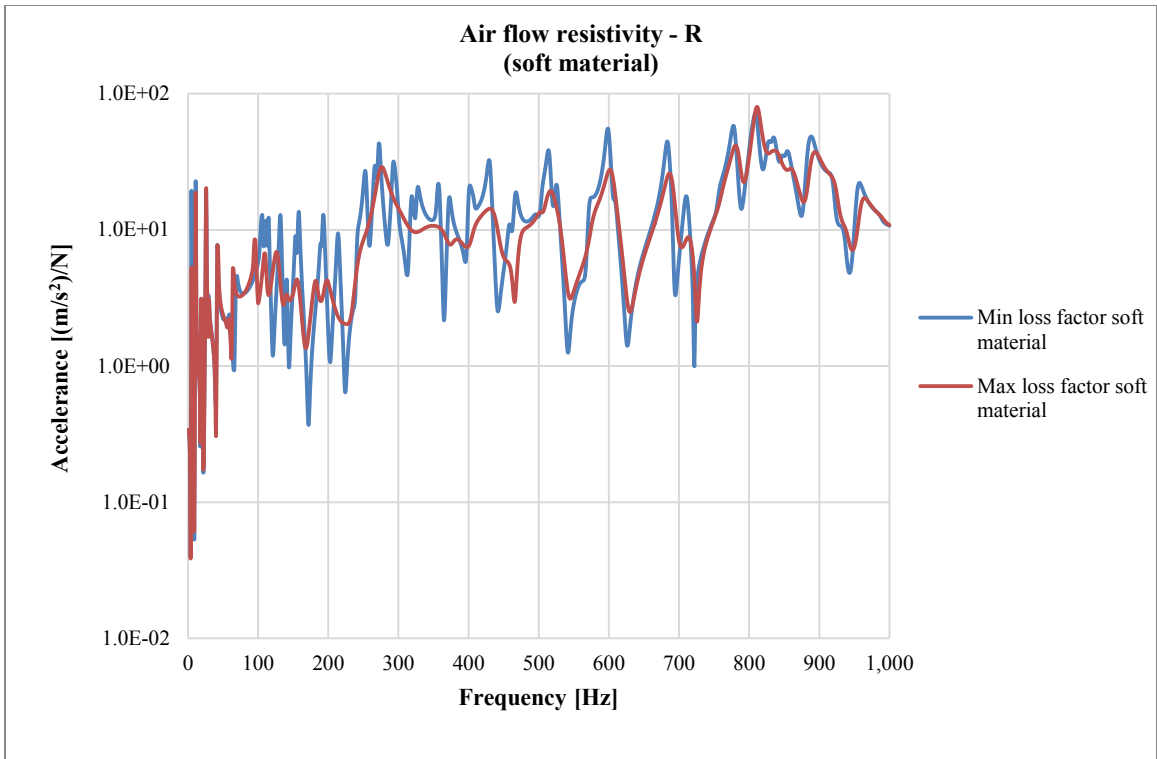


Figure 0.32: Effect of the input air flow resistivity on the output frequency response.

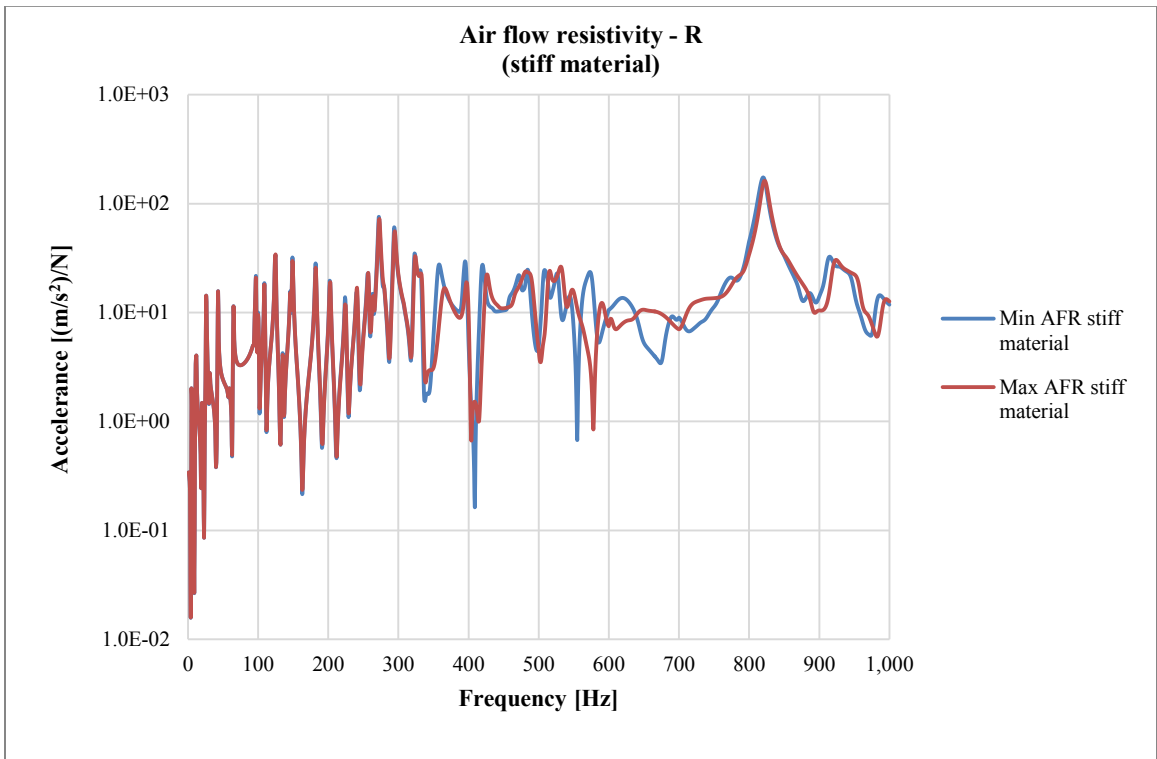


Figure 0.33: Effect of the input air flow resistivity on the output frequency response.

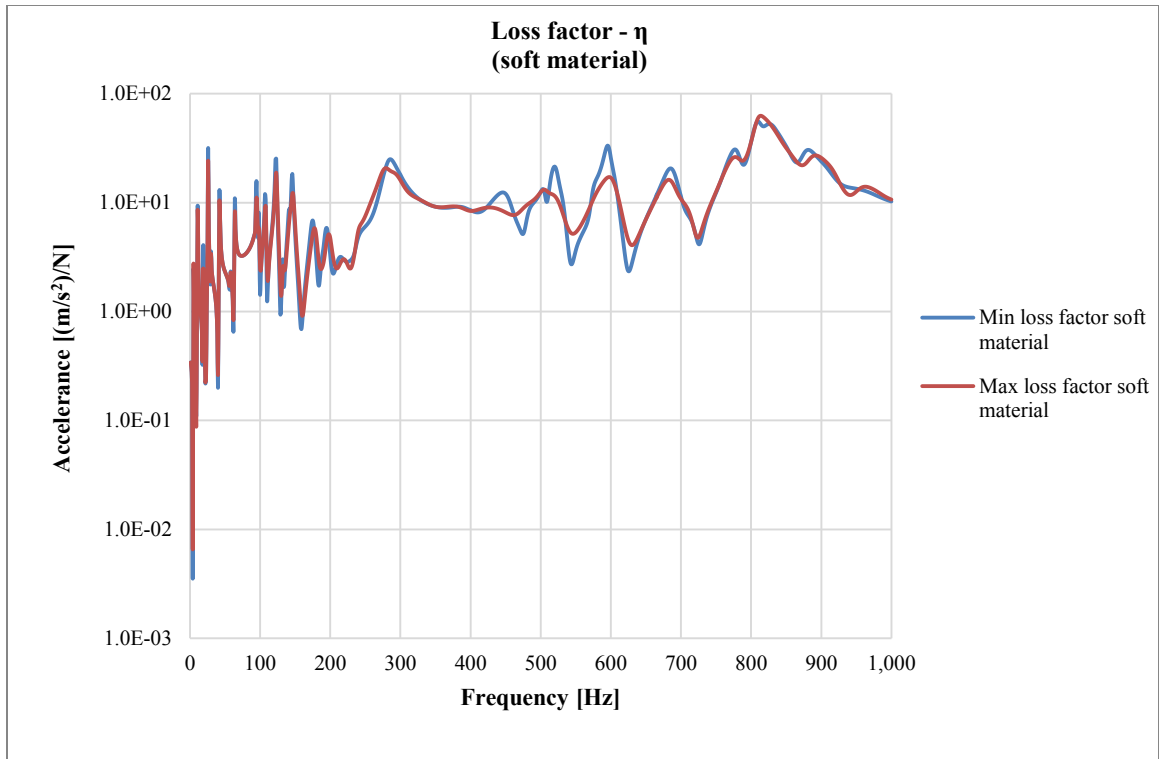


Figure 0.34: Effect of the input air flow resistivity on the output frequency response.

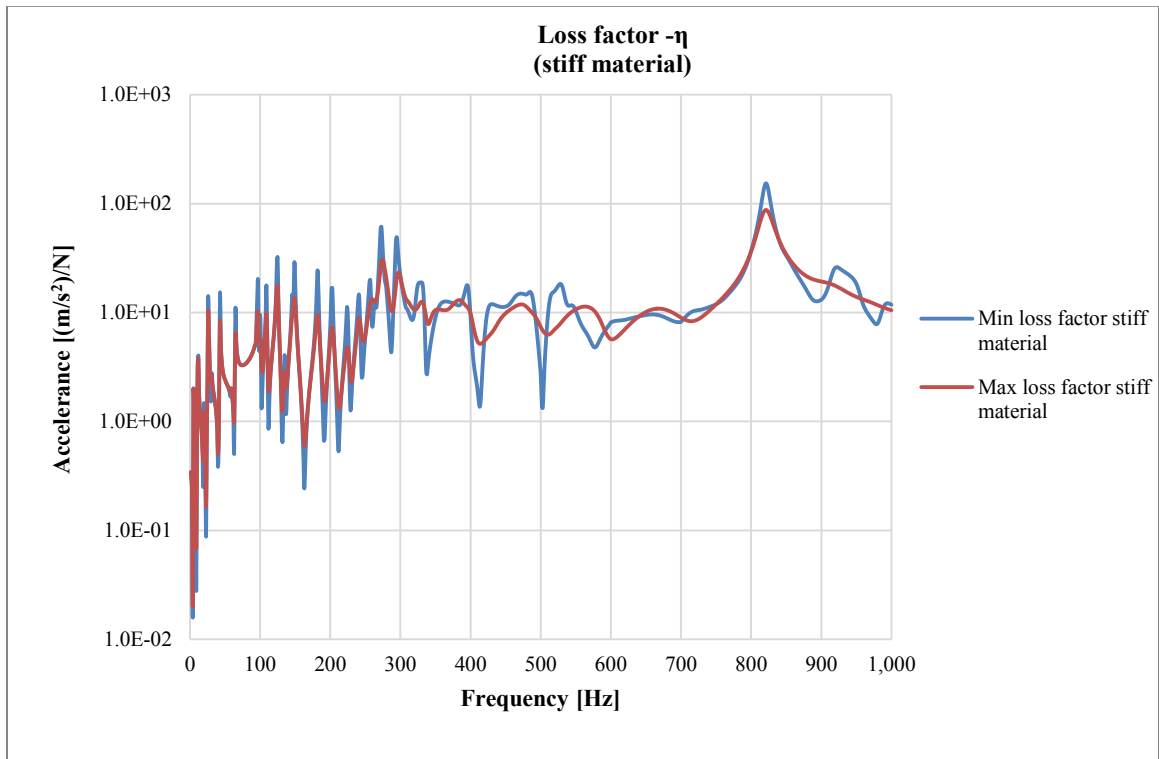


Figure 0.35: Effect of the input air flow resistivity on the output frequency response.

3.5.2.3 *Young's modulus of the skeleton*

Figure 0.36 shows the two frequency responses related to the maximum and minimum Young's modulus of the porous skeleton. From the comparison between the two curves it can be noticed that the stiffness of the porous material has a considerable impact on the response of the system. In particular the treatment with a lower Young's modulus shows a significantly higher damping level with respect to the stiffer one. This phenomenon can be explained by the fact that the energy dissipations occurring within a porous treatment are related to the deformation of the skeleton, which is inversely proportional to its Young's modulus.

Furthermore, due to the large difference between the Young's modulus of the plate (210 GPa) and the maximum Young's modulus of the skeleton of the porous material (800 KPa), it can be observed that Bode plot do not present any frequency shift, as the contribution of the porous treatment to overall stiffness of the system is negligible.

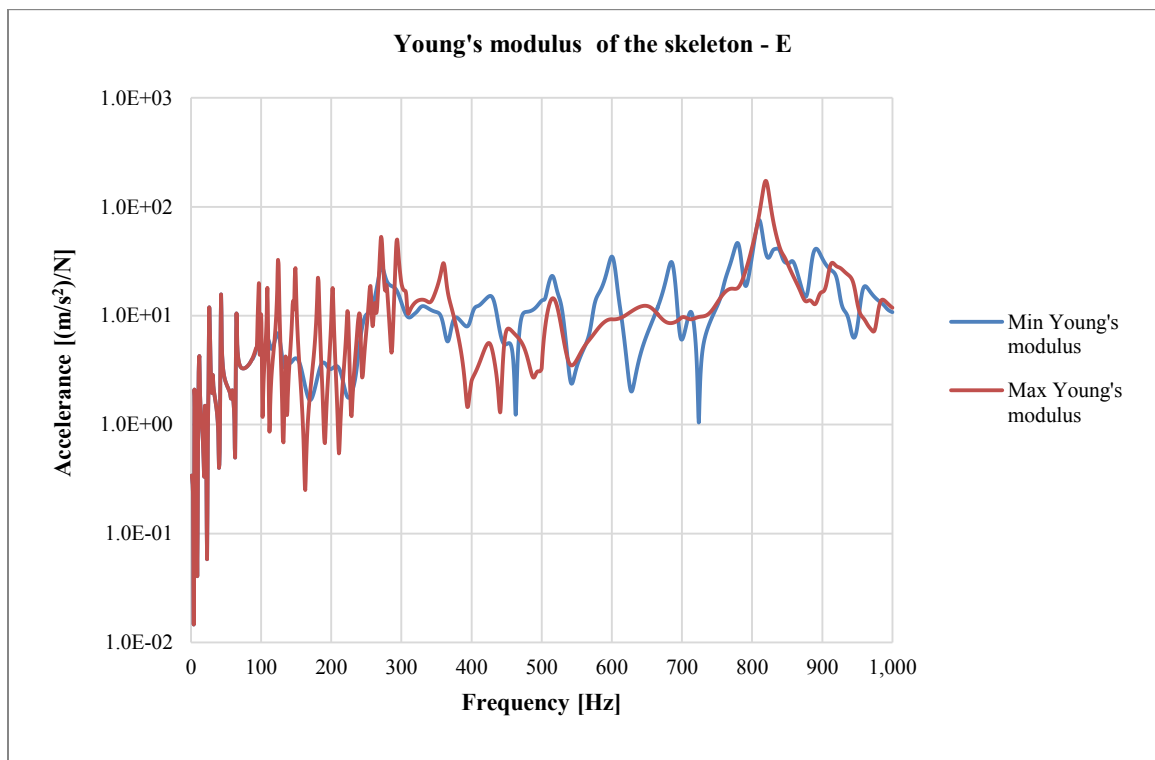


Figure 0.36: Effect of the input Young's modulus parameter on the output response.

3.5.3 *Negligible parameters*

The comparison among the results obtained with different values of tortuosity, viscous characteristic length and thermal characteristic length, shows that those parameters do not affect the frequency response of the system to a mechanical excitation, as the FRF curves are found to be coincident. From a physical standpoint this results indicates that the shape of the porous skeleton does not affect the dynamic response of the treated plate, while from the point of view of the numerical analysis it suggest that these three input variables can be neglected in the simulations.

3.6 **Vibration damping performances of poroacoustic treatments**

This section compares the vibration damping performance of different poroacoustic treatments provided by the suppliers and presents the possible benefits related to the adoption of new materials with ideal characteristics.

3.6.1 *Performance index*

The first step for evaluating the vibration damping performance of different treatments is the definition of a quantity allowing the comparison between them. Considering that for a system the vibration damping is related to the reduction of the amplitude of its response, the FRF curves might be used as graphical tool for the comparison. However, because the FRF are obtained through a single output point and that they take different values according to the frequency, their interpretation is sometimes ambiguous. For these reasons, it is necessary to introduce a new index that facilitates the comparison among the responses obtained with the different treatments, which must be related to the overall vibration level of the system. An index of this kind is the average RMS acceleration in 1/3 octave band (\overline{RMS}_{Ab}), which is defined as in (0.13). In the equation N is the number of points of the structure over which the acceleration RMS is averaged, f_{h_b} and f_{l_b}

are the upper and lower limits of the 1/3 octave band considered, f_s is the sampling step of the frequencies and A is the calculated acceleration.

$$\overline{RMS}_{A_b} = \frac{1}{N} \sum_{n=1}^N \left(\sqrt{\frac{1}{\left(\frac{f_{h_b} - f_{l_b}}{f_s}\right)} \sum_{f=f_{l_b}}^{f_{h_b}} (A(f))^2} \right)_n \quad (0.13)$$

3.6.2 Comparison between different materials

The comparison among the vibration damping performance of the different treatments is conducted by means of numerical simulations. The same FE model, composed by an acoustic treatment completely attached to the surface of a steel plate, is used for all the treatments and only the materials properties of the porous trim are changed. The RMS acceleration is averaged over the responses of all the nodes of the panel for each of the 1/3 octave bands.

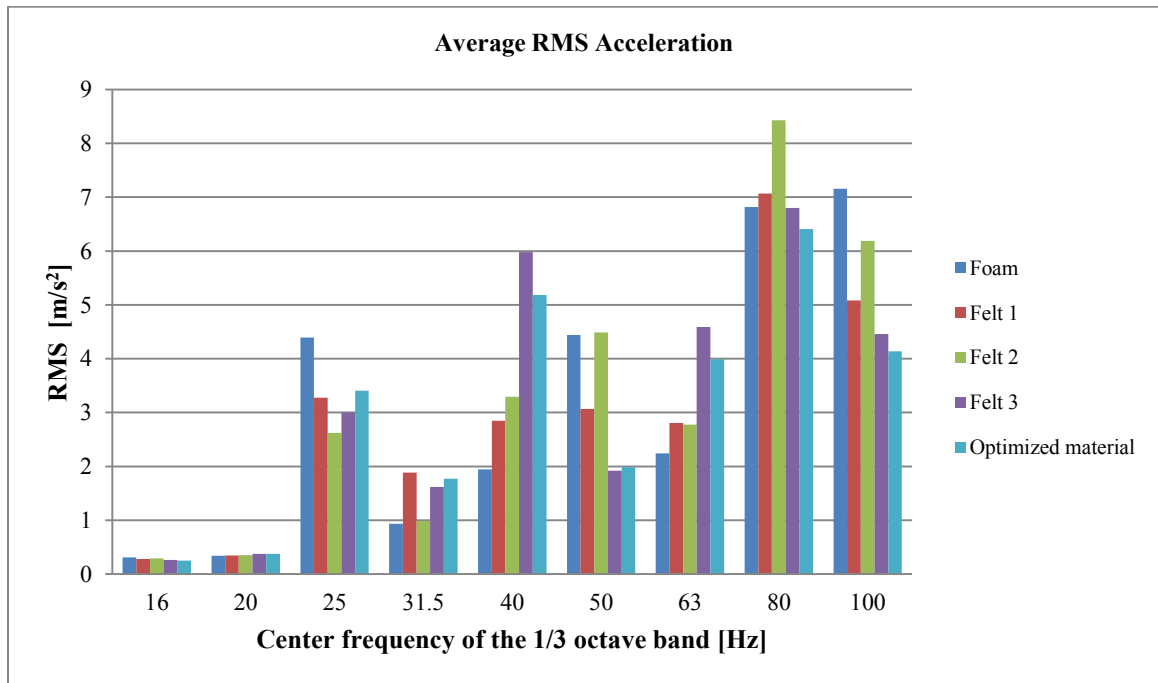


Figure 0.37: Average RMS acceleration of the treated plate in 1/3 octave bands between 14.1 and 112 Hz.

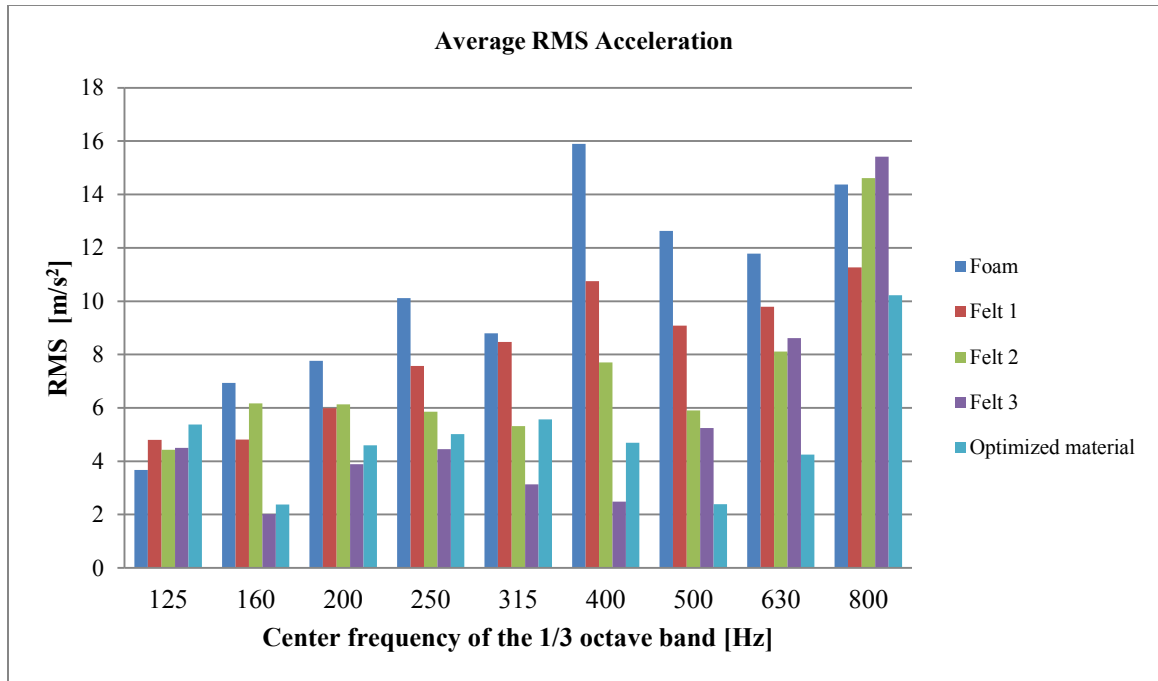


Figure 0.38: Average RMS acceleration of the treated plate in 1/3 octave bands between 112 and 891 Hz.

In total five different treatments are compared, four of which chosen among the ones made available from the suppliers and the other one virtually created imposing the ideal characteristics found with the sensitivity analysis.

ρ_s [Kg/m ³]	R [Ns/m ⁴]	Ω	E_s [Pa]	η
827	735007	0.85	105000	0.49

Table 0.5: Material properties of the optimized treatment.

Examining the results presented in Figure 0.37 and Figure 0.38 it is possible to determine for each frequency band which material, among the ones taken into consideration, possess the best damping characteristics (i.e. the one which shows to the lowest average RMS acceleration).

Furthermore, the weighted mean of the average RMS acceleration is calculated for each treatment, thus providing a unique index of its damping performance for the whole range of frequencies examined. The results are presented in Figure 0.39. On the same plot, the densities of

the treatments are also reported, in order to compare the impact of each treatment on the overall weight of the vehicle.

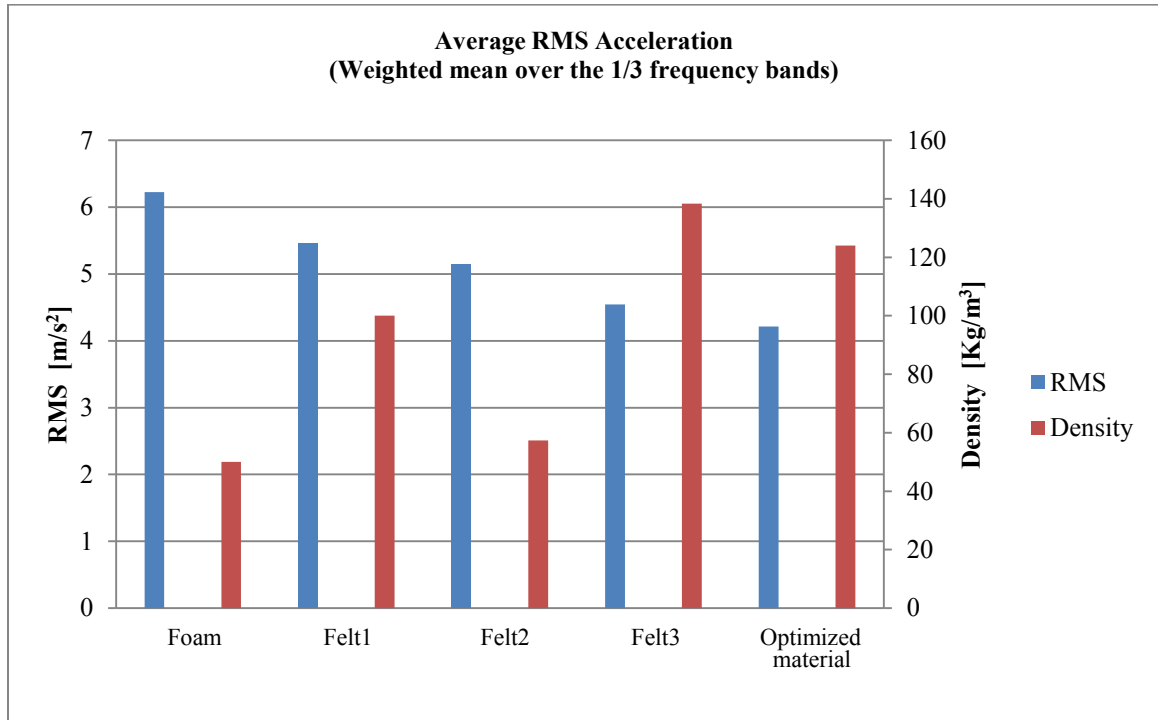


Figure 0.39: Weighted mean calculated over the 1/3 frequency bands of the average RMS acceleration of the plate treated with different poroacoustic materials.

Examining the results in Figure 0.39, it can be observed that among the existing materials Felt3 is the one that offers the best performances in terms of vibration damping. From the comparison, it also emerges that the two treatments that show the lowest value of acceleration RMS are also the heaviest ones. It must be noted, however, that the density and the vibration reduction are not directly correlated.

As for the ideal treatment, the fact that it allows reaching the lowest average vibration level and that its density is smaller than the one of Felt 3, confirms that it is possible to further improve the performance of the porous treatments by acting on their material properties.

3.7 Use of the poroacoustic treatments on a vehicle for damping the vibration of the floor

The current solution employed for the control of noise and vibration on the floor of the vehicles involves the use of various layers of different materials, as depicted in Figure 0.40.

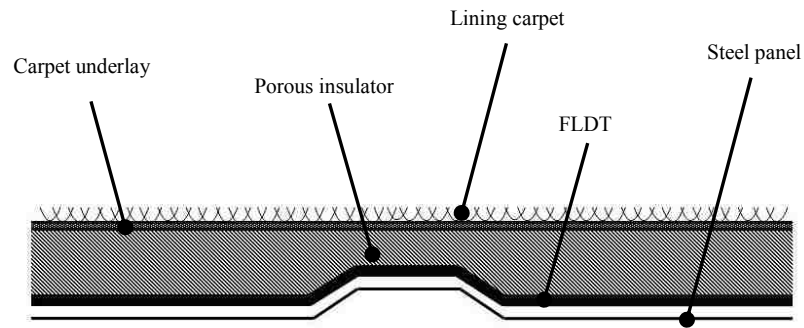


Figure 0.40: Layout of the treatments applied to the floor of a mid-segment vehicle.

The first layer is composed of the viscoelastic damping treatments, which are made of a bituminous material that is thermally bonded to the panels of the floor. In order to reduce the overall weight of the car body, the damping treatments are applied only to the areas of the floor that show a particularly elevated vibration level, rather than its whole surface. These regions are usually identified with the finite element analysis, which allows the topological optimization of the viscous layer.



Figure 0.41: Example of damping treatments layout on a vehicle's floor.

On the top of the damping treatments there is another layer composed of the noise insulating treatments, which are made of porous materials like foam or felt. These treatments are usually placed in the most critical regions of the floor from the point of view of noise transmission, like the wheel arches and the area under the rear seats. The porous treatments are usually glued to the lining carpet, which is made of rubber and fibers. The carpet is distributed over the whole floor and it is joined to the car body by means of fasteners. Each of the three layers described above has a specific function: the damping treatment reduce the vibration level and the transmission through the structure borne path, the porous trim insulate the passenger compartment acting on the airborne path, and the carpet serves as an aesthetic finish and reduce the reverberation within the cabin. However, since the results obtained in the course of this research work suggest that the porous treatments may be used to damp the vibration of the car body panels, the two functions of vibration damping and noise insulation might be integrated into a unique component. For this reason in the following sections a series of numerical tests are conducted to investigate the possibility of removing the standard FLDT and using the poroacoustic treatments in their place to damp the vibration of the floor.

3.7.1 Comparison among different layouts of the treatments

This section aims to assess the overall vibration levels of the floor that can be achieved by attaching the viscoelastic and poroacoustic treatments to its surface in different configurations.

In particular, five layouts are examined:

- Layout 1: Standard FLDT only, thickness 2 or 4 mm
- Layout 2: Poroacoustic treatment distributed over the whole surface of the floor and completely glued to the steel panels, thickness 10, 20, 30 or 40 mm.
- Layout 3: Poroacoustic treatment placed on the same surface as the FLDT in layout 1 and completely glued to the steel panels, thickness 10, 20, 30 or 40 mm.

- Layout 4: FLDT thickness 2 mm, and poroacoustic treatment distributed over the whole surface of the floor and completely glued to the steel panels, thickness 10, 20, 30 or 40 mm, the
- Layout 5: FLDT thickness 2 mm, and poroacoustic treatment placed on the same surface as the FLDT in layout 1 and completely glued to the steel panels, thickness 10, 20, 30 or 40 mm.

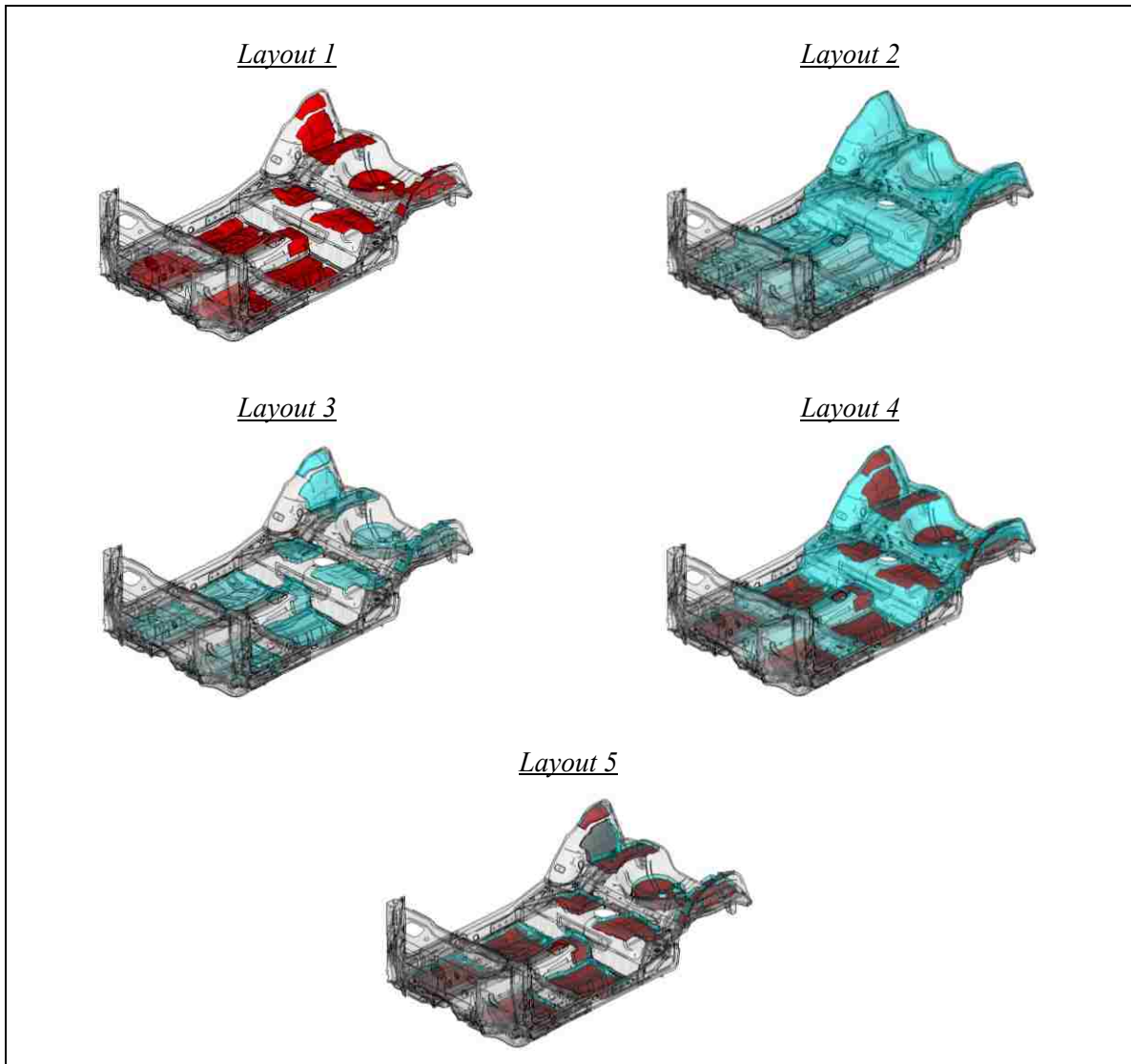


Figure 0.42: Alternative treatments layouts compared.

3.7.1.1 Performances evaluation method

In order to evaluate the vibration damping performance of the different layouts it is necessary to compare the average vibration level of the floor when each of them is employed. The procedure used for the evaluation is similar to the one described in 3.6.1. The structure is excited with a dynamic load along the z-axis, applied in correspondence of the right rear suspension mount, and the frequency response is measured for an elevated number of nodes, randomly chosen on the surface of the floor, as depicted in Figure 0.43. After that, the average RMS is calculated, for each 1/3 octave band, according to the equation (0.13).

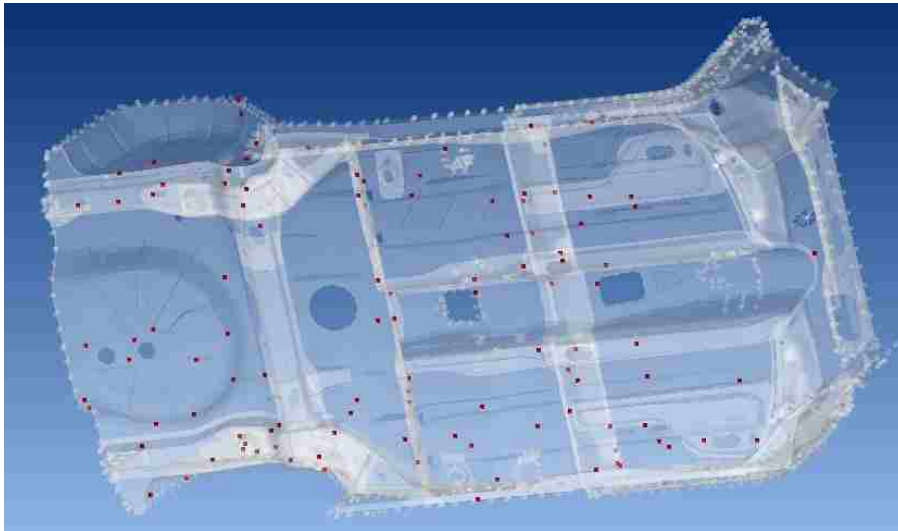


Figure 0.43: Randomly selected response nodes for the evaluation of the average vibration level of the floor.

For facilitating the graphical comparison the average RMS is normalized (i.e. it is referred to the mean value among the various configuration in each frequency band), as indicated in (0.14).

$$\overline{RMS}_{norm} = \frac{\overline{RMS}_{A_b,j}}{\frac{1}{M} \sum_{M=1}^M (\overline{RMS}_{A_b,i})} \quad (0.14)$$

In the equation, j indicates the current configuration of the floor (treatment, thickness, etc.) and m all the other M configurations examined.

In order to have a unique indicator of the average vibration level obtained with each configuration, the mean value of $\overline{RMS}_{A_b, norm}$ is averaged among all the 1/3 octave bands contained in the investigated range of frequencies, as indicated in (0.15).

$$\overline{RMS}_{mean} = \frac{1}{K} \sum_{k=1}^K \overline{RMS}_{A_b, norm_k} \quad (0.15)$$

In the equation, k indicates the band in which the average RMS is calculated and K the total number of bands contained in the frequency range taken into consideration.

In addition to the indicators described above also, the overall mass of the treatments is considered as a performance index for the comparison of the various layouts.

3.7.1.2 *Analysis of the results*

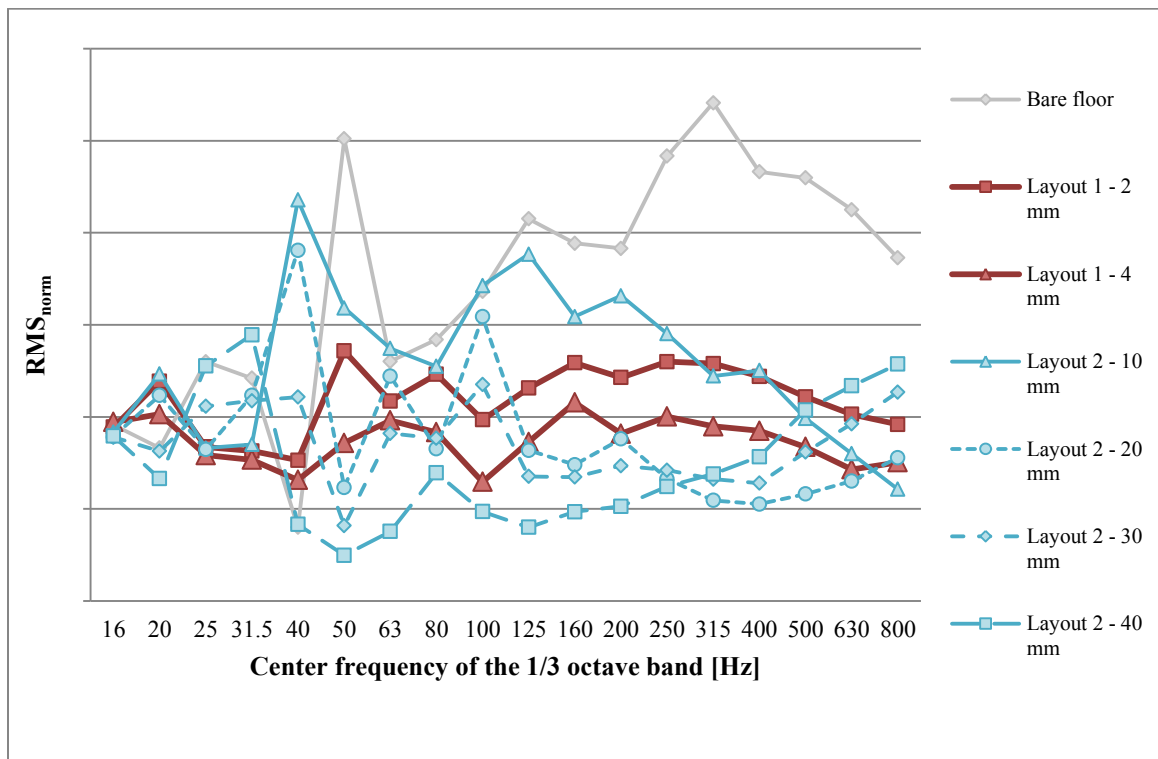


Figure 0.44: Comparison among the normalized average RMS acceleration in 1/3 octave measured on the bare floor and on the floor treated as in layout 1 and layout 2.

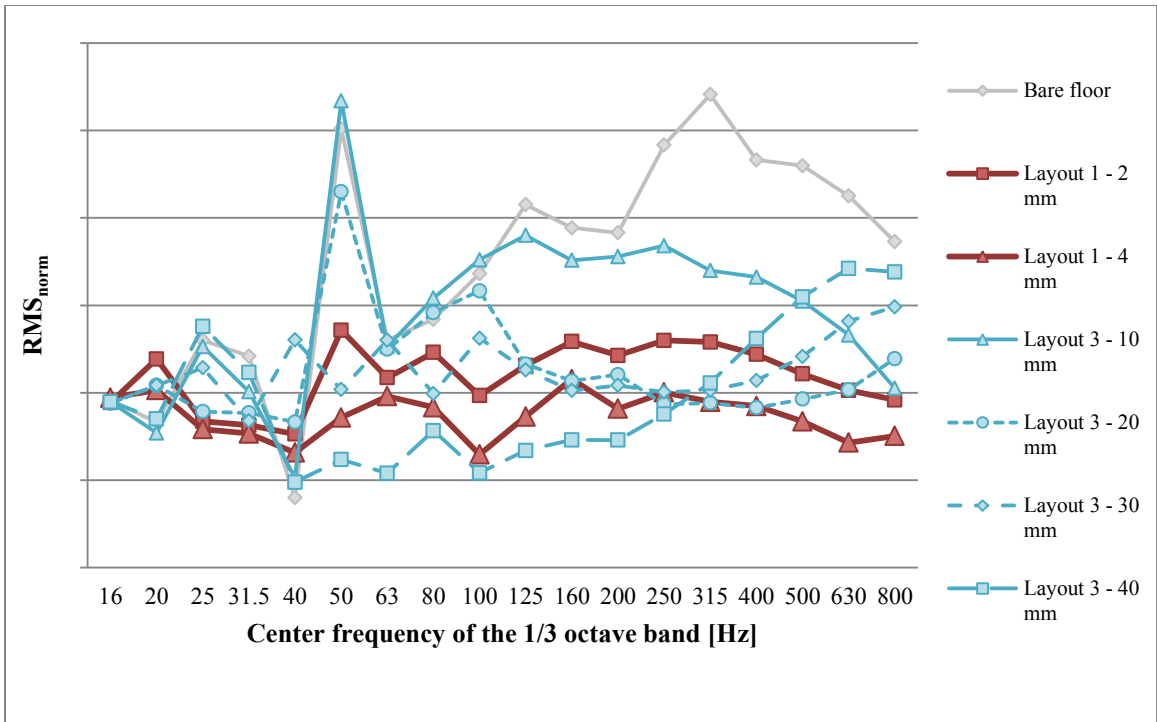


Figure 0.45: Comparison among the normalized average RMS acceleration in 1/3 octave measured on the bare floor and on the floor treated as in layout 1 and layout 3.

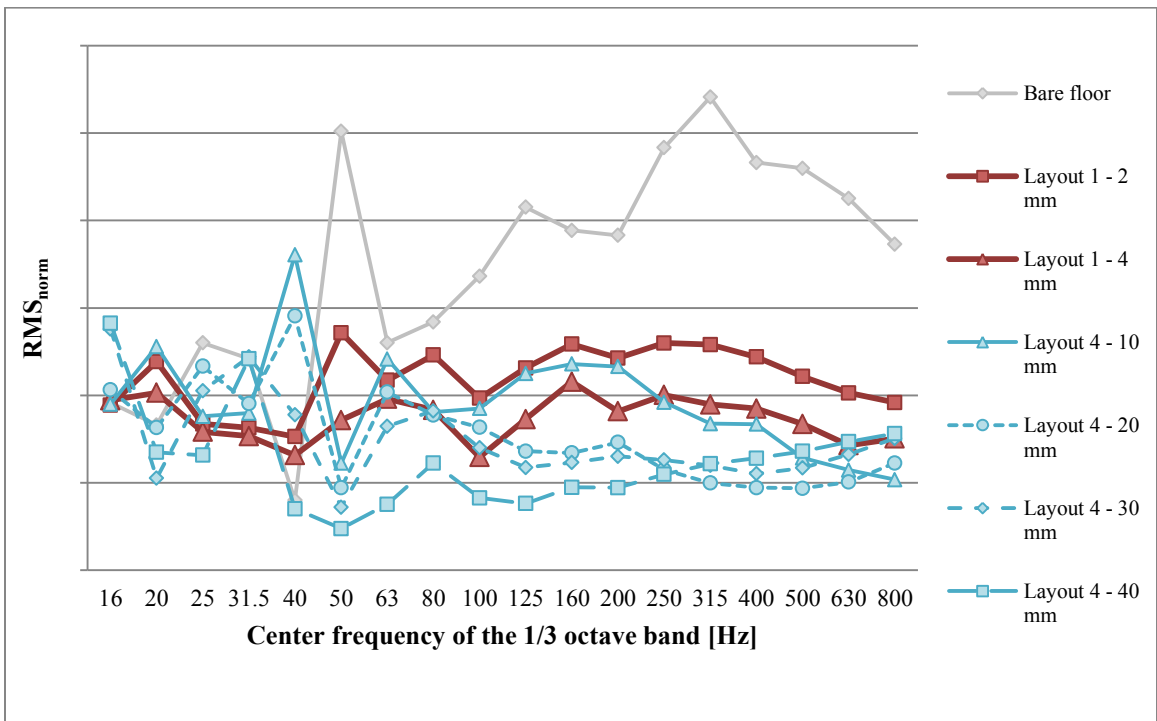


Figure 0.46: Comparison among the normalized average RMS acceleration in 1/3 octave measured on the bare floor and on the floor treated as in layout 1 and layout 4.

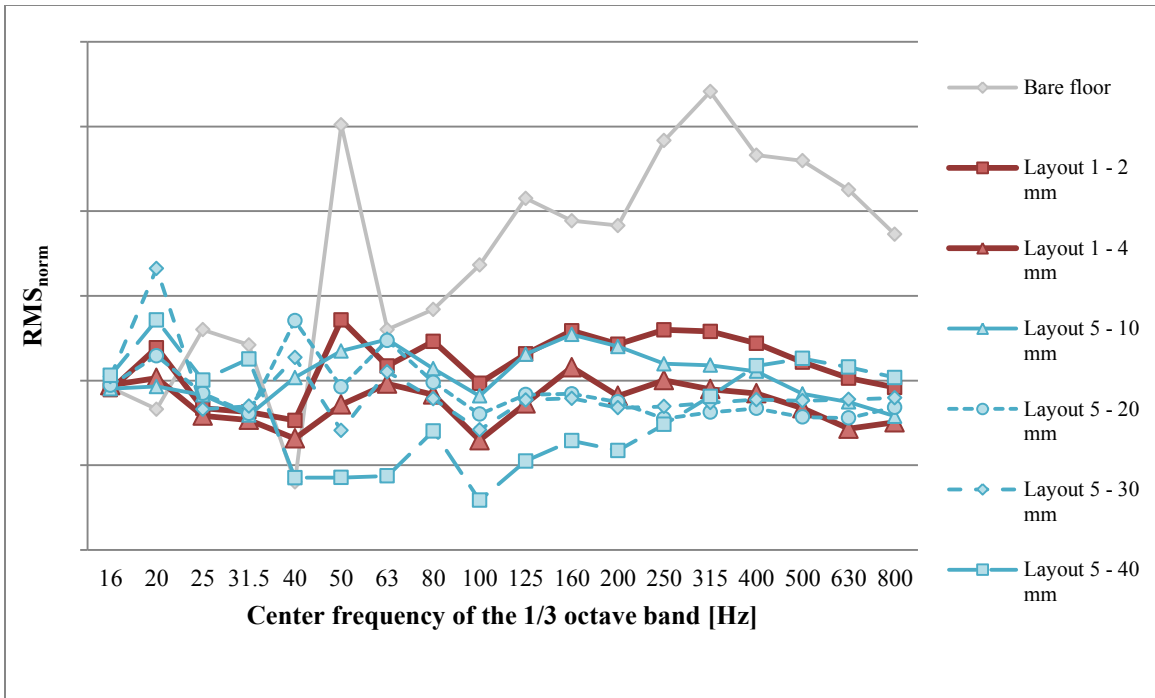


Figure 0.47: Comparison among the normalized average RMS acceleration in 1/3 octave measured on the bare floor and on the floor treated as in layout 1 and layout 5.

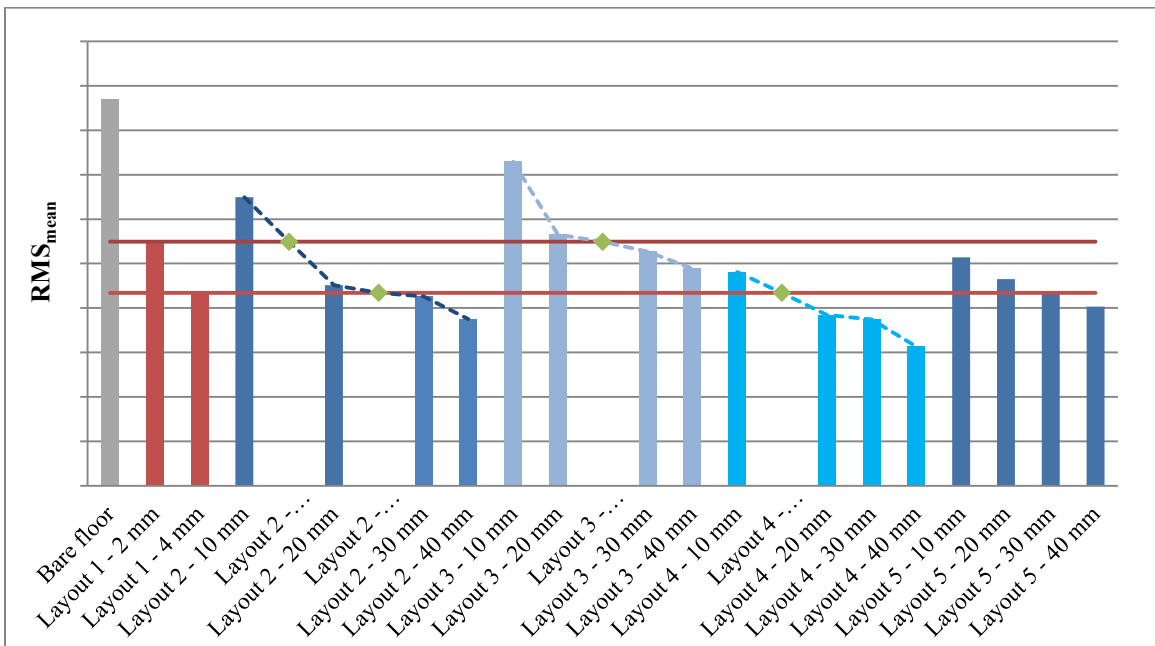


Figure 0.48: Comparison among the mean value of the normalized average RMS acceleration over the frequency range 0-1000 Hz, calculated for the bare floor and for the floor with the different layouts of the treatments

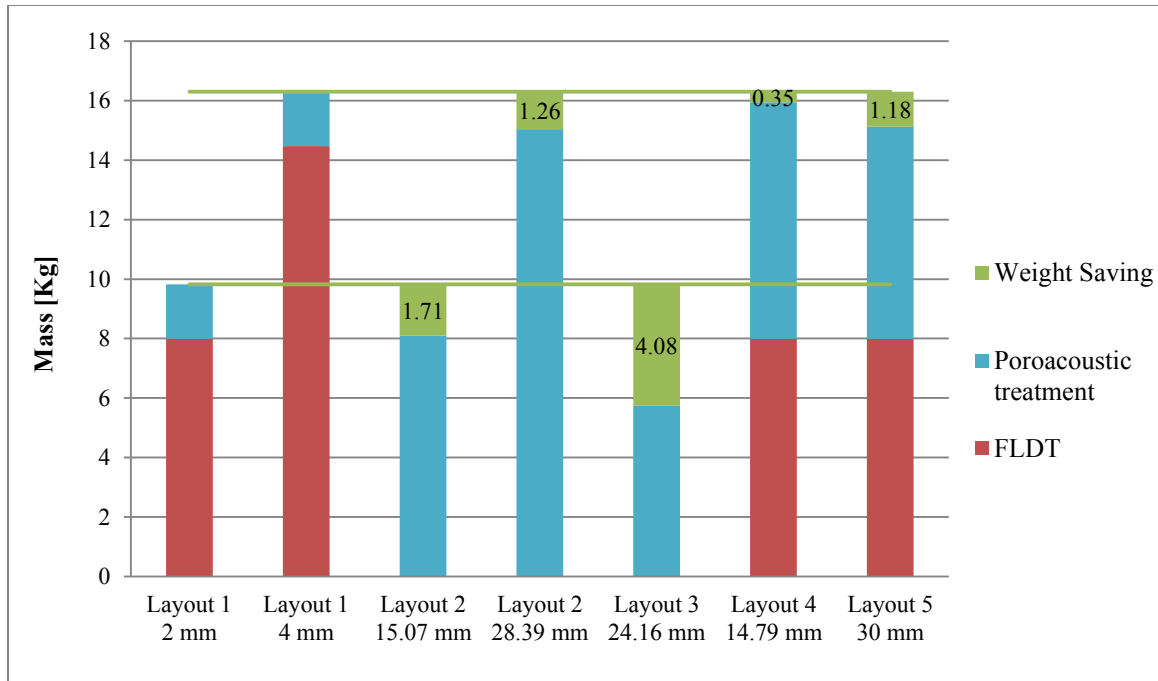


Figure 0.49: Comparison among the mass of the treatments in the various layouts and weigh saving achievable with the alternative solutions proposed.

Reviewing the results obtained with each of the five layouts examined, the following observations can be made:

- Layout 2:** Making reference to the diagram in Figure 0.44 it can be noticed that this alternative layout of the treatments is less effective than the standard solution of layout 1 for the reducing the vibration level of the floor in the lower frequency bands. Furthermore, in correspondence of the last frequency bands an anomalous increase of the RMS for the thicker porous treatments can be observed; which is attributable to the frequency shift of the resonant peaks caused by the mass increase. The same anomaly can be found also for all the other alternative layouts.

The diagram in Figure 0.48 shows that the configuration of layout 2 allows reaching the same average vibration level of the floor as the standard solution with a 2 and 4 mm of viscous material by using a thickness of the porous material equal respectively to 15.07 and 28.39 mm, but with a weight reduction of 1.71 and 1.26 kg.

- **Layout 3:** With the employment of this layout, the level of vibration obtainable with a 4 mm viscoelastic layer distributed as in layout 1 could be achieved only using a porous treatment with a thickness higher than 40 mm, which, however, would exceed the dimensional constraints of the passenger cabin. On the other hand employing a 24.16 mm layer of poroacoustic material it is possible to reach same level of vibration as layout 1 with 2 mm of FLDT, but with a weight reduction equal to 4.08 kg.
- **Layout 4:** Using this layout the performance of layout 1 with a 4 mm FLDT can be achieved by applying a 14.79 mm thick layer of porous material in addition to the 2 mm viscoelastic layer. The mass reduction in this case is very limited (0.38 kg).
- **Layout 5:** The results obtained with this layout confirm that the use of both the FLDT and the poroacoustic treatments for damping the vibration of the floor is beneficial only from the point of view of the overall thickness of the treatments. The weight savings are quite limited if compared to the solutions where the viscoelastic materials have been completely removed.

CHAPTER 4

CONCLUSIONS AND RECOMMENDATIONS

4.1 Introductory comments

One of the strategies employed for controlling the noise within a vehicle cabin consists in limiting its transmission along the structure borne path. In today's vehicles, applying a layer of viscoelastic material to the car body panels to damp their vibration usually does this. In the course of the present thesis an alternative solution has been studied which should allow removing these viscoelastic-damping treatments from the vehicle, introducing possible improvements in terms of cost and weight. The novelty of the solution proposed consists in the use of the poroacoustic treatments for not only the sound absorption and insulation, as they are employed now, but also for the vibration damping.

In order to reduce the costs and time that an experimental study would have required, the research work was carried out for the most part by means of numerical simulations conducted with a FEA tool based on Biot's theory of poroelasticity. This methodology, which has been employed before in other research activities in the field of vibroacoustic, has been validated by means of experimental tests to confirm the trustworthiness of its results. Taking advantage of the flexibility of the simulations, which unlike the experimental tests allow the investigation of different materials simply by changing the input parameters of the model, a brief sensitivity analysis has been conducted. The purpose of this sensitivity analysis was to evaluate which characteristics of the porous treatments make them suitable to be used as vibration dampers. Furthermore, the use of sensitivity analysis was also intended to evaluate whether any of the properties of the porous material required by the Biot model have an influence on the frequency response of the treated panels. The numerical simulations have also been used to compare the vibration damping performances of various porous materials, for the purpose of determining which, among them, could be used for the implementation of the technical solution proposed.

Finally, an example of a potential application to a car body floor has been proposed to demonstrate the possibility to remove the standard viscoelastic layer treatments by handing over their vibration damping function to the poroacoustic materials, which are already used on the vehicle for the acoustic insulation.

4.2 Conclusions

Taking into consideration the outcomes of the research activities conducted in the course of this thesis project it is possible to draw the following conclusions:

- The results of the experimental tests conducted on the steel plate have demonstrated that attaching the porous acoustic treatments to the surface of a panel it is possible to reduce the amplitude of its vibrations and therefore to limit the transmission of the noise through the structure borne path.
- The comparisons between the experimental results acquired from the tests and the numerical results obtained with a finite element solver have confirmed the validity of the numerical simulation for the analysis of the frequency response of panels treated with poroacoustic materials. In particular, it has been demonstrated that the software is capable of representing the effect of different materials as well as different coupling conditions between the plate and the poroacoustic treatment.
- Some of the modeling aspects have been examined, in particular the meshing technique, the effects of the acoustic cavity and the selection of the frequencies for the computation of the reduced impedance matrices. As regards the meshing technique, it has been introduced a criterion for dimensioning the mesh of the structural components and it has been shown how the frequency response varies depending on the kind of elements used. A significant simplification of the numerical simulations has been introduced demonstrating that the presence of an acoustic cavity has a negligible effect on their frequency response to a mechanical excitation. Moreover, it has also been demonstrated

that it is possible to further reduce the computational cost of the simulations by using a variable sampling step for the calculation of the frequency dependent impedance matrices, without affecting the accuracy of the results.

- The numerical sensitivity analysis has identified the properties of the poroacoustic treatments, which modify their vibration damping performance as well as the ones which have no influence on the frequency response of a treated panel.
- According to the sensitivity analysis the ideal characteristic of a porous material used for vibration damping are:
 - Low porosity and a high solid density, which increase the mass of the system
 - High airflow resistivity and structure loss factor, which cause an elevated energy dissipation
 - Low Young's modulus, which gives rise to higher deformations and therefore promotes the dissipation mechanisms.
- The sensitivity analysis has highlighted that the variations of the three parameters related to the geometry of the porous skeleton (tortuosity, viscous and thermal characteristic lengths) have no effect on the frequency response of a treated panel.
- Comparing the vibration damping performances of four different poroacoustic materials, which have been chosen among the ones that are currently made available from the suppliers, it has been possible to identify the most promising one, which is the treatment referred as Felt 3.
- The ideal material tested along with the other four existing treatments has demonstrated that it is possible to further improve the vibration damping performance of the porous materials by adjusting their properties.
- The comparison among the vibration level of the floor obtained with different treatments layouts confirmed that it is possible to completely replace the standard viscoelastic layer

damping treatments with the poroacoustic materials. This innovative solution allows decreasing the overall weight of the car body and it may bring benefits in terms of production costs.

- The outcomes of the analysis carried out on the floor of the vehicle also indicate that the best trade-off between vibration damping and weight reduction can be achieved by exclusively employing the poroacoustic treatments rather than a combination of poroacoustic treatments and standard FLDT. Furthermore, they have also demonstrated that by optimizing the topological layout of the porous treatments it is possible to reduce their impact on the mass of the vehicle, yet leaving the vibration level unchanged.

4.3 Recommendations

The research work that has been conducted in the course of this thesis constitutes only the preliminary stage in the development of an innovative solution that can combine the two functions of vibration damping and sound insulation in a unique treatment. The purpose of this thesis, indeed, is to motivate further research on this kind of solution, which may lead to its application to production vehicles. In this respect, the following recommendation should be taken into consideration for the future studies:

- For the frequency response analysis of the bare plate an improvement on the correlation of the results of the numerical analysis with the ones of the experimental tests might be achieved with a more precise measurement of the thickness of the component (eventually using with an ultrasonic gauge to determine its local value at various points), and with the employment of a panel with a more strict flatness tolerance. In addition to that also the influence of the hangs should be investigated more in depth by comparing different methods to suspend the plate and evaluating how they affect the output results.
- As regards the numerical simulations conducted on the treated panels, measuring the properties of the porous treatments directly on the samples rather than relying on the

specifications provided from the supplier could improve the accuracy of the results. In fact, since the treatments are constituted by aggregates of recycled fibers their characteristics usually present a very high variability from one sample to another.

- The most important improvement that should be done in the numerical simulation software is the introduction of a more detailed representation of the joining conditions between the treatments and the panel. The principal issue is that the software is not capable of representing the sliding contact that occurs in the areas of the porous treatment that are not bonded to the plate, but simply leaning on it.
- In the numerical simulation software, a further improvement should be the introduction of the topological optimization support. This tool, which is already implemented into many structural FE solvers, is necessary to define the optimal layout of the damping treatments on the vehicle.
- In the course of this thesis project, not being in possession of the tools necessary for the measurement of the Biot parameters and given the limited number of treatments for which these parameters have been provided from the suppliers, the sensitivity analysis has been conducted only by using the numerical simulations. For this reason, the results obtained with the numerical sensitivity analysis should be verified through experimental tests conducted on a high number of materials with known characteristics.
- With a deeper understanding of the role that each material property has on the frequency response of a treated panel it should be possible to create new poroacoustic treatments with optimized vibration damping performances.
- The research conducted in the present thesis has only investigated the possibility to employ the porous materials for damping the vibration of the car body panels, without addressing their acoustic performance. However, it must be taken into account that even if these materials are already employed in vehicles for the noise insulation and

absorption, their application as vibration dampers would require some design modification that could negatively affect these two functions. For instance bonding the porous treatment to the car body panels, which has been demonstrated from both the numerical and the experimental results to be necessary for damping the vibration, might reduce the sound insulation effect that is now obtained by leaving a certain air gap between the structure and the acoustic treatment. In a similar way, modifying the material properties of the porous treatments to improve their vibration damping performance might reduce their ability to dissipate the energy of the sound pressure waves. Based on these considerations, an important step towards an actual vehicle application should be the multi-target optimization of the treatment, so that they can offer the best trade-off between the acoustic and the vibration damping performances.

- An important aspect that has not been considered in this thesis, and that should be carefully evaluated in the future, is the economic impact of the new solution. In particular it should be determined if the removal of the FLDT can lead to some cost reduction in addition to the weight saving.

REFERENCES/BIBLIOGRAPHY

- [1] Nicholas Roy, Sylvain Germès, Benjamin Lefebvre, and Etienne Balmès, "Damping Allocation in Automotive Structures using Reduced Models," SDTools, Leuven, Belgium, conference paper 2006.
- [2] Lorenzo Morello, Lorenzo Rosti Rossini, Giuseppe Pia, and Andrea Tonoli, "Noise, Vibration, Harshness," in *The Automotive Body*. Italy: Springer, 2011, vol. II, ch. 11, pp. 239 - 263.
- [3] Pranab Saha, "Developing Vehicle Sound Packages," *SOUND & VIBRATION*, pp. 11 - 13, October 2001.
- [4] Francesco Pompoli and Paolo Bonfiglio, "I materiali fonoassorbenti," in *Materiali poroelastici e le loro applicazioni fonoisolanti e fonoassorbenti*. Ferrara, 2010.
- [5] Mohan D. Rao, "Recent applications of viscoelastic damping for noise control in automobiles and commercial airplane," *Journal* , no. 262, pp. 457-474, October 2002.
- [6] Yang Yue, Quiang Liu, Liu Xie, Meng Zhang, and Fuquan Zhao, "Study on Influence of High-Performance Acoustic Materials on a Vehicle's NVH Performance," in *FISITA 2012 World Automotive Congress*, Beijing, China, 2012.
- [7] X. Sagartzazu, L. Hervella, and J. M. Pagalday, "Review in Sound Absorbing Materials," *Archives of Computational Methods in Engineering*, vol. 15, no. 3, pp. 311-342, September 2008.
- [8] Free Field Technologies, *Actran 12.1 users'guide.*, 2012.

- [9] D. L. Johnson, J. Koplik, and R. Dashen, "Theory of dynamic permeability and tortuosity in a fluid-saturated porous media," *Journal of Fluid Mechanics*, vol. 176, pp. 379-402, 1987.
- [10] Y. Champoux and J. F. Allard, "Dynamic tortuosity and bulk modulus in air saturated porous media," *Journal of Applied Physics*, vol. 70, pp. 1975-1979, 1991.
- [11] J. F. Allard and N. Atalla, *Propagation of sound in porous media*, 2nd ed.: John Wiley and Sons, 2009.
- [12] M. E. Delany and E. N. Bazley, "Acoustical properties of fibrous absorbent materials," *Applied Acoustics*, vol. 3, no. 2, pp. 105-116, 1970.
- [13] F. P. Mechel, "Ausweitung der Absorberformel von Delany and Bazley," *Acoustica*, vol. 35, pp. 210-213, 1976.
- [14] Y. Miki, "Acoustical properties of porous materials - modifications of Delany-Bazley models," *Journal of the Acoustical Society of Japan*, vol. 11, pp. 19-24, 1990.
- [15] J. F. Allard and Y. Champoux, "New empirical equations for sound propagation in rigid frame fibrous materials," *Journal of the Acoustical Society of America*, vol. 91, pp. 3346-3353, 1992.
- [16] M. Biot, "Theory of propagation of elastic waves in fluid-saturated porous solid," *Journal of the Acoustical Society of America*, vol. 28, no. 2, pp. 168-191, 1956.
- [17] N. Kobayashi, Y. Uno, and H. Yamakoa, "Dynamic behavior analysis of vehicle acoustic trim using FEM," in *Acoustics'08 Paris*, Paris, 2008, pp. 3761-3766.
- [18] J. F. Allard, *Propagation of sound in porous media: Modelling sound absorbing materials*.

London: Elsevier Applied Science, 1993.

- [19] Nouredine Atalla, Raymond Panneton, and Patricia Debergue, "A mixed displacement-pressure formulation for poroelastic materials," *Journal of the Acoustical Society of America*, vol. 104, no. 3, pp. 1444-1452, 1998.
- [20] Patricia Debergue, Raymond Panneton, and Nouredine Atalla, "Boundary conditions for the weak formulation of the mixed (u,p) poroelasticity problem," *Journal of the Acoustical Society of America*, vol. 106, no. 5, pp. 2383-2390, 1999.
- [21] Olivier Dazel and Nicolas Dauchez, "The Finite Element Method for Porous Materials," in *Materials and Acoustics Handbook*.: Hermes Science Publishing, 2010.
- [22] Luca Guj, Theophane Courtois, and Claudio Bertolini, "A FE Based Procedure for Optimal Design of Damping Package, with Presence of the Insulation Trim," *SAE International Journal of Passenger Cars - Mechanical Systems*, vol. 4, no. 2, pp. 1291 - 1303, May 2011.
- [23] Thomas D. Rossing, "Experimental modal testing," in *Handbook of Acoustics*.: Springer, 2007, pp. 1129-1130.
- [24] Brian J. Schwarz and Mark H. Richardson, "EXPERIMENTAL MODAL ANALYSIS," in *CSI Reliability Week*, Orlando Florida, 1999.
- [25] Yeon June Kang and J. Stuart Bolton, "Finite element modeling of isotropic elastic porous materials coupled with acoustical finite elements.," *Journal of the Acoustical Society of America*, vol. 98, no. 1, pp. 635-643, 1995.
- [26] Raymond Panneton and Nouredine Atalla, "Numerical prediction of sound transmission through finite multilayer systems with poroelastic materials," *Journal of the Acoustical*

- Society of America*, vol. 100, no. 1, pp. 346-354, 1996.
- [27] N. Dauchez, S. Sahraoui, and N. Atalla , "Investigation and modeling of damping in a plate with a bonded porous layer," *Journal of Sound and vibration*, vol. 265, pp. 437-449, 2003.
- [28] Christian Glandier, Ralf Lehmann, Takashi Yamamoto, and Yoshinobu Kamada, "Vibro-acoustic FEA Modeling of Two Layer Trim Systems," in *SAE Noise and Vibration Conference and Exhibition*, Grand Traverse, Michigan, United States, 2005.
- [29] Peter Göransson, "Acoustic and vibrational damping in porous solids," *Philosophical Transactions of the Royal Society*, vol. 364, pp. 89-108, 2006.
- [30] Christopher J. Cameron, Per Wennhage, and Peter Göransson, "Prediction of NVH behaviour of trimmed body components in the frequency range 100-500 Hz," *Applied Acoustics*, vol. 71, pp. 708-721, 2010.
- [31] Norimasa Kobayashi, Masami Habuchi, and Hiroo Yamakoa, "FEM System Development for Dynamic Response Analysis of Acoustic Trim," *SAE International Journal of Passenger Cars - Mechanical Systems*, vol. 2, no. 1, pp. 1487-1493, 2009.
- [32] A. Duval et al., "Trim FEM simulation of a dash and floor insulator cut out modules with structureborne and airborne excitations," in *Acoustics'08 Paris*, Paris, 2008, pp. 3779-3784.
- [33] Gregorio Bergeretti, Simulazione del comportamento vibroacustico dei trattamenti acustici di origine automobilistica, 2011.
- [34] Andrew N. Norris, "Flexural waves on narrow plates," *Journal of the Acoustical Society of America*, vol. 113, no. 5, pp. 2647-2658, May 2003.

- [35] Reza Madjlesi, "Application of FEM and SEA in predicting vibro-acoustic behavior of flat ribbed panel structure," *Canadian Acoustics*, vol. 35, no. 3, 2007.
- [36] O. C. Zienkiewicz, *The Finite Element Method: Its Basis and Fundamentals*, 6th ed. Berkeley, California: Elsevier, 2005, vol. 1.
- [37] Giovanni Belingardi, *Il Metodo degli Elementi Finiti nella Progettazione Meccanica*. Torino: Levrotto&Bella, 1995.
- [38] Alan F. Duncan, Frank C. Su, and Walter L. Wolf, "Understanding NVH Basics," in *IBEC*, 1996.
- [39] Jorge P. Arenas and Malcolm J. Crocker, "Recent Trends in Porous Sound-Absorbing Materials," *Sound & Vibration*, pp. 12-17, July 2010.
- [40] B. Lagrain, L. Boecks, E. Wilderjans, J. A. Delcour, and W. Lauriks, "Non-contact ultrasound characterization of bread crumb: Application of the Biot–Allard model," *Food research international*, vol. 39, pp. 1068-1074, 2006.
- [41] Taylor & Francis Group, "Reducing noise in the automotive interiors," in *Textile advances in the automotive industry*, Roshan L. Shishoo, Ed. Manchester, England, 2008, pp. 200-227.
- [42] MSC Software, "Dynamic Analysis," in *MSC Nastran user's guide.*, 2012, pp. 43-132.
- [43] George A. Papagiannopoulos and George D. Hatzigeorgiou, "On the use of the half-power bandwidth method to estimate damping in building structures," *Soil Dynamics and Earthquake Engineering*, vol. 31, no. 7, pp. 1075–1079, July 2011.

VITA AUCTORIS

NAME: Carlo Gambino

PLACE OF BIRTH: Asti, Italy

YEAR OF BIRTH: 1989

EDUCATION: Liceo scientifico “Galileo Galilei”, diploma di liceo scientifico, Nizza Monferrato, Italy, 2003

Politecnico di Torino, Corso di laurea di I livello in ingegneria dell’autoveicolo, Torino, Italy, 2011

Politecnico di Torino, Corso di laurea magistrale in automotive engineering, Torino, Italy, 2013

University of Windsor, M.A.Sc. in Mechanical Engineering, Windsor, ON, 2015